博士論文

Magnetic Rotational Properties of Biogenic Micro-crystals Initiating Urinary Tract Stones and Gout

尿路結石・痛風の原因となる

生体由来微結晶の磁気回転特性

武 内 裕 香

広島大学大学院先端物質科学研究科

2015 年 3 月

目次

1. 主論文

    Magnetic Rotational Properties of Biogenic Micro-crystals Initiating Urinary Tract Stones and Gout
    (尿路結石・痛風の原因となる生体由来微結晶の磁気回転特性)
    武内　裕香

2. 公表論文

    (1) Magnetic Rotation of Monosodium Urate and Urinary Tract Stones for Clinical Treatment Applications
    Yuka Takeuchi, Yoko Sugawara, Tadashi Sugawara, Masakazu Iwasaka
    IEEE Transactions on Magnetics, **50** (11), 6101204 (2014).

    (2) Two-stage magnetic orientation of uric acid crystals as gout initiators
    Y. Takeuchi, Y. Miyashita, Y. Mizukawa, M. Iwasaka
    Applied Physics Letters, **104**, 024109 (2014).

3. 参考論文

    (1) Effects of magnetic fields on dissolution of arthritis causing crystals
    Y. Takeuchi and M. Iwasaka
    Journal of Applied Physics **117** 17D152 (2015).

    (2) Magnetic rotations of uric acid crystals and uranic crystals by static magnetic fields of up to 500 mT
    Y. Takeuchi, Y. Mizukawa and M. Iwasaka
    35th Annual International Conference of the IEEE Engineering in Medicine and Biology Society (EMBC2013), Conf Proc IEEE Eng Med Biol Soc. 2013:3261-4, Osaka, Japan, July 3-7 (2013).

主論文

Table of Contents

Chapter 1. Introduction

Chapter 2. Magnetic Field Effects and *in vivo* Crystals

Chapter 3. Two-Stage Magnetic Orientation of Uric Acid Crystals

Chapter 4. Magnetic Rotation of Monosodium Urate Crystal

Chapter 5. Conclusions and Future Plans

1

Introduction

1.1 Background of Magneto-Science

Magnetism has numerous applications: refrigerator doors and magnets used for attaching reminders to blackboards are some obvious examples of permanent magnet applications. However, use of magnets is not limited to such direct applications. A television set includes many magnetic cores and magnetic transformer cores. An electric motor uses magnetic materials, and electric meters are interwoven with these materials. Numerous magnetic materials are existent and a majority of them contain iron. Elements such as iron, cobalt, nickel, and gadolinium are attracted to magnets. Why does iron exhibit magnetism and is attracted to magnets? These fundamental questions have not yet been answered similar to the question about "why nature exists?" has not been answered.

Human beings first encountered magnetism with the discovery of natural magnets. By 600 BC, a natural magnet had already been produced in Magnesia, Greece, and supposedly, the existence of magnetism was widely known to the world. Natural magnets are oxidized iron and rocks that have been turned into permanent magnets by lightning or volcanism. It was widely known to the world that natural magnets were also found in a region of a province in China bearing a name that meant "benevolence". During the same time period, "magnet" was written as "benevolent stone" in Chinese, and the character for "benevolent stone" also appeared in Japanese literature in the Nara era. Legend has it that the etymology of the word "magnet" came from the appearance of iron pieces adhering to magnets called mercy stones.

Although the existence of magnetism has been well known for centuries, only in recent years have magnets been used in technological applications. Previously, magnets were primarily used only as magnetic needles to find the azimuth because in addition to attracting iron, they were known to have directional characteristics and show north and south. *W. Gilbert*, the attending doctor to the British Queen *Elizabeth I*, inferred that the

earth was a giant globe magnet and gave a correct explanation of the directional characteristics of magnetism. He conducted extensive research on magnets and published "De Magnete" in 1600. Consequently, He is referred to as the founder of the theory of magnetism.

This understanding ultimately made it possible to create artificial magnets from steel in the 18th century. *H. Oersted* discovered that an electric current generates a magnetic field, which in turn led to the discovery of a link between electric and magnetic forces. The momentum at that time spurred scientists, such as *A. Ampere* and *M. Faraday*, to develop the foundations of electromagnetism.

K. Onnes in the Netherlands discovered superconduction in 1911[1], and the development of superconductors using electric magnets, which allow electric current to flow without any significant heat loss, began in earnest. High-temperature superconduction was discovered in 1986, which contributed to outstanding progress in superconductivity research and the development of scientific technology for the application of superconductivity.

Compared with conventional electric magnets, superconductive magnets can generate a magnetic field in excess of 10 Tesla. Superconductive magnets of this type make it possible for scientists to observe interesting phenomena that are impossible to see under normal circumstances. For example, typical magnets strongly attract iron, nickel, and other metals when these metals are placed close to the magnets, but generally do not attract aluminum and copper, nor are they repulsed by them. Superconductive magnets also attract iron when it is placed close to them. However, their strong magnetic fields (in excess of 10 Tesla) also repulse substances such as aluminum, water, and other elements that are considered to be non-reactive to magnets. These unprecedented phenomena are expected to be applied in a wide range of areas and are considered the genesis of the latest advances in the field of magneto-science.

1.2 Magnetism

All materials exhibit magnetism. When a magnetic field is applied, a material is magnetized depending on its inherent magnetic susceptibility (Figure 1.1). The magnetization M (A/m) depends on the magnetic field strength H (A/m) and is expressed as equation (1.1):

$$M = \chi H, \qquad\qquad\qquad (1.1)$$

where χ (dimensionless value) is the magnetic susceptibility. Depending on whether the value of the magnetic susceptibility is positive or negative, the material is classified as paramagnetic or diamagnetic, respectively. Paramagnetic materials are slightly magnetized in the same direction as the direction of the magnetic field (magnetic susceptibility: 10^{-3}–10^{-6}). Examples of paramagnetic materials include aluminum and copper. On the other hand, ferromagnetic materials, such as iron and nickel, respond strongly to weak magnetic fields and have a large magnetic susceptibility ($\sim 10^3$). In addition, they undergo spontaneous magnetization and their spin directions are aligned in specific directions. Diamagnetic materials are slightly magnetized in the direction opposite to the direction of the magnetic field (magnetic susceptibility: $\sim -10^{-6}$) and include plastics, water, and proteins.

The effect of a weak magnetic field on diamagnetic and paramagnetic materials is only 10^{-6}–10^{-9} that of ferromagnetic materials because the volume magnetic susceptibility of diamagnetic and paramagnetic materials is only 10^{-3}–10^{-6}. Therefore, the effects of weak magnetic fields (1 Tesla or less) have not been confirmed. However, magnetic effects can be observed in magnetic materials with very small magnetic susceptibilities if the magnetic field is sufficiently strong.
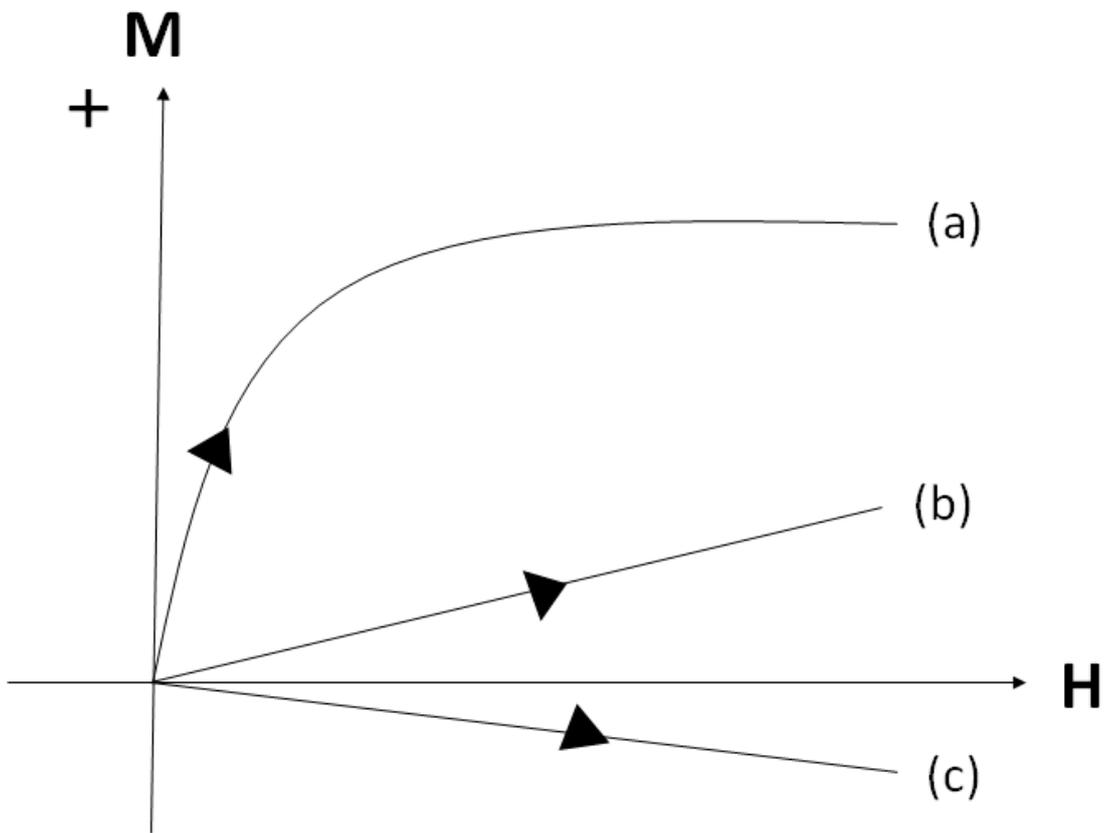
Fig. 1.1. Magnetization curve: (a) ferromagnet. (b) paramagnet. (c) diamagnet.

Reference

[1] H. Kamerlingh Onnes, Leiden Comm. 120 b, 122b, 124 c (1911).

2

Magnetic Field Effects and In vivo Crystals

2.1 Magnetic Field Effects

2.1.1 Properties of Diamagnetism

In the mid-17th century, the existence of diamagnetic materials was revealed. Diamagnetism is a property of magnetic repellency, because a diamagnet is magnetized in the direction opposite to the applied magnetic field. The values of χ for diamagnets are very small, and the diamagnetic susceptibility exhibits minimal temperature dependency. Diamagnetism is observed only after a magnetic field is applied externally, whereas paramagnetism is the result of the natural behavior of the atoms, molecules, and electrons in paramagnetic materials. In addition, molecular diamagnetic susceptibilities are approximately 2–3 orders of magnitude less than molecular paramagnetic susceptibilities. Therefore, diamagnetism is often neglected in magnetic fields of millitesla or less. Think about why diamagnetism appears.

Diamagnetism occurs as a result of the movement of electron in orbitals. Consider that electrons move with an angular frequency ω in a circular orbit with a radius r. Assuming that the magnetic field direction is the +z axis and the electronic orbital is in the xy plane, the direction of an energetically stable electronic orbital is clockwise given the negative charge of the electron. It is also assumed that changes in the electron orbit are negligibly small due to the applied magnetic field. When the force that binds the electrons to the nucleus depends only on r, it can be assumed that the mass of the atom is m, and the balance of the force F with no applied magnetic field can be expressed using the following equation (2.1):

$$F(r) = mr\omega_0^2,\qquad(2.1)$$

where ω_0 is the angular velocity when no magnetic field is applied. This equation can

then be expressed as equation (2.2) considering the Lorentz force when a magnetic field is applied:

$$F(r) = mr\omega^2 + er\omega\mu_0 H , \tag{2.2}$$

where e is the charge of an electron, μ_0 is the magnetic permeability, and H is the magnetic strength. By eliminating F(r) from equations (2.1) and (2.2), we obtain equation (2.3):

$$\omega^2 - \omega_0^{\,2} = -\frac{er\mu_0 H}{m} . \tag{2.3}$$

It is given that $\Delta\omega \equiv \omega - \omega_0 \ll \omega$, because $\omega \simeq \omega_0$ when the applied magnetic field H is small. The value of $\Delta\omega$ can be estimated using equation (2.4):

$$\Delta\omega \approx -\frac{er\mu_0 H}{2m} . \tag{2.4}$$

Here, the magnetic moment was induced in the $-Z$ direction. On the other hand, the magnetic dipole moment m of the circular current I generated due to the motion of the electron is given as $m = IS = I\pi r^2$. The current I is given as in equation (2.5), because the current is the amount of charge flowing per unit time:

$$I = \frac{-e\Delta v}{2\pi r} . \tag{2.5}$$

Therefore, the change in the magnetic moment can be estimated using equation (2.6):

$$\Delta m \approx -\frac{er\Delta v}{2} \approx -\frac{e^2 r^2 \mu_0 H}{4m} . \tag{2.6}$$

The magnetic dipole moment $\angle m$ occurs due to application of the magnetic field H in the opposite direction. This diamagnetic behavior is referred to as Larmor diamagnetism.

2.1.2   The Nature of Magnetic Field

Magnetic field effects on non-magnetic materials, such as diamagnetic and paramagnetic materials that have been conventionally considered to have little influence on magnetic fields, have been clarified with the recent advances in superconducting technology. In fact, understanding magnetic field effects on biomaterials has helped enable the elucidation of mechanisms in living systems placed within electromagnetic fields. For example, a greater understanding of the influence of magnetic fields on the behavior of radical species and their mechanical effects on biomaterials and biochemical reactions has become possible. Known mechanisms of magnetic field effects are listed in Table 2.1.

Table 2.1. Kind of magnetic field and magnetic field effect.

Category	Mechanism	Magnetic effect
DC magnetic fields	Diamagnetic torque	Magnetic orientation
	Zeeman splitting	Magnetic effect to chemical reaction
Gradient magnetic fields	Magnetic force	Moses effect
AC magnetic fields	Eddy current	Magnetic nerve stimulation

Magnetic fields can be distinguished roughly as direct current (DC) magnetic fields and alternating current (AC) magnetic fields. DC magnetic fields are steady magnetic fields with a spatially constant magnetic field strength. In the case of AC magnetic fields, the magnetic field strength varies with direction (i.e., there is a gradient). This magnetic field orientation phenomenon is known to cause magnetic effects when a steady magnetic field is applied. In addition, if a DC magnetic field and light are applied simultaneously, a photochemical magnetic field effect can be observed due to the generation of radical pairs. This phenomenon is thought to be involved in the magnetic sensing of animals. It is also known that a magnetic force will interact under a gradient (AC) magnetic field in proportion to the strength and the gradient of the magnetic field. For example, when a magnetic force is applied under a gradient magnetic field,

diamagnetic materials move in the weak direction of the magnetic field, while paramagnetic materials move in the strong direction, which can be advantageous.

Living materials have been classified on the basis of their magnetism under the influence of DC and AC magnetic fields. The influence of an AC magnetic field is determined by the magnetic properties of the material and the currents induced by the magnetic field. The elucidation of biological effects under strong magnetic fields has received attention because magnetic fields that are 500,000 times stronger than the Earth's magnetic field are now used in some medical applications due to the development of the superconducting technology.

2.1.3 *Magnetic Orientation*

The thermal energy of materials in the vapor or liquid phases is attributed to the random rotation of their molecules. When an external magnetic field is applied, the molecules are arranged in the direction of the received magnetic torque. The thermal energy of a material is *2/kT* at temperature *T*. The magnetic anisotropy of a molecule is oriented in a magnetic field when the magnetic energy of the field is greater than the thermal energy of the molecule. Thus, magnetic orientation stabilizes the dominant magnetic energy by disturbing the thermal energy.

Red blood cells

Red blood cells have the important function of accepting and delivering oxygen. These cells are shaped like pancakes with a diameter of approximately 8 μm and have dents in their centers. When there is no magnetic field, red blood cells point in random directions, but when a magnetic field is applied, they point unidirectionally [1,2]. In fact, red blood cells are thought to be more susceptible to magnetic field effects than other tissue cells because of their flat shape, which imparts particularly strong anisotropy to the diamagnetic susceptibility of the cell membrane lipids. *Higashi* [3] reported that measurement of the light transmission rate of a suspension of red blood cells exposed to a high magnetic field indicated that the cells were completely oriented at 3–4 T. A red blood cell is largely composed of iron–protein hemoglobin, but the differences in the magnetic properties of the cell components do not affect the intensity of the orientation. The cell components that cause the magnetic field orientation have magnetic anisotropy and are oriented unidirectionally; further, they are well integrated within the cell. In addition, compared with such magnetic energy, the energy generated by the magnetic shape anisotropy is negligibly small. Given that red blood cells that contain oxyhemoglobin exhibit approximately the same degree of orientation as those with deoxyhemoglobin, it was concluded that the diamagnetism of the membrane lipids make a more significant contribution to the orientation than the paramagnetism of hemoprotein. Furthermore, *Murayama* [4] found that sickle-shaped red blood cells, which are seen in the inherited disease sickle-cell anemia and result in deterioration of the oxygen transport function, are oriented in a magnetostatic field of just 0.35 T, with their long axes at right angles to the direction of the magnetic field.

Red blood cell membranes

The diamagnetic anisotropy of the red blood cell membrane lipid bilayer and membrane-spanning proteins mainly contribute to the orientation of the red blood cells. The red blood cell membrane consists of a phosphatide-based lipid bilayer in which membrane-spanning proteins with alpha helix structures are scattered. Because the phosphatide has all of its hydrocarbon chains aligned perpendicularly to the magnetic field, the cell's surface is positioned parallel to the magnetic field [5,6]. Meanwhile, the membrane-spanning proteins are directed along the long axis of the alpha helix portion parallel to the magnetic field and act to position the cell membrane's surface at a right angle to the magnetic field. It should be noted that spectrin, a membrane-lining protein that accounts for a quarter of the membrane proteins, forms an interconnected network structure in the interior of the cell membrane, which serves as the cellular cytoskeleton. This three-dimensional conformation is shaped like a string of beads and has no significant magnetic anisotropy.

Flagella

A bovine sperm is 55 μm in length and has a flat oval head and a tail [7]. The entire sperm is surrounded by a single cell membrane. The nucleus is located in the head and contains extremely condensed DNA. The tail consists of flagella, through the center of which an axial filament runs longitudinally. The axial filament consists of 2 simplex microtubules surrounded by 9 duplex microtubules. A microtubule consists of protofilaments with tubulin dimers running longitudinally. In duplex microtubules, a simplex microtubule and an incomplete microtubule consisting of 11 protofilaments are fused. Bovine sperm are oriented parallel to the magnetic field, even when the tails are removed, thus indicating that the magnetic anisotropy originates from the head [8].

Fibrinogen

The magnetic orientation of fibrinogen has been well researched [9-12]. Fibrin is a protein involved in clot formation and acts to clot blood when exposed to air outside of the body by transforming into fibrin. This polymer has many benzene rings positioned unidirectionally. *Torbet, et al.* [13] found that fibrin is oriented parallel to the magnetic field direction under a magnetic field of 10 T. This behavior has also been reported by *Yamagishi* [14], and the mechanism of such magnetic orientation is thought to be due to the diamagnetic-susceptibility anisotropy of peptide groups peculiar to the protein. The substance polymerizes to form fibrin fibers that interconnect in a network-like fashion and pectize the entire solution.

In general, biological materials that have many benzene rings that are oriented in the same direction will be oriented in a magnetic field of approximately 1 T. However, often, the movement is limited because biological materials are large molecules. For instance, even though the diamagnetic anisotropy of red blood cells is large and it is relatively easy to orient them, it takes several milliseconds for red blood cells to become orientated in a magnetic field.

As shown in the above, the effects of magnetic fields on biological molecules and macromolecules, such as proteins in solution, have been thoroughly studied in magnetic fields of up to 10 Tesla (T). However, there are few reports concerning the possible applications of magnetically controlled crystallization as a therapeutic method. Of several kinds of physical stimulation, a direct-current magnetic field is a candidate that can provide noncontact noninvasive treatments of living tissue. It is reported that the biogenic crystals of guanine, revealed that it shows distinct magnetic orientation and light-scattering anisotropy under magnetic fields in the range of 100 to 500 mT [15-17]. Guanine is shows by the molecular formula $C_5H_5N_5O$, is one of the key is a four substances of the double helix structure of DNA (adenine, cytosine, guanine, thymine). Of these, adenine, guanine has a structure known a purine base, a uric acid results as a final product in which they are metabolized. The purine base is a collective term for substances having a purine skeleton. This included purine bases, purine nucleoside, purine nucleotides, such as ATP, and the nucleic acid. The purine as a raw materials for uric acid is categorized those from food and those synthesized in the body. Uric acid is a metabolite produced in the process of DNA is finally metabolism. We focused on the uric acid which is a degraded product of DNA.

2.1.4   Superconductivity Magnet

An external view of a superconductive magnet is shown in Figure 2.1. The magnet is cooled to cryogenic temperatures to reduce resistance and thus heat loss. A superconductive magnet consists of a coil of wire made from a superconducting material through which an electric current flows, resulting in the generation of a magnetic field according to Ampere's law. Each loop of the coil generates a magnetic field, and therefore, the larger the number of loops, the greater is the total magnetic field. The magnetic field distribution is the strongest at the center and gradually weakens towards the edge.

Today, various phenomena have been clarified by exposing a weak magnetic material to the strong magnetic field generated using a superconducting magnet [18-26]. However, superconducting magnets require the use of liquid helium as a refrigerant. Liquid helium is a finite material, and its use contributes to the high cost of superconducting magnets. In addition, the influence of such strong magnetic forces on the human body and the surrounding environment are a concern. Furthermore, the requirement of greater cooling efficiencies has led to the need for larger support structures, and as the size of the apparatus has increased, the locations where superconducting magnets can be used have becoming increasingly restricted.

Fig. 2.1. The appearance of the superconducting magnet.

2.1.5   *Magnetic Anisotropy*

In aeolotropic substances, both susceptibility anisotropy and shape anisotropy can exist. A crystal is an example of a material with susceptibility anisotropy. Uniaxial (tetragonal, trigonal, and hexagonal) and biaxial (orthorhombic, monoclinic, and triclinic) crystals also have susceptibility anisotropy. However, a cubic crystal is isotropic with respect to its magnetism. There are three principal values for the susceptibility tensor, with one of them different than the other two in uniaxial crystals and all three different in biaxial crystals. All three values are the same in cubic crystals. The relationship between the direction of the main axis and the direction of the crystal axis determines the crystal structure. For instance, in monoclinic crystals, the crystal axis agrees with one of the magnetic axes, and in orthorhombic crystals, each of the three magnetic axes correspond to a crystal axis [27]. A polymetric fiber also has susceptibility anisotropy, with the value of the magnetic susceptibility different in the direction perpendicular to the fiber-axis direction. Because the molecular chains in a polymeric fiber orient themselves in the fiber-axis direction, the susceptibility anisotropy of the monomer units is reflected as the aeolotropicity of the fiber. The susceptibility anisotropy of both crystals and fibers originates from the magnetic susceptibility anisotropy of the chemical bonds, and more generally due to the aeolotropicity of the electron distribution. Particles with shape anisotropy, such as cylindrical and disk-like particles, exhibit susceptibility anisotropy due to both their shape anisotropy and the susceptibility anisotropy unique to each material. Shape anisotropy contributes to the susceptibility anisotropy because the size of the magnetic moment induced under a magnetic field differs depending on the direction of the particle with respect to the magnetic field [28]. For ferromagnetic bodies, this effect is referred to as a demagnetizing field. It is not observed for diamagnetic materials.

2.1.6   *Diamagnetic Anisotropy*

Diamagnetic materials can also exhibit anisotropy. Aromatic compounds such as benzene are examples. These molecules adopt a planar structure with a π-electron system existing above and below the plane. Consider the molecular aspects of the magnetic susceptibility of benzene separately from the bidirectional parallel and vertical magnetic force lines. A magnetic moment occurs in the direction opposite to that of the magnetic field direction because an intramolecular electric current (ring current effect) flows along the ring according to Lenz's law when a magnetic field is vertically applied with respect to the benzene ring. The benzene ring experiences rotational interactions due to the magnetic field, and the direction of rotation of the magnetic moment is perpendicular to the magnetic field because his magnetic moment is unstable. However, such an electric current is not generated when a magnetic field is applied perpendicular to the surface of the benzene ring.

Thus, in diamagnetic aromatic compounds, the magnetic anisotropy can be expressed using the following equation (2.7), where $\chi_\perp$ is the magnetic susceptibility with the magnetic field applied perpendicular to the benzene surface, and $\chi_{//}$ is the magnetic susceptibility with the magnetic field applied vertically with respect to the benzene surface:

$$\triangle\chi = \chi_\perp - \chi_{//}. \qquad\qquad (2.7)$$

Here, the signs of $\chi_\perp$ and $\chi_{//}$ are both negative, and the absolute value of $\chi_\perp$ is greater. The susceptibility anisotropy is the key magnetic parameter determining the magnetic orientation. Because a smaller absolute value indicates a more stable diamagnetic magnetization ($M = \chi B$) in a given magnetic field, diamagnetic materials that naturally experience repulsion from a magnetic field are subject to a torque in the direction of the lesser magnetic susceptibility ($\chi_\perp$ or $\chi_{//}$). Therefore, magnetic orientation occurs along the molecular axis parallel to the magnetic direction when the shape of the molecule and the electron distribution are similar.

① **Ambient field**

② **Unstable**
Applied magnetic field

③ **Unstable**
Magnetic field **Ring current**
Applied magnetic field

④ **Stable**
Rotation
Applied magnetic field
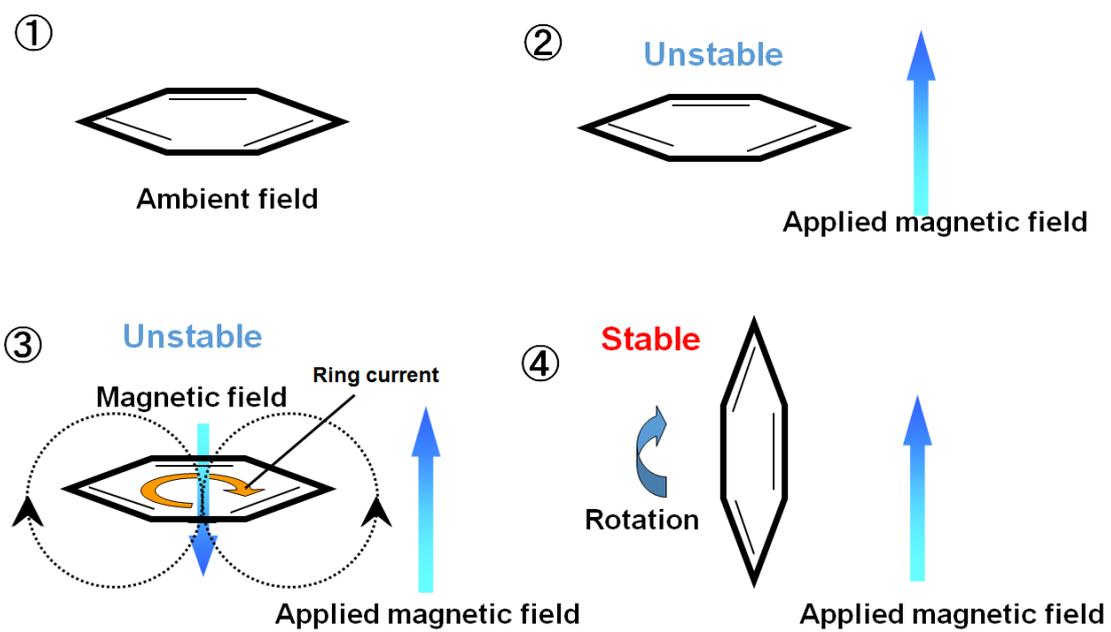
Fig. 2.2. Aromatic ring placed in a magnetic field.

2.1.7 Magnetic Energy

When a magnetic field is applied to a material, the material obtains magnetic energy:

$$E = -\frac{VB^2 \chi}{2\mu_0}.$$

(2.8)

A material with uniaxial anisotropy under a static magnetic field can be shown to follow equation (9) by using its main axis. Applied magnetic fields can be classified as static magnetic fields, rotating magnetic fields, or modulated magnetic fields. In a material where $\chi_3 < \chi_2 < \chi_1$, magnetization occurs most easily on the χ_1 axis, followed by the χ_2 axis, while magnetization along the χ_3 axis is difficult. The χ_1 axis is therefore uniaxially oriented under a static magnetic field, and the magnetic energy can be expressed as in equation (2.9) for a uniaxial crystal with $\chi_3 = \chi_2 < \chi_1$ is placed in a magnetic field applied in the direction of the Z-axis:

$$E_2 = -\frac{VB^2}{2\mu_0}(\chi_1 - \chi_2)\cos^2\theta.$$

(2.9)

where θ is defined as the angle between the χ_1 axis and the magnetic field B [29]. This expression indicates that the χ_1 axis is related to the magnetic field direction. The level of relationship (coefficient of $\cos^2\theta$) is proportional to the volume V and the magnetic susceptibility difference. If the axis that is most easily magnetized is parallel to the magnetic field B, the material is stable in this direction, because the magnetic energy E takes a minimum value. However, the difference in the magnetic energy for an arbitrary direction and the direction of the stable axis is small when the magnetic field B is weak. Therefore, the orientation of the material becomes random due to thermal agitation. On the other hand, the difference in the magnetic energy between any direction and the stable direction increases when the magnetic field increases. As a result, orientation in the stable direction overcomes the thermal agitation when the difference in the magnetic energy exceeds the thermal energy.

2.1.8   Magnetic Torque

A magnetic moment is generated in the interior of a crystal when a magnetic field is applied to the crystal:

$$M = \chi\, B / \mu_0. \tag{2.10}$$

Torque results because the magnetic field interacts with the magnetic moment [30]. The magnetic torque T interacting with the diamagnetic magnetization M due to the presence of a ring current in the magnetic field B is given by $T = B \times M$. Because the diamagnetic magnetization M, which is caused by the aeolotropicity of the diamagnetic susceptibility increases as the size of the molecule increases, the torque T is large:

$$T = VM \times B = V(\chi\, B) \times B / \mu_0. \tag{2.11}$$

When a material having magnetic anisotropy is placed in a magnetic field as shown Figure 2.3, the magnetic torque acting on the object can be determined using equation (2.11), because the magnetic moment is defined as $B\chi_1\sin\theta$, 0, $B\chi_2\cos\theta$ [29]:

$$T = \frac{VB^2}{\mu_0}(\chi_1 - \chi_2)\cos\theta\sin\theta. \tag{2.12}$$

A material with magnetic anisotropy orients due to the magnetic torque and according to the magnetic susceptibility when a magnetic field is applied. Magnetic torque is therefore very useful in the fields of materials science and biomaterials. Moreover, the development of new materials can be expected by considering other possible types of substances with magnetic anisotropy.
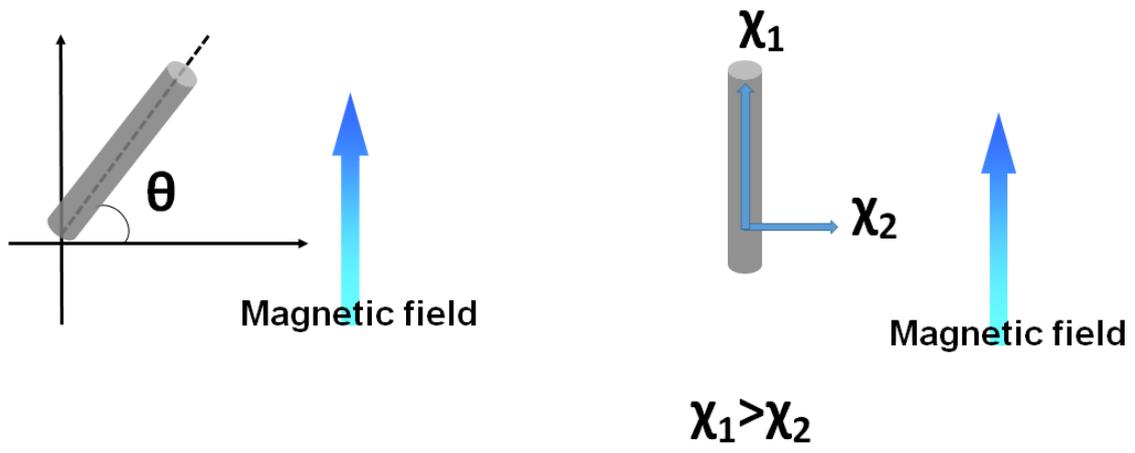
Fig. 2.3. Application of a magnetic field to the object with magnetic anisotropy.

2.2   In vivo crystals

2.2.1   In vivo Crystals

In vivo crystals include crystals that function within the body partly due to their crystalline structure (Table 2.2) and include, for example, crystals in bone and crystals that cause diseases. At present, the crystallization of calcium oxalate (urinary calculus) has been most extensively studied. Body tissues that have crystalline structures include bone tissue and hard tissue, which mainly contain calcium phosphates, such as hydroxyapatite. *In vivo* crystals that relate to disease include urinary calculi, gallbladder calculi, knots, and crystals in the synovial fluid, which cause arthritis and include basic calcium phosphates such as monosodium urate (MSU), calcium pyrophosphate dihydrate, and hydroxyapatite.

Table 2.2. Crystalline material *in vivo.*

Region	Main components that deposit
Bone, cartilage	Calcium phosphate
Dental tissue (enamel, cementum, dentin)	Calcium phosphate
<Those involved in the disease>	
Urinary lithiasis	Calcium oxalate, Calcium phosphate, Uric acid
Gallbladder calculus	Cholesterol
Nodal cell	Calcium phosphate
Intra-articular crystal	Monosodium urate, Calcium pyrophosphate dehydrate, Calcium phosphate

2.2.2 *Uric Acid*

Uric acid is largely present as a sodium salt in body fluids. Body fluids for which the pH does not significantly change barely contain precipitated MSU crystals, which are the causative agent of gout arthritis. On the other hand, in the urinary tract where pH values do vary, uric acid crystals are deposited. Uric acid crystals are one of the causative agents of urinary tract stones.

The solubility of sodium urate in normal serum at pH 7.4 is regarded as 7.0 mg/dL, which is approximately 370 μM when converted to molar concentration. The total quantity of uric acid in the body of a healthy person is approximately 1,200 mg. In addition, each day approximately 500 mg of uric acid is excreted in urine and an additional 200 mg in sweat and digestive juices. However, 90% of the uric acid that is filtered by the renal glomerulus is reabsorbed from the convoluted tubule into the capillaries. Uric acid transporter (URAT 1, urate transporter in the human kidney) and organic anion transporter 4 (OAT 4) are located on the luminal side of the renal proximal tubular epithelium cell and transport uric acid into the cells [31]. Glucose transporter 9 (GLUT 9) is expressed in the tubule basement membrane and reabsorbs uric acid from cells and transports it to the blood vessels [32].

2.2.3 Gout

Gout was the first disease in which a crystalline material found in the synovial fluid was confirmed to be the cause. At present, slightly more than 1% of the Japanese population suffers from gout; it is as frequent as rheumatoid arthritis. A gout attack occurs due to hyperuricemia and, particularly, due to an excessive amount of uric acid in the synovial fluid that is precipitated and deposited as MSU crystals onto soft tissue, such as synovial membranes. The solubility of uric acid is 6.8 mg/dL *in vivo*, and when this concentration is exceeded, MSU crystals may be precipitated. The first metatarsophalangeal joint is a typical site of gout possibly due to the lower temperature of the periphery of the toes; this area is often subject to minor injuries or physical stimuli, and there is a difference in the permeability of the joint capsule for the synovial fluid (solvent) and the uric acid (solute) despite a tendency for hydrarthrosis due to constant placement of weight, etc [33]. In the area of the Achilles tendon, one of the sites where MSU crystals are often deposited, the MSU crystals are frequently deposited on the insertion tendon rather than on other tendons, suggesting that the formation of MSU crystals may be related to biomechanical or local factors [34].

Numerous cases have been reported where patients with gout felt discomfort in the diseased area before the gout attack occurred. The discomfort is considered the herald, and heat (calor), swelling (tumor), redness (rubor), and acute pain (dolor) follow within 24 h after the herald. The dolor reaches a peak at 8–12 h after its initial occurrence, and for attacks within the lower limbs, acute dolor often causes gait disturbance or walking difficulty. During an initial gout attack, the dolor is remitted in 10–14 days, even without treatment and no symptoms are observed until the next attack.

Although hyperuricemia is an essential condition for gout, only one in 20–30 patients with hyperuricemia suffer from gout. It is clear that the more the serum urate concentration increases, the greater is the risk of a gout attack, and when the serum urate concentration is 9 mg/dL or greater, the possibility that a gout attack will occur within five years is 20%–60% [35, 36]. However, because MSU crystals have been detected in joints of patients with gout (through a puncture) that were not having attacks, it is clear that the deposition of MSU crystals does not immediately lead to an attack [37-40].

The incidence of gout arthritis necessarily accompanies the deposition of MSU crystals. However, this type of arthritis is not caused only by crystal deposition, because there have been cases where no arthritis has developed despite the presence of crystalline MSU [41-44]. It follows that other *in vivo* factors must affect the

crystallization of MSU. Therefore, it is speculated that the incidence of gout is affected by the ease with which MSU crystallizes in the body and the individual differences in inflammatory reactions to MSU crystals.

2.2.4 *The Mechanism of Gout*

A gout attack is inflammation reactions that result from monosodium utrate (MSU) crystals were deposited into a joint cavity. Firstly, uric acid cannot be completely dissolved if the uric acid in the blood becomes excessive. Uric acid is combined with the sodium in the blood to form MSU crystal, and the crystals were deposited in the joint tissue as needle-shaped crystals. Then MSU crystals that are deposited in the joint tissue fall off into an articular cavity by physical stimulus or the rapid change in uric acid value. Then, inflammatory cells such as white blood cells are migrated if peeling fallen monosodium urate crystals are released into the articular cavity (Figure 2.4). MSU crystals that are deposited in the interior of a joint excite synoviocytes, macrophages, and monocytes and induce the production of inflammation-causing cytokines, such as tumor necrosis factor (TNF)-α, interleukin (IL)-1β, IL-6, and IL-8. As a result, the MSU crystals themselves trigger an acute inflammation attack and extend the duration. The IL-8 concentration in the joint fluid at the time of a gout attack has been determined to range from 5 to 10 times that present in patients with osteoarthritis. Furthermore, MSU crystals activate phospholipase C and phospholipase D in polymorphonuclear neutrophil leukocytes and monocytes, and through the acceleration of tyrosine phosphorylation, result in the production of active oxygen and additional proinflammatory cytokines. It has also been reported that MSU crystals can lead to an increase in phospholipase A_2 activity and activate the biosynthesis of many compounds from arachidonic acid to leukotriene. Finally, MSU crystals have been shown to cause the release of proinflammatory mediators, including cyclooxygenase (COX) and lipoxygenase that generate metabolites of arachidonic acid, and soluble mediators, such as protease in lysosome, bradykinin, and kallikrein from phagocytes, synoviocytes, and other cells, thus perpetuating the inflammation. Inflammatory mediators are physiologically active substances discharged from the cells infiltrating to a damaged organization and area of inflammation and white blood cells (Figure 2.5).
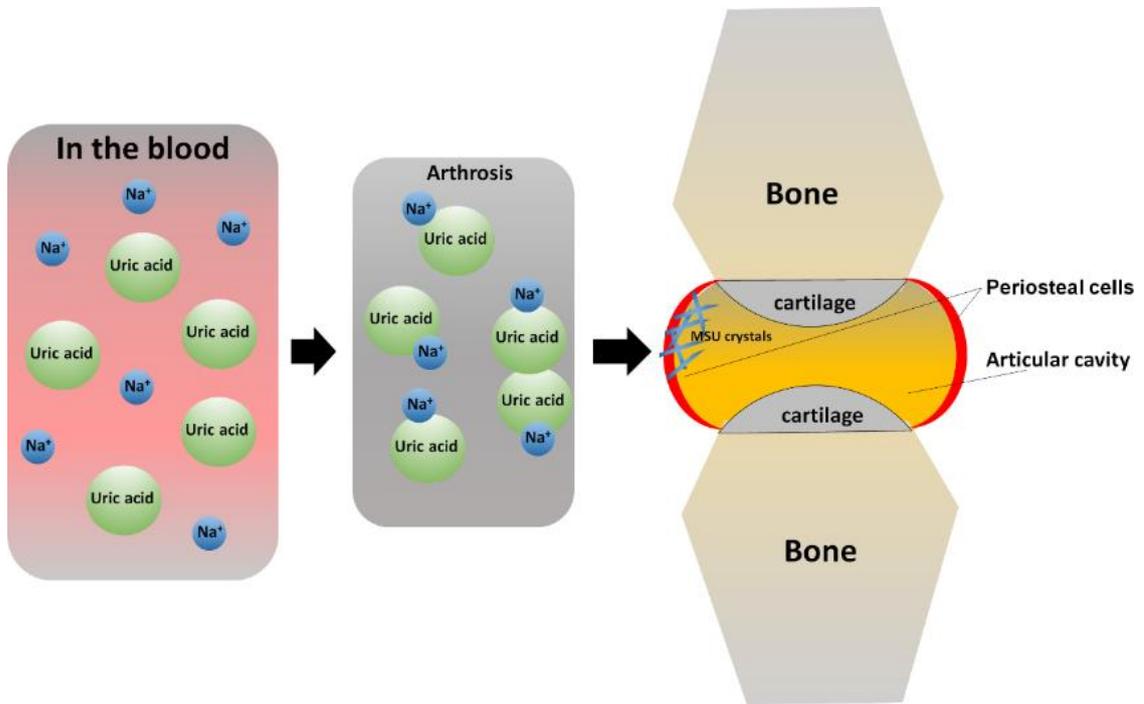
Fig. 2.4. Sideration of gout arthritis by MSU crystals.
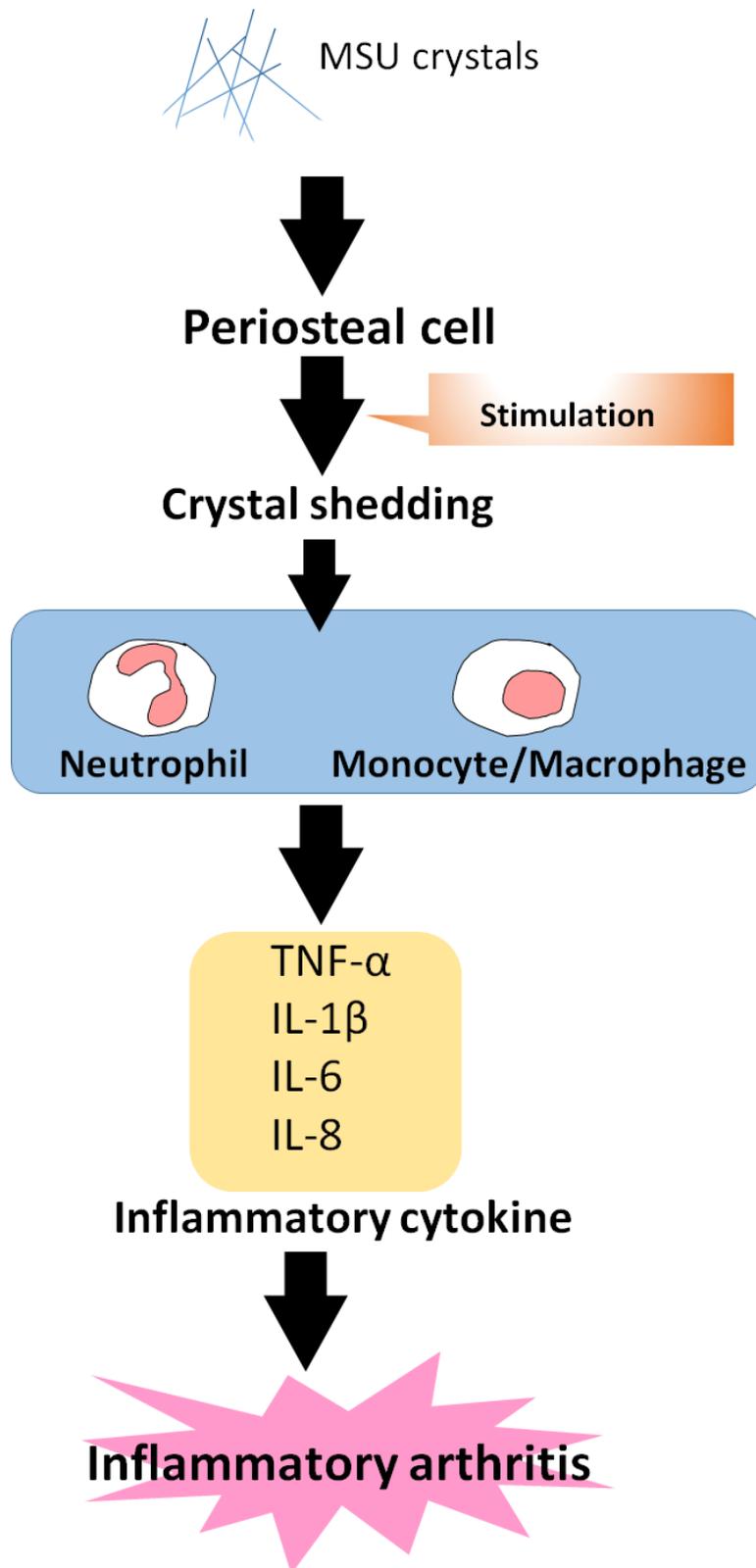
Fig. 2.5. Inflammatory mediators involved in goutly attack.

2.2.5 Diagnostic Approaches for Gout

Various crystals are deposited in joint fluids. Gout is a form of acute arthritis caused by the precipitation of MSU crystals in joints. The treatment for gout arthritis is the control of uric acid levels (measured in the serum) through alimentary and antihyperuricemic treatment. However, gout arthritis can still develop despite the control of serum uric acid levels over a long period of time. Diagnostic methods other than measurement of serum uric acid levels are therefore desired for the estimation of the effects of therapy and the treatment duration. Alternatives include the use of a polarizing microscope, X-ray analysis, dual-energy computed tomography (DECT), magnetic resonance imaging (MRI), and echography [45, 46]. Each of these techniques has certain merits and demerits.

For cases of gout with obvious pathogenesis, which is the presence of MSU crystals, puncturing the joint and collecting synovial fluid to confirm the existence of characteristic MSU crystals by using a polarizing microscope is recommended for a definite diagnosis [47, 48]. However, identifying MSU crystals by puncturing a joint such as the ankle joint in order to collect the synovial fluid can rarely be implemented, because, as mentioned above, the procedure is difficult , requires invasion of the patient, and has proven unsuccessful in as many as 25% of the acute cases[49].

Ultrasonography, on the other hand, is minimally invasive with a low cost and is therefore, widely used for various medical diagnoses. Moreover, the ability to achieve dynamic, multi-planar, and multi-joint evaluations in a short period of time is advantageous; therefore, this technique is expected to see increased use in both clinical and research settings [50-54]. However, the success of an ultrasonography evaluation largely depends on the proficiency of and the procedures followed by the ultrasound examiner and the performance of the device. Furthermore, the field of view is limited. Characteristic signals and contrast patterns for *gouty tophi* have not yet been observed in MRIs [55].

In the case of computed tomography (CT), substance discrimination is performed by determining the CT values, which are dependent on the density of the substance (as the substance density increases, the CT value also increases) [56]. Thus, substances with similar densities cannot be distinguished using CT. For example, it is often the case that hematomas and calcifications have the same CT values.

While the index for material discrimination using DECT is often only the CT value, this method is more multilateral and accurate than normal CT. Component analysis of urinary tract stones, and particularly, the differentiation of uric acid stones

and calcium stones, has been reported using Dual energy CT (DECT). Because DECT is also non-invasive, it is expected to be a leading alternative as an appropriate diagnostic method for gout [57-60]. However, data at two different energies must be collected at the same site; therefore, this method involves increased exposure to X-rays. In addition, the devices are expensive and large; thus, their number is limited. Furthermore, DECT cannot be used for early diagnosis.

Consequently, although a less invasive and more accurate technique for the diagnosis of gout is anticipated, none has yet been established. If small nodules of crystallized MSU can be detected, it may be possible to predict the sites in which crystalline arthritis is likely to occur. It may also be possible to diagnose atypical cases of crystalline arthritis.

2.2.6   Treatment of Gout

It has been clearly demonstrated that hereditary and environmental factors lead to hyperuricemia. However, it is necessary to decrease the serum urate level using drug treatment when hyperuricemia cannot be controlled by removal of negative environmental factors. The antihyperuricemic treatments generally include a uricosuric drug (i.e., benzbromaron and probenecid) to increase the excretion of uric acid and a urate synthesis inhibitor (i.e., allopurinol, an inhibitor of xanthine oxidase) to decrease uric acid production.

These drugs are administered on the basis of the patient's level and type of hyperuricemia. Allopurinol is generally administered to patients with hyperuricemia due to excess production of uric acid, while benzbromaron is preferentially administered to patients suffering from hyperuricemia due to reduced excretion of uric acid [61]. Because allopurinol can lead to side effects, such as elevated concentrations of oxypurinol and allopurinol in the blood, which has been observed in renal failure cases, the dose of allopurinol is carefully monitored with respect to creatinine clearance. Patients taking allopurinol can also suffer from the Stevens–Johnson syndrome, a critical eruption of the mucous membrane of the eye if they have the *HLA-B*5801* genotype, and thus, must be screened prior to the administration of allopurinol. Finally, allopurinol has also been associated with side effects such as leukopenia, congestive hepatopathy, and anaphylaxis [62]. On the other hand, with uricosuric agents including benzbromaron, there is a risk of generating urinary stones due to an increase in the amount of uricotelic acid in the urine [63-66]; therefore, urinary management including the alkalinization of urine is necessary. Consequently, the use of drug treatment to sufficiently lower serum uric acid levels is difficult.

Patients taking uric acid excretion agents often develop urinary tract calculi in the urine due to the relatively high levels of urinary uric acid. Therefore, the administration of allopurinol is often preferable to that of uricosuric drugs. However, for patients who cannot take allopurinol to prevent the overproduction of uric acid due to its side effects, there are no alternative drugs. Thus, there is no truly effective treatment for gout, and this disease remains an unmet medical need.

Reference

[1] T. Higashi, S. Sagawa, N. Ashida and T. Takeuchi, "Orientation of glutaraldehyde-fixed erythrocytes in strong," Bioelectromagnetics, Vol. 17, No. 4, pp. 335 (1996).

[2] T. Higashi, A. Yamagishi, T. Takeuchi and M. Date, "Effects of static magnetic fields of erythrocyte rheology," Bioelectrochem Bioenerg, Vol. 36, No. 2, pp. 101 (1995).

[3] T. Higashi, A. Yamagishi, T. Takeuchi, N. Kawaguchi, S. Sagawa, S. Onishi, and M. Date, "Orientation of erythrocytes in a strong static magnetic field," Blood, Vol. 82, No. 4, pp. 1328 (1993).

[4] M. Murayama, "Orientation of Sickled Erythrocytes in a Magnetic Field," Nature, Vol. 206, pp. 420 (1965).

[5] M. Murayama, "Molecular mechanism of red cell "sickling"," Sience, Vol. 153, pp. 145 (1966).

[6] M. Chabre, "Diamagnetic anisotropy of proteins and magnetic orientation of biological membranes and protein assemblies," Biophysical Effects of Steady Magnetic Fields. Springer-Verlag, New York, pp. 28 (1986).

[9] C. E. Chidsey, L. Takiff, R. A. Goldstein and S.G. Boxer, "Effect of magnetic fields on the triplet state lifetime in photosynthetic reaction centers: Evidence for thermal repopulation of the initial radical pair," Proc. Natl. Acad. Sci. U S A. Vol. 82, No. 20, pp. 6850 (1985).

[10] H. M. Kingma, R. van Grondelle, and L. N. M. Duysens, "Magnetic-field effects in photosynthetic bacteria. I. Magnetic-field-induced bacteriochlorophyll emission changes in the reaction center and the antenna of Rhodospirillum rubrum, Rhodopseudomonas sphaeroides and Prosthecochloris aestuarii," Biochim. Biophys. Acta. Vol. 808, No. 3, pp. 363 (1985).

[11] H. Kingma, R. van Grondelle and L. N. M. Duysens, "Magnetic field effects in photosynthetic bacteria. II. Formation of triplet states in the reaction center and the antenna of Rhodospirillum rubrum and Rhodopseudomonas sphaeroides. Magnetic field effects," Biochim. Biophys. Acta. Vol. 808, pp. 383 (1985).

[12] A. Yamagishi, "Biological systems in high magnetic field," J. Mag. Mag. Mat. Vol. 90&91, pp. 43 (1990).

[13] J. Torbet, J. M. Freyssinet, and G. Hudry-Clergeon, "Oriented fibrin gels formed by polymerization in strong magnetic fields," Nature, Vol. 289, pp. 91, (1981).

[14] A. Yamagishi, T. Takeuchi and M. Date, "Diamagnetic orientation of polymerized molecules under high magnetic field" J. Phys. Soc. Jpn. Vol. 58, pp. 2280 (1989).

[15] M. Iwasaka, "Effects of static magnetic fields on light scattering in red chromatophore of goldfish scale," J. Appl. Phys. Vol. 107, 09B314 (2010).

[16] M. Iwasaka and Y. Mizukawa, "Light reflection control in biogenic micro-mirror by diamagnetic orientation," Langmuir. Vol. 29, pp. 4328 (2013).

[17] M. Iwasaka, Y. Miyashita, Y. Mizukawa, K. Suzuki, T. Toyota, and T. Sugawara, "Biaxial Alignment Control of Guanine Crystals by Diamagnetic Orientation," Appl. Phys. Express, Vol. 6, 037002 (2013).

[18] M. Fujiwara, M. Tamaru, M. Hara, K. Suzuki, and K. Mukai, "Magnetic Orientation of 1,3,5-Triphenyl-6-oxoverdazyl Radical Crystals," J. Phys. Chem. B Vol. 111, pp. 9492 (2007).

[19] M. Fujiwara, M. Fukui, and Y. Tanimoto, "Magnetic Orientation of Benzophenone Crystals in Fields up to 80.0 KOe," J. Phys. Chem. B Vol. 103, pp. 2627 (1999).

[20] T. Kohama, H. Takeuchi, M. Usui, J. Akiyama, M. G. Sung, K. Iwai, and S. Asai, "In-Situ Observation of Crystal Alignment under a Magnetic Field Using X-ray Diffraction," Mater. Trans. Vol. 48, pp. 2867 (2004).

[21] C. Uyeda, R. Takashima, and K. Tanaka, "Origin of diamagnetic anisotropy which induces magnetic rotation of non-magnetic particles,"Appl. Phys. Lett. Vol. 86, 094103 (2005).

[22] C. Wu, S. Li, K. Sassa, Y. Chino, K. Hattori, and S. Asai, "Theoretical Analysis on Crystal Alignment of Feeble Magnetic Materials under High Magnetic Field," Mater. Trans. Vol. 46, pp. 1311 (2005).

[23] T. Kawai, R. Iijima, Y. Yamamoto, and T. Kimura, "Crystal Orientation of N,N'-Dicyclohexyl-2,6-naphthalenedicarboxamide in High Magnetic Field," J. Phys. Chem. B Vol. 105, pp. 8077 (2001).

[24] S. Li, K. Sassa, K. Iwai, and S. Asai, "A Novel Process to Fabricate of Highly Textured Ceramics in a High Magnetic Field," Mater. Trans. Vol. 45, pp. 3124 (2004).

[25] Y. Kawamura, I. Sakurai, A. Ikegami, and S. Iwayanagi, "Magneto-Orientation of Phospholipids," Mol. Cryst. Liq. Cryst. Vol. 67, pp. 77 (1981).

[26] G. Sazaki, E. Yoshida, H. Komatsu, T. Nakada, S. Miyashita, and K. Watanabe, "Effects of a magnetic field on the nucleation and growth of protein crystals、"J. Cryst. Growth. Vol. 173, pp. 231 (1997).

[27] J. F.Nye "Physical Properties of Crystals", Clarendon Press, Oxford (1984).

[28] S. Asai "Electromagnetic Processing of Materials", Springer (2012).

[29] T. Kimura, "Study on the Effect of Magnetic Fields on Polymeric Materials and Its Application" Polym. J. Vol. 35, pp. 823 (2003).

[30] S. Tsukui and T. Kimura "Magnetic Alignment of Magnetically Biaxial Diamagnetic Rods under Rotating Magnetic Fields" Jpn. J. Appl. Phys. Vol. 51, 057301 (2012)

[31] K. R. Maples and R. P. Mason, "Free radical metabolite of uric acid." J. Biol. Chem. Vol. 263, No. 4, pp. 1709 (1988).

[32] M. Hosoyamada, "Transporter" Hyperuricemia and gout, Vol. 18, No. 1 pp. 1 (2010).

[33] P. A. Simkin, "The pathogenesis of podagra,"Ann. Intern. Med. Vol. 86, pp. 230 (1977).

[34] N. Dalbeth, R. Kalluru, O. Aati, A. Horne, A. J. Doyle and F. M. McQueen,"Tendon

involvement ill the feet of patients with gout : a dual-energy CT study" Ann. Rheum. Dis. Vol. 72, pp. 1545 (2013).

[35] E. W. Campion, R. J. Glynn, L. O. DeLabry, "Asymptomatic hyperuricernia. Risks and consequences in the Normative Aging Study" Am. J. Med. Vol. 82, pp. 421 (1987).

[36] K. C. Lin, H. Y. Lin, and P. Chou, "The interaction between uric acid level and other risk factors on the development of gout among asymptomatic hyperuricemic men in a prospective study" J. Rheumatol. Vol. 27, pp. 1501 (2000).

[37] E. Pascual, E. Batlle-Gualda, A. Martinez, J. Rosas and P. Vela, "Synovial fluid analysis for diagnosis of intercritical gout" Ann. Intern. Med. Vol. 131, pp. 756 (1999).

[38] C. M. Burns and R. L. Wortrnann,"Latest evidence on gout management : what the clinician needs to know." Ther. Adv. Chronic. Dis. Vol. 3, pp. 271 (2012).

[39] J. G. Puig, E. de Miguel and M. C. Castillo, A. L. Rocha, M. A. Martínez and R. J. Torres,"Asymptomatic hyperuricemia: impact of ultrasonography." Nucleosides Nucleotides Nucleic Acids. Vol. 27, pp. 592 (2008).

[40] C. Pineda, L. M. Amezcua-Guerra, C. Solano, P. Rodriguez-Henríquez, C. Hernández-Díaz, A. Vargas, F. Hofmann and M. Gutiérrez. "Joint and tendon subclinical involvement suggestive of gouty arthritis in asymptomatic hyperuricemia : an ultrasound controlled study" Arthritis. Res. Ther. Vol. 13, pp. R4 (2011).

[41] J. Li-Yu, G. Clayburne, M. Sieck, A. Beutler, M. Rull, E. Eisner and H. R. Jr. Schumacher, "Treatment of chronic gout. Can we determine when urate stores are depleted enough to prevent attacks of gout?" J. Rheumatol. Vol. 28, pp. 577 (2001).

[42] E. Pascual and F. Sivera,"Time required for disappearance of urate crystals from synovial fluid after successful hypouricaemic treatment relates to the duration of gout" Ann. Rheum. Dis. Vol. 66, pp. 1056 (2007).

[43] J. S. Bomalaski, G. Lluberas and H. R. Jr Schumacher," Monosodium urate crystals in the knee joints of patients with asymptomatic nontophaceous gout" Arthritis. Rheum. Vol. 29, pp. 1480 (1986).

[44] A. Weinberger, H. R. Schumache and C. A. Agudelo, "Urate crystals in asymptomatic metatarsophalangeal joints" Ann. Intern. Med. Vol. 91, pp. 56 (1979).

[45] F. M. McQueen, A. Doyle, and N. Dalbeth, "Imaging in gout what can we learn from MRI, CT, DECT and US? " Arthritis. Res. Ther. Vol. l3 pp. 246 (2011).

[46] N. Dalbeth, A. Doyle, and F. M. McQueen, "Imaging in gout; Insights into the pathological features of disease" Curr. Opin. Rheumatol. Vol. 24, pp. 132 (2012).

[47] H. R. Schumacher and A.J. Reginato,"Atlas of Synovial Fluid Analysis and Crystal Identification" Philadelphia, Lea & Febiger, (1991).

[48] A. Malik, H. R. Schumacher, J. E. Dinnella and G. M. Clayburne, "Clinical diagnostic criteria

for gout; Comparison with the gold standard of synovial fluid crystal analysis" J. Clin. Rheumatol. Vol. l5, pp. 22 (2009).

[49] A. Swan, H. Amer, and P. Dieppe, "The value of synovial fluid assays in the diagnosis of joint disease: A literature survey" Ann. Rheum. Dis. Vol. 61, pp. 493 (2002).

[50] R. G. Thiele and N. Schlesingcr, "Ultrasonography shows disappearance of monosodium urate crystal deposition on hyaline cartilage after sustained normouricermia is achieved" Rheumatol. Int. Vol. 30, pp. 495 (2010).

[51] W. Grassi, G. Meenagh, E. Pascual and E. Filippucci, "'Crystal clear: sonographic assessment of gout and calcium pyrophosphate deposition disease" Semin. Arthruis. Rheum. Vol. 36, pp. 197 (2006).

[52] R. G. Thiele and N. Schlesinger," Diagnosis of gout by ultrasound" Rheumatology. Vol. 46, pp. 1116 (2007).

[53] S. A. Wright, E. Fihppucci, C. McVeigh, A. Grey, M. McCarron, W. Grassi, G. D. Wright and A. J. Taggart, "High-resolution ultrasonography of the first metatarsal phalangeal joint in gout? A controlled study" Ann. Rheum. Dis. Vol. 66, pp. 859 (2007).

[54] C. Schueller-Weidekamm, G. Schueller, M. Aringer, M. Weber and F. Kainberger, "Impact of sonography in gouty arthritis; Comparison with conventional radiography, clinical examination, and laboratory findings," Eur. J. Radiol. Vol. 62, pp. 437 (2007).

[55] J. S. Yu, C. Chung, M. Recht, T. Dailiana and R. Jurdi, "MR imaging of tophaceous gout" American Journal of Roentgenology." Vol. 168, pp. 523 (1997).

[56] J. C. Gerster, M. Landry, L. Dufresne and J. Y. Meuwly,"Imaging of tophaceous gout: computed tomography provides specific images compared with magnetic resonance imaging and ultrasonography", Ann. Rheum. Dis. Vol. 61, pp. 52 (2002)

[57] N. M. Kulkarni, B. H. Eisner, D. F. Pinho, M. C. Joshi, A. R. Kambadakone, D. V. Sahani, "Determination of renal stone composition in phantom and patients using single-source dua1-energy computedtomography" J. Comput. Assist. Tomogr. Vol. 37, pp. 37 (2013).

[58] M. A. Desai, J. J. Peterson, H. W. Garner, H. W. Garner, and , J. M. Kransdorf, "Clinical utility of dual-energy CT for evaluation of tophaceous gout" Radiographics. Vol. 31, pp. 1365 (2011).

[59] K. N. Glazebrook, L. S. Guimaraes, N.S. Murthy, D. F. Black, T. Bongartz, N. J. Manek, S. Leng, J. G. Fletcher and C. H. McCollough, "Identification of intra articular and perarticular uric acid crystals with dual-energy CT: Initial evaluation" Radiology. Vol. 261, pp. 516 (2011).

[60] H. K. Choi, A. M. Al-Arfaj, A. Eftekhari, P. L. Munk, K. Shojania, G. Reid and S. Nicolaou, "Dual energy computed tomography in tophaceous gout" Ann. Rheum Dis. Vol. 68, pp. 1609 (2009).

[61] H. Okabe, T. Hosoya, M. Hikita, M. Saji, K. Ichida, and I. Ohno "Analysis of urolithiasis in patients with gout and hyperuricemia using ultrasonography" Jpn. J. Rheumatol. Vol. 9, pp. 239 (1999).

[62] F. Perez-Ruiz, P. Gomez-Ullate, J. J. Amenabar, S. Zarraga, M. Calabozo, A. M. Herrero-Beites and J. M. Nolla, "Long-term efficacy of hyperuricaemia treatment in renal transplant patients" Nephrol. Dial. Transplant. Vol. 18, pp. 603 (2003).

[63] S. I. Hung, W. H. Chung, L. B. Liou, C. C. Chu, M. Lin, H. P. Huang, Y. L. Lin, J. L. Lan, L. C. Yang, H. S. Hong, M. J. Chen, P. C. Lai, M. S. Wu, C. Y. Chu, K. H. Wang, C. H. Chen, C. S. Fann, J. Y. Wu and Y. T. Chen, "HLA-B"5801 allele as a genetic marker for severe cutaneous adverse reactions caused by allopurinol" Proc. Natl. Acad. Sci. USA. Vol. 102, pp. 4134 (2005).

[64] N. Kaniwa, Y. Saito, M. Aihara, K. Matsunaga, M. Tohkin, K. Kurose, J. Sawada, H. Furuya, Y. Takahashi, M. Muramatsu, S. Kinoshita, M. Abe, H. Ikeda, M. Kashiwagi, Y. Song, M. Ueta, C. Sotozono, Z. Ikezawa, and R. Hasegawa; JSAR research group, " HLA-B locus in Japanese patients with antiepileptics and allopurinol-related Stevens-Johnson syndrome and toxic epidermal necrolysis" Pharmaco-genomics. Vol. 9, pp. 1617 (2008).

[65] C. Lonjou, N. Borot, P. Sekula, N. Ledger, L. Thomas, S. Halevy, L. Naldi, J. N. Bouwes-Bavinck , A. Sidoroff, C. de. Toma, M. Schumacher, J. C. Roujeau, A. Hovnanian and M. Mockenhaupt; RegiSCAR study group, "A European study of HLA-B in Stevens-Johnson syndrome and toxic epidermal necrolysis related to five high-risk drugs" Pharmacogenet Genomics. Vol. 18, pp. 99 (2008).

[66] K. R. Hande, R. M. Noone and W. J. Stone, "Severe allopurinol toxicity; Description and guidelines for prevention in patients with renal insufficiency"Am. J. Med. Vol. 76, pp. 47 (1984).

3

Two-Stage Magnetic Orientation of Uric Acid Crystals

3.1 Introduction

In recent years, it has been shown that approximately one of every seven men is ailing from urinary tract stone disease [1]. Urine is produced by the kidneys and passed through the ureters. It is then discharged through the urethra into the bladder and accumulates. These components make up the urinary tract. Urinary calculus is a disease that involves the formation of calculi in the urinary tract. Urinary tract calculi are classified as upper urethra lithiasis and lower urethra lithiasis, the latter of which is the formation of calculi in the bladder and urethra. Of the people that have a urinary tract calculus, 95% suffer from upper urethra lithiasis. Urinary tract calculi are also classified by their ingredients, which include calcium oxalate, calcium phosphate, uric acid, and cystine. The focus of our research has been on uric acid crystals. It is well known that urinary calculi have a large impact on the development of gout [2-5]. Both gout and hyperuricemia, which are diseases associated with eating habits, are related to the formation of urinary calculi [6-8]. While a therapeutic agent that acts as a uric acid excretion stimulator has been developed, to improve the quality of life of patients suffering from gout, another approach for controlling the formation of uric acid crystals needs to be developed.

3.2 Experiment Section

3.2.1 Materials

Uric acid ($C_5H_4N_4O_3$) is an organic compound with a molecular weight of 168.11, and it is a tasteless and odorless white solid at room temperature (Figure 3.1(a)). It has maximum absorption at a wavelength of about 292 nm. X-ray diffraction analysis of uric acid revealed that it adopts a monoclinic crystal structure with unit cell dimensions of $a = 14.464$ Å, $b = 7.403$ Å, $c = 6.208$ Å, and $\beta = 65.10°$ [9, 10]. Growth in the (100) plane of the crystal was investigated in real time using atomic force microscopy [9, 10]. The crystals grow in layers on the (100) plane, but initially extended in a spiral and then grow in a uniform direction (Figure 3.1(b)). Each layer consists of parallel ribbons of uric acid molecules hydrogen bonded head-head and tail-tail, with the ribbon plane perpendicular to the bc plane. The ribbons in adjacent layers are hydrogen bonded and offset by ~62° (Figure 3.2). There is no hydrogen bonding between ribbons within a layer [11].

Uric acid is poorly soluble in both water and organic solvents (polar and nonpolar) under neutral conditions. The oxypurine structure of uric acid is thought to be the cause of its poor water solubility. The solubility decreases when the hydroxyl groups in the α- and γ-positions of the purine ring are substituted. Uric acid adopts the enol form in aqueous solution because of tautomerism. The value of pK_{a1} (8-OH) is 5.6 and that of pK_{a2} (2-OH) is 10.3. Therefore, uric acid is present as a basic anion at the 8-position (enolic hydroxyl group) under physiological conditions at pH 7.4 [12].
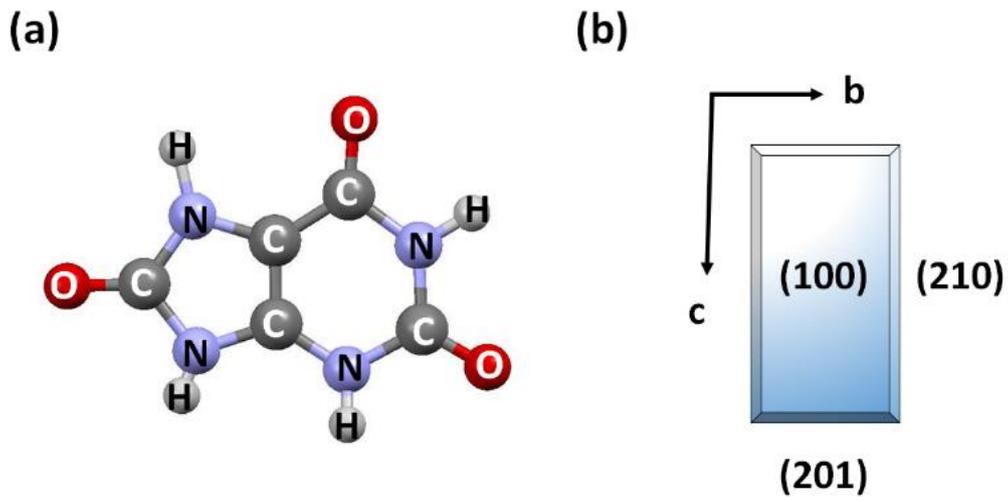
Fig. 3.1. (a) Diagram of Uric acid molecule. (b) Schematic of uric acid crystal.
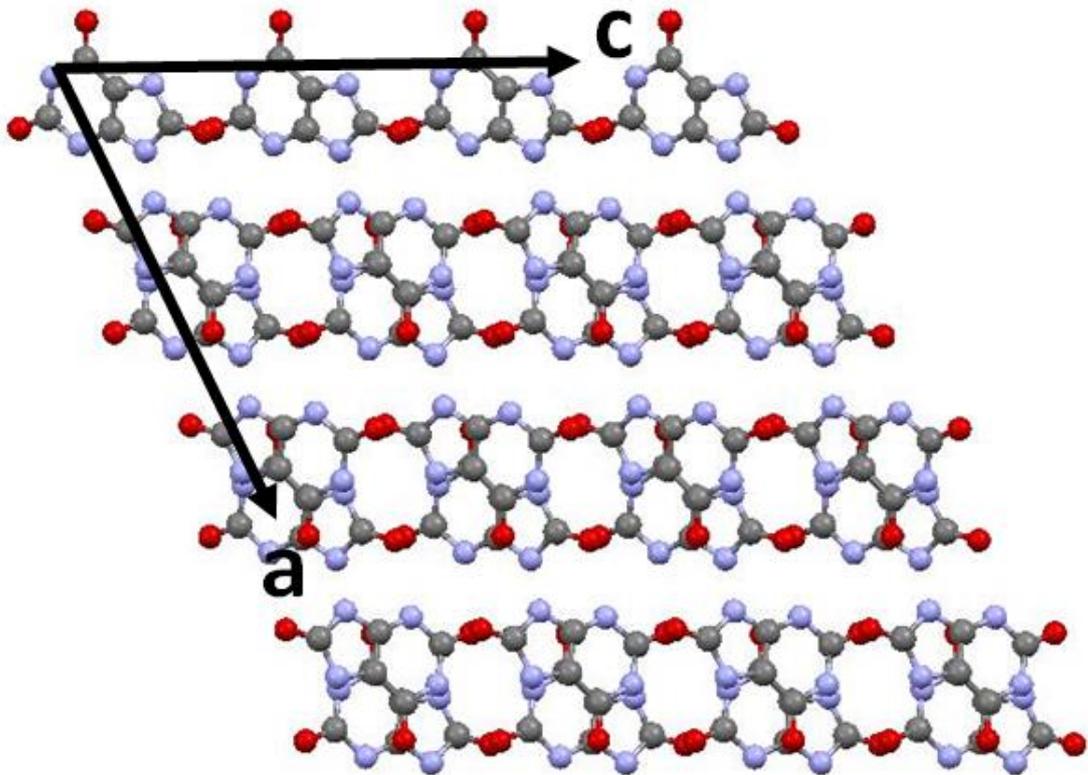
Fig. 3.2. Crystal structures of uric acid.

Uric acid powder (216-00222, 98% purity, 10 mg, Wako, Osaka, Japan) was completely dissolved in an aqueous solution of sodium hydroxide (0.075 mol/L, 5.0 mL), and then hydrochloric acid (2.88 mol/L, 1.3 mL) was added to precipitate uric acid crystals in the bottom of the incubation tube upon neutralization, as shown in Figure 3.3. The crystals were rectangular in shape. In the bottom of the two cover glass and microchamber gaps space (580 micron height) used in microscopic observation, the uric acid crystal that almost precipitated was observed by gravity. The crystals that are substantially adjacent on the bottom of cover glass, or the crystals that are slightly floating because of the influence of Brownian motion were observed.

(a)   **(b)**
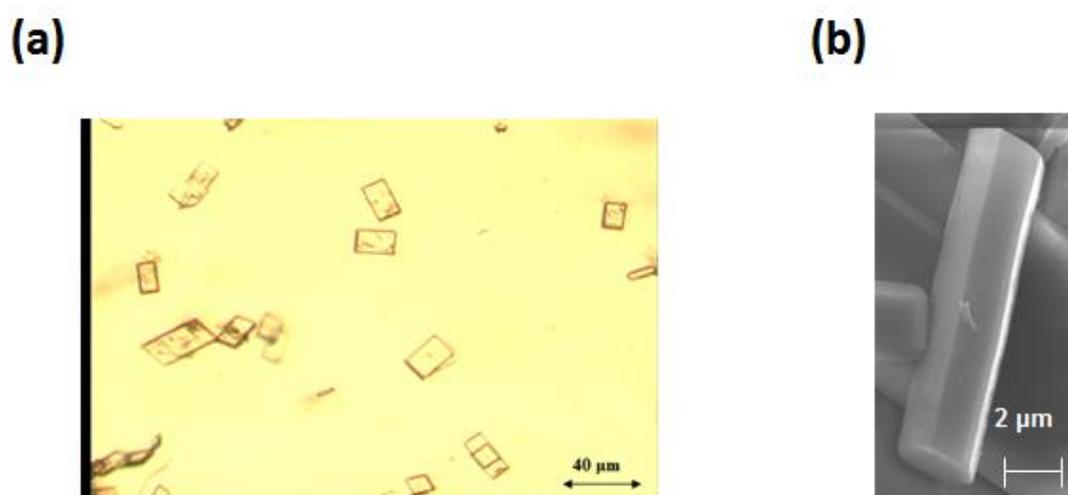
Fig. 3.3. (a) A microscope image of uric acid crystals. (b) A scanning electron microscope image of a uric acid crystal.

3.2.2   Measurements

Charge-coupled device camera observations

The obtained crystals were transferred to a microchamber (9 mm × 9 mm, 0.3 mm thick) with a cover glass window (18 mm × 18 mm, 0.12–0.17 mm thick). The microchamber was positioned in a charge-coupled device (CCD) microscope, which was then placed in an electromagnet (resistive type, 50 mm between magnetic poles; Hayama Co. Ltd., Fukushima, Japan), as shown in Figure 3.4(a) and (b), to observe the dynamic motion of the uric acid crystals. The reasons the samples were sealed with cover glass and microchamber is the solution is not dried. Magnetic fields of up to 500 mT were generated by the electromagnet. The magnetic field was generated within 1 s. Images of the crystals were recorded on an MPEG-2 recorder, and the obtained static images were analyzed with capture and analysis software (Image-J).

.

Reflected light intensity measurements

Figure 3.4(c) shows the configuration for the measurement of reflected light. Spectroscopic measurement of the reflected light was carried out in a fiber-optic measurement system. The magnetic field was generated by an electromagnet (Figure 3.4(b)). The obtained white uric acid crystal suspension was transferred to a quartz cell ($1.0 \times 1.0 \times 4.5$ mm^3). The light source used was a halogen lamp, which provided a continuous stream of light. The magnetic field, light source, and fiber-optic measurement system were orthogonal.

(a)

Cover glass

18 mm

18 mm

0.12-0.17 mm

0.3 mm

9 mm

9 mm

Chamber

0.12-0.17 mm

Sample

(b)

Magnetic field

Light

Electromagnet

Sample

CCD microscope

PC

(c)

Light

Quartz cell

Magnetic field

Detected fiber
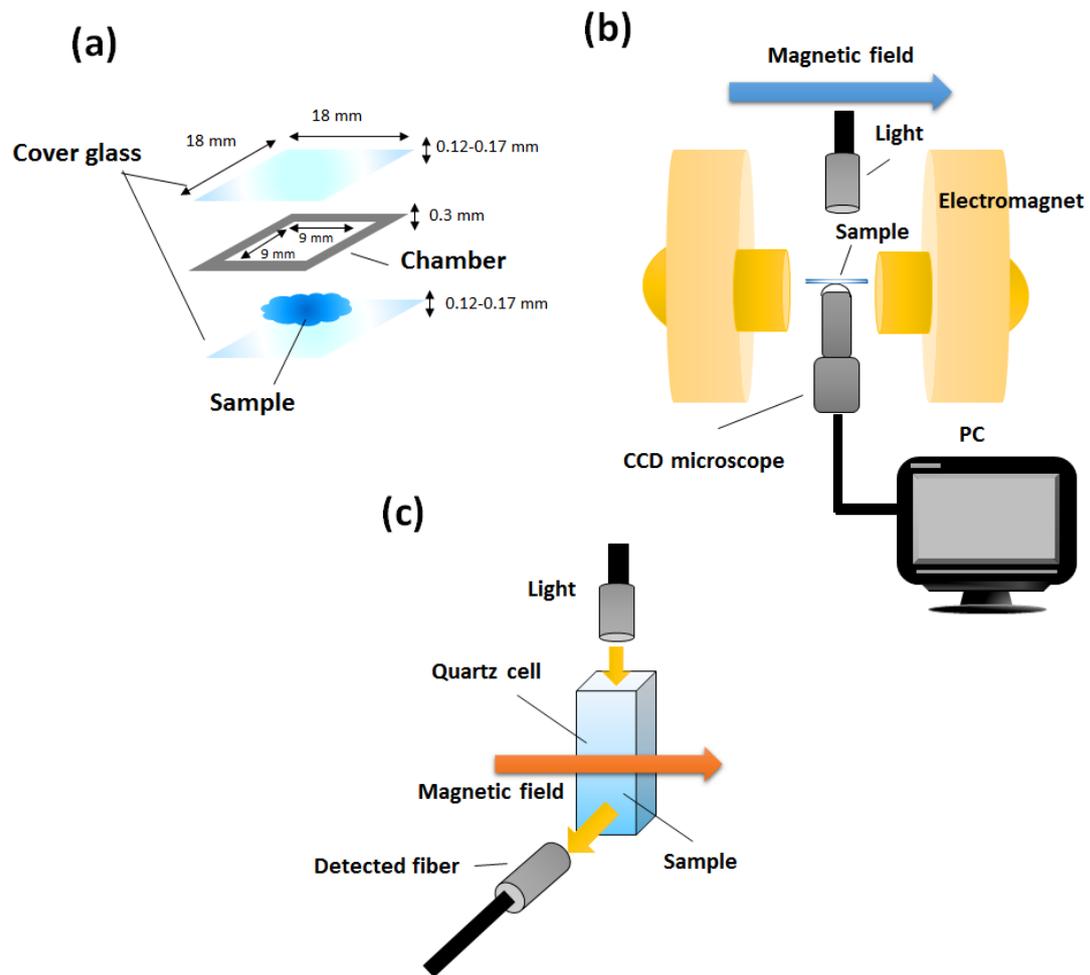
Sample

Fig. 3.4. Experimental system. (a) The configuration of the sample. (b) Observed experimental system under magnetic field. (c) The experimental system in the measurement of the reflected light intensity.

3.3   Results and Discussion

3.3.1   Two-stage Magnetic Orientation Observed by CCD Camera Observation

Figure 3.5 shows photographs of the uric acid crystals and the change of angular velocity both with and without a static magnetic field of several hundred millitesla. The X and Y axes are defined as the directions parallel and perpendicular to the magnetic field, respectively. The Z axis is the direction of observation, and is perpendicular to the magnetic field. The observed crystals showed two stages of orientation. In the first stage, the length (morphological long axis) of the crystal rotated around the Z axis with an angular velocity of ω_z, and consequently the length was perpendicular to the magnetic field. The second stage of magnetic rotation occurred around the Y axis with an angular velocity of ω_y, which caused the morphologically largest surface of the crystal to be oriented perpendicular to the magnetic field. As the magnetic field increased, the duration of rotation shortened and rapid rotation of the crystals was observed. These phenomena occurred between 200 and 500 mT. When the magnetic field was 130 mT, the crystal rotated around the Z axis with an angular velocity ω_z and was oriented perpendicular to the magnetic field, but a second magnetic rotation did not occur. This suggests that there was an insufficient amount of energy for the second rotation for this sized crystal. The crystal showed no movement in the absence of a magnetic field. After turning off the magnetic field, the relaxation process of the orientation takes place due to thermal agitation of the crystal, interaction of surrounding solution and a Brownian motion. For example, in the ferromagnet, magnetic moment orientation is likely kept even after the magnetic field disappears, but in the diamagnetic material, after the magnetic field disappears, it advances to a random orientation because the induced magnetism moment disappears.

Figure 3.6 shows the relationship between the magnetic field and the angular velocity in uric acid crystals with an area of 1000 mm^2. The applied magnetic field was changed between 130 and 500 mT. As mentioned above, the angular velocity increased as the strength of the magnetic field increased, and tended to saturate in the vicinity of 400 mT. Figure 3.7 shows how the ω_z and ω_y angular velocities were determined.

The uric acid molecule is diamagnetic and the uric acid crystal does not contain paramagnetic or strong magnetic species. Thus, it is possible to conclude that the orientation of the crystal was induced by the diamagnetic anisotropies in the recrystallized uric acid. The speed of diamagnetic rotation decreased when the maximum strength of the magnetic field decreased.
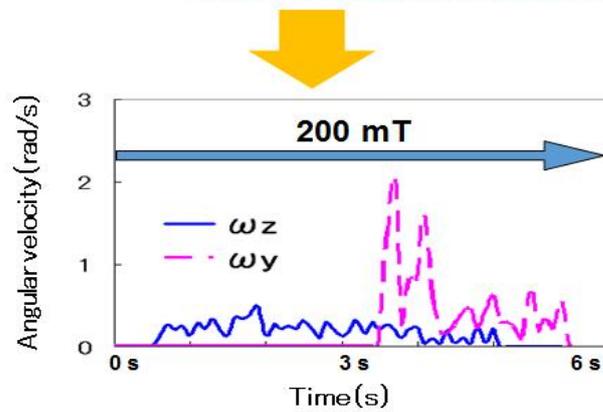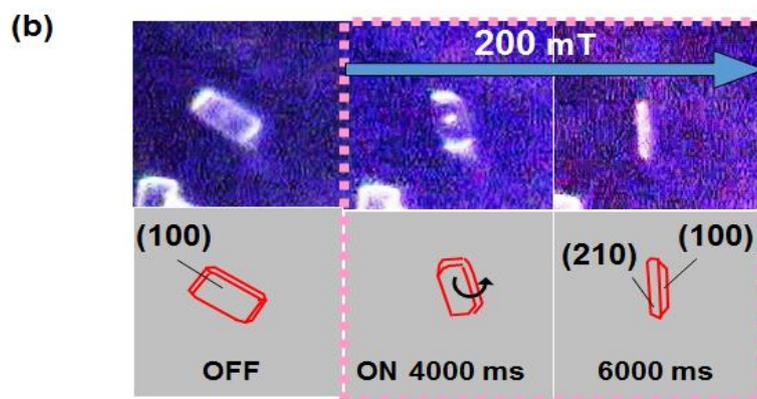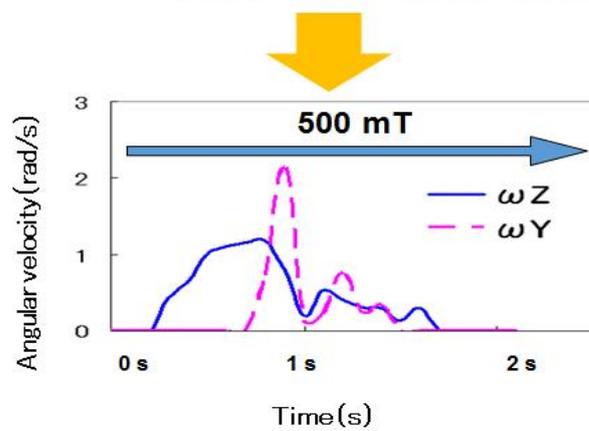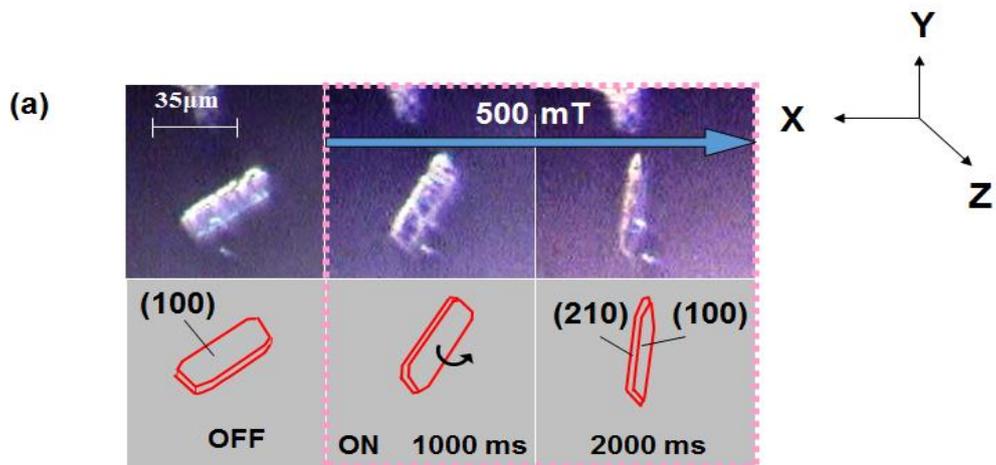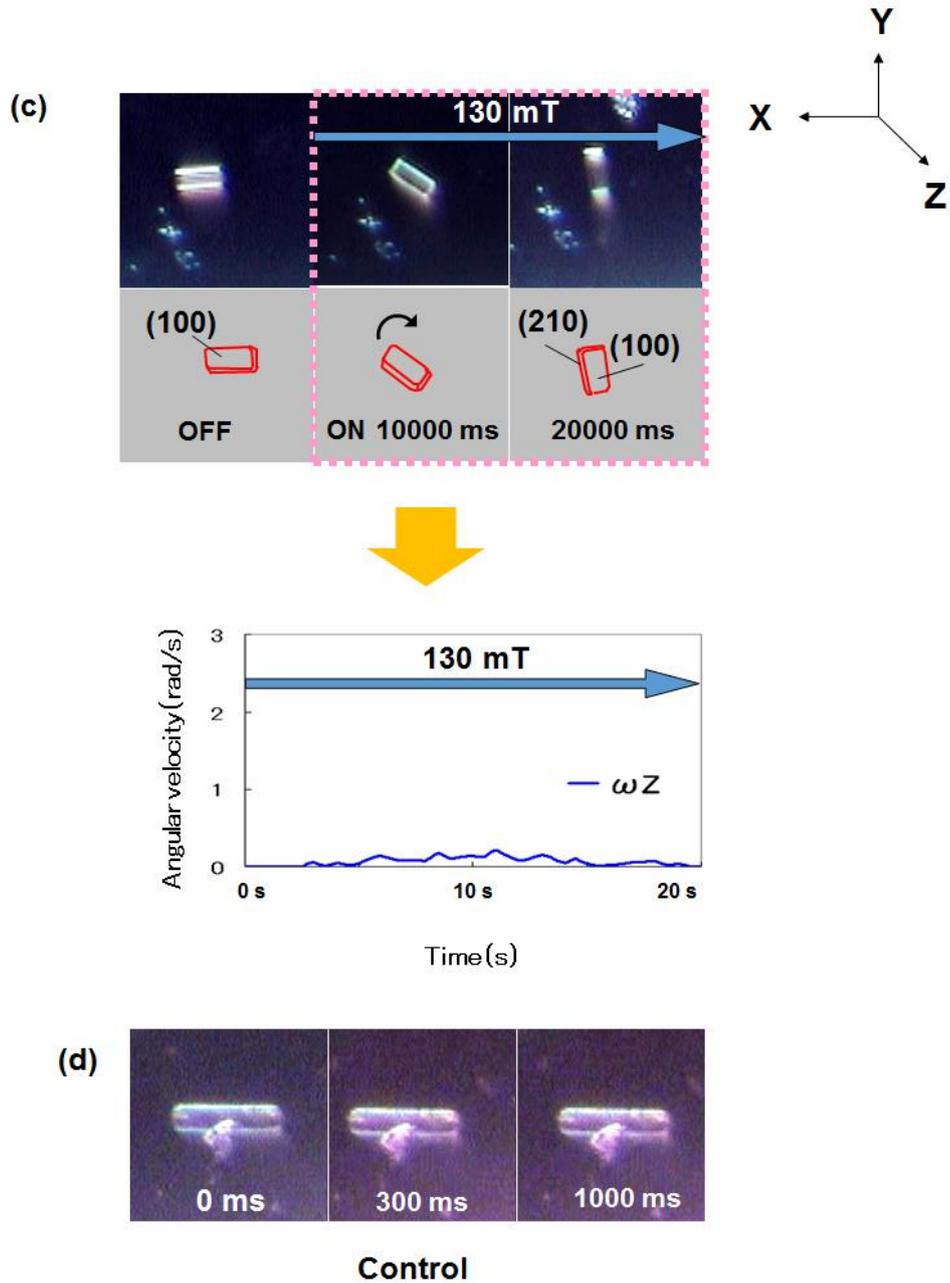
Fig. 3.5. (a)-(c) Microscopic images showing the two stages of magnetic orientation of uric acid crystals under magnetic fields of several hundreds of mT. The graphs show the change in angular velocity over time after the magnetic field is applied. The solid line is the angular velocity of a uric acid crystal around its Z-axis. The dotted line is the angular velocity around the Y-axis. (d) Microscopic images of uric acid crystals not exposed to a magnetic field.
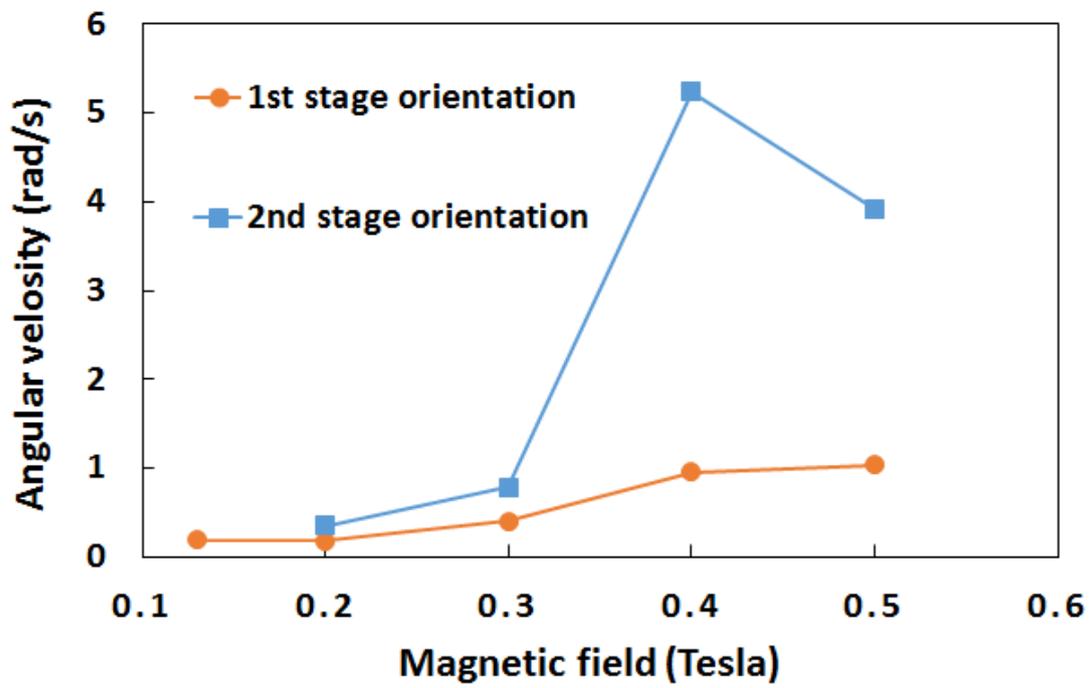
Fig. 3.6. Magnetic field dependence on the angular velocity of the uric acid crystals.
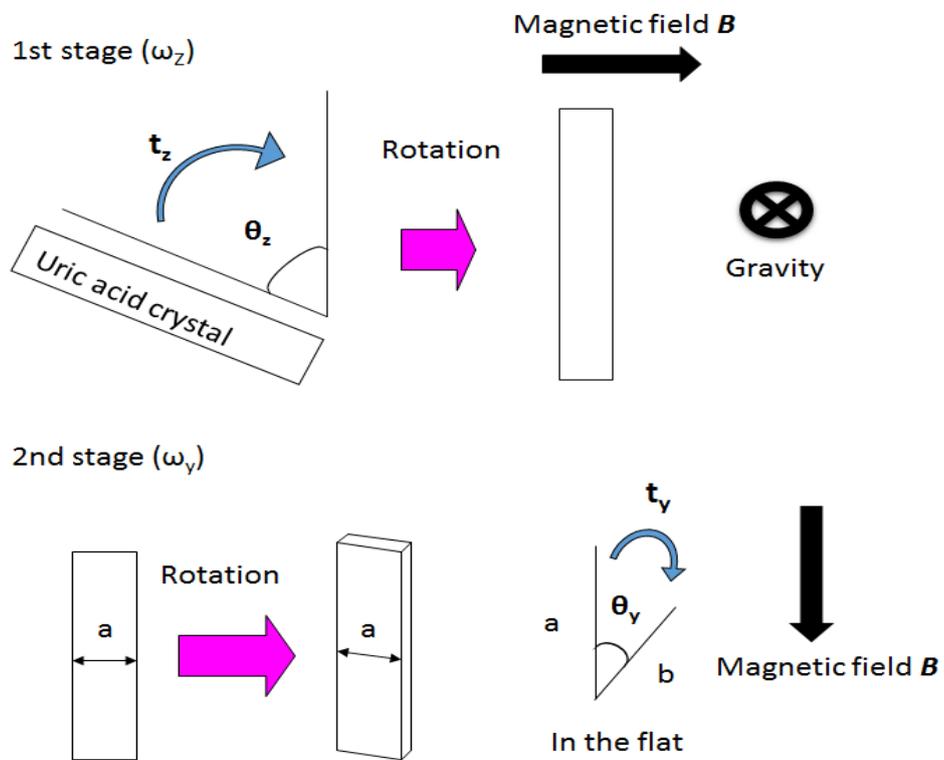
Fig. 3.7. Method of calculating the angular velocity.

Figure 3.8(a) shows the relationship between the angular velocity of the diamagnetically rotating crystals and the area of the largest surface of the crystal for applied magnetic fields of up to 300 mT. The angular velocity clearly increased as the area of the largest surface of the uric acid crystal decreased. These results indicate that the orientational speed of the crystal was negatively correlated with the surface area of the largest face of the crystal. In other words, the orientational speed increases as the average moment of inertia decreases.

Figure 3.8(b) shows the relationship between the angular velocity and the aspect ratio of the diamagnetically rotating crystals for an applied magnetic field of up to 300 mT. The aspect ratio was calculated by measuring the length and width of the largest surface of a crystal, whose area was between 800 and 1100 μm^2. The angular velocity of diamagnetic rotation clearly increased with decreasing aspect ratio. This indicates that a thinner crystal shape results in faster angular velocity, and the crystal shape definitely has an effect on the angular velocity.
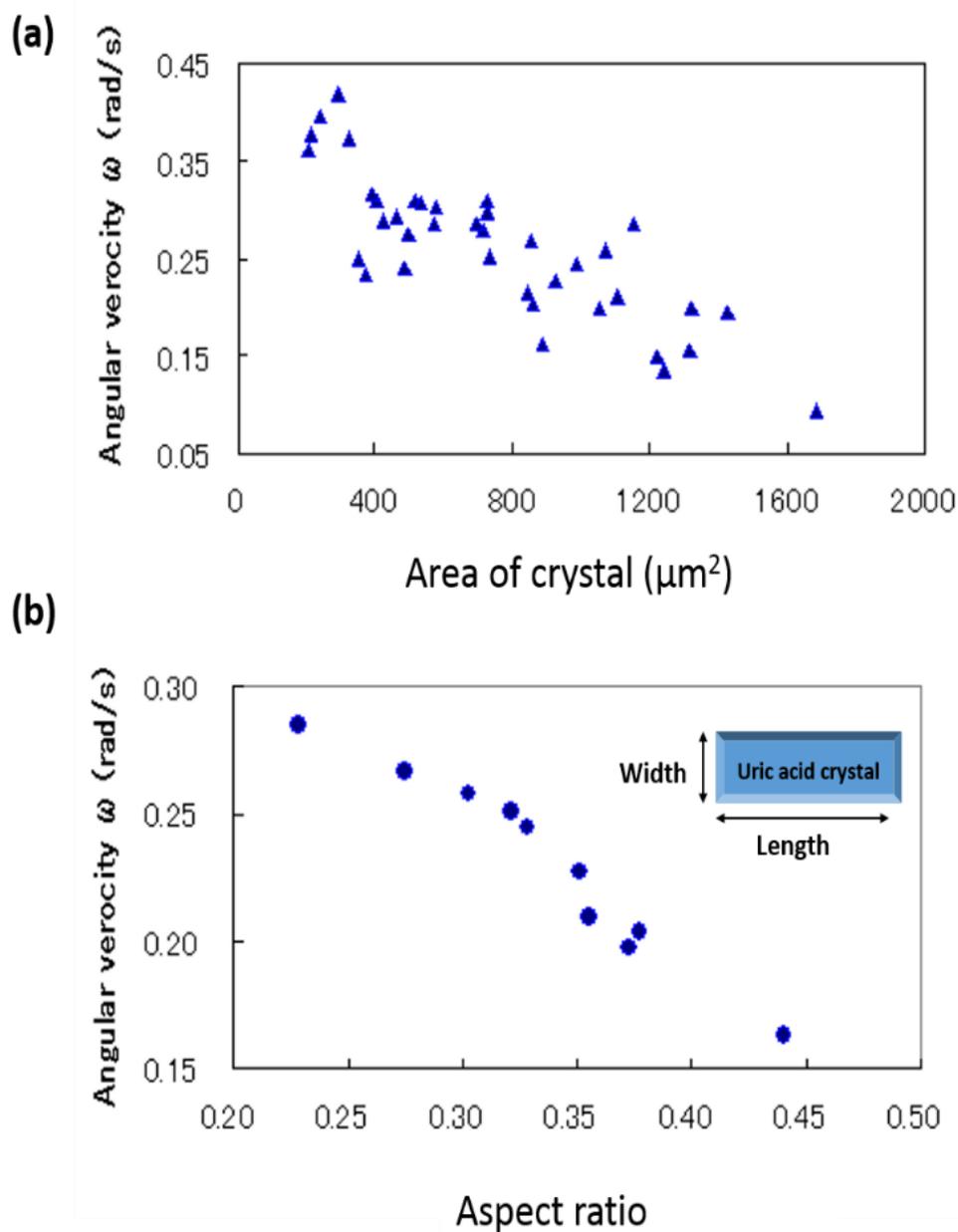
Fig. 3.8. (a) Dependence of angular velocity of the area of each uric acid crystal diamagnetically rotating around an applied magnetic field of 300 mT. (b) Dependence of angular velocity on the aspect ratio of uric acid crystals diamagnetically rotating around an applied magnetic fields at 300 mT.

45

3.3.2 The Calculation of the Magnetic Susceptibility Anisotropy

Research of magnetic susceptibility of monocrystalline which indicates diamagnetism has revealed remarkable anisotropy effect in aromatic compound. With the assumption of a principal value of molecular susceptibility tensor as κ, perpendicular susceptibility on a molecular surface as κ_3 and inside molecule as κ_1 or κ_2, κ_3 obviously becomes more negative than κ_1 or κ_2 in aromatic compound.

L.Pauling explained peculiar anisotropy seen in diamagnetic susceptibility of aroma molecule. He assumed that six-πelectrons of benzene were not localized but form "Ring Current". The vibration frequency of the electron that circulates around benzene intramolecular is assumed to be *v*. Then, the size of "Ring Current" which form six-πelectrons becomes $i=-6ev=-6e\ (\omega/2\pi)$. If a benzene molecule is placed on a magnetic field ***B*** perpendicular to a magnetic field, ω increments by $\Delta\omega$. $\Delta\omega$ can be formulated as follows.

$$\Delta\omega=eH/2m. \tag{3.1}$$

Therefore,

$$\Delta i=-3e^2H/2\pi m. \tag{3.2}$$

As the magnetic moment generated by closed ring current equals M=iF, Δi is assigned. He assumed F=$a^2\pi$ and analyzed [13,14] the anisotropy of the diamagnetic susceptibility of aromatic molecules and obtained the diamagnetic anisotropy of molar benzene as -49.4×10^{-6} cm^3 mol^{-1} based on the following equation:

$$\Delta\kappa = -\frac{3e^2a^2}{2m}, \tag{3.3}$$

where *e* is the elementary charge, *a* is the distance between two carbon atoms, and *m* is the mass of an electron. In the case of a five-membered ring compound, $\Delta\kappa$ is calculated to be -14.2×10^{-6} cm^3 mol^{-1}. The molar diamagnetic anisotropy of a uric acid molecule is estimated to be -63.6×10^{-6} cm^3 mol^{-1}, because it contains both six- and five-membered rings.

The anisotropy of volumetric susceptibility $\Delta\chi$ is given by $\Delta\chi=\Delta\kappa\rho/M$, where ρ

is density and M is molar mass. $\Delta\chi$ is calculated to be -3.7×10^{-7}. The diamagnetic anisotropic energy ΔE can be estimated using the following equation:

$$\Delta E = -\frac{\Delta\chi V B^2}{2\mu_0} \, , \tag{3.4}$$

where V is the volume of the crystal, and μ_0 is magnetic permeability in a vacuum. We calculated the average volume of uric acid crystals as 1.9×10^{-10} cm^3 based on the length and width of each crystal on its broadest surface and thickness, which were determined from the images of rotating crystals under magnetic fields of more than 200 mT. The thickness was measured using images of completely aligned crystals. ΔE of the crystals at 130 and 200 mT using the averaged volume is 6.3×10^{-11} and 1.4×10^{-10} erg, respectively. ΔE at 200 mT is therefore about 10^4 times larger than the thermal energy kT at 300 K, which is 4.14×10^{-14} erg. It is speculated that the constraint factors such as the viscosity of the surrounding water and friction with the glass surface limit the velocity of diamagnetic rotation of the crystals, and consequently only the one-stage rotation occurred at 130 mT.

3.3.3 *Reflected Light Intensity Changes*

We measured the change in reflected light intensity for a suspension of floating uric acid crystals to verify the magnetic orientation. The reflected light intensity was continuously measured both with and without applied magnetic fields of several hundred millitesla, as shown in Figure 3.9(a)–(c). The changes in light intensity were detected using a spectrometer. The wavelength was measured as the average between 500 and 700 nm.

The reflected light was measured in three orthogonal directions and the magnetic field direction was fixed, as shown Figure 3.9(a)–(c). The light direction is the *X* axis, and the magnetic direction is the *Y* axis. The reflected light intensity decreased with an applied magnetic field of 500 mT when the observation direction was the *Z* axis, and the reflected light intensity increased with the magnetic field off in Figure 3.9(a). The reflected light intensity decreased with an applied magnetic field of 500 mT when the observation direction was the *Y* axis (i.e., the magnetic and observation directions were parallel) in Figure 3.9(b). The reflected light intensity decreased with an applied magnetic field of 500 mT when the observation direction was the *X* axis (i.e., the light and observation directions were parallel.) in Figure 3.9(c). The reason why the reflected light intensity decreased is considered to be because the reflecting surface was not facing the light direction because of magnetic orientation. It is suggested that the reflecting surface is the (100) plane, which is a largest surface. Therefore, the light direction was not parallel to the *a* axis of the crystal (Figure 3.10).

Next, we measured the reflected light intensity when changing the light direction. The reflected light intensity increased when a magnetic field of 500 mT was applied and the observation, magnetic, and light directions were parallel, and the reflected light intensity decreased with no magnetic field in Figure 3.11. The change is small compared with Figure 3.9(a)–(c) because a mirror was attached to the detector and optical fiber of the experiment system structure. The reason why the light intensity increased is considered to be that the reflecting surface faced the light direction because of magnetic orientation. This indicates that the (100) plane of the crystal was parallel to the magnetic field direction (Figure 3.12). By changing the combination of the magnetic, light, and observation directions, the behavior of the orientation of the crystal can be determined. This orientation behavior is consistent with the experimental microscopy results, because the (100) plane of the uric acid crystal is orthogonal to the magnetic direction.

We also determined the relationship between the magnetic field and the reflected light intensity. The experimental system was the same as that shown in Figure 3.9(c).

The measured wavelength was between 600 and 650 nm. Figure 3.13 shows the reflected light intensity for magnetic fields between 50 and 500 mT. The changes were determined by the time to reach saturation after the magnetic field was applied. As the magnetic field decreased, the time to reach saturation decreased. This shows that the orientation speed decreases as the magnetic field decreases. Figure 3.14 shows the rate of change of the reflected light intensity by changing the magnetic field strength. In the case of 300 and 500 mT magnetic fields, the change rate of the reflected light intensity was about 2.5%. The reflected light intensity changed about by 1.7% at 130 mT and by about 1.5% at 95 mT. However, the reflected light intensity only slightly changed (0.2%) at 50 mT. Thus, a magnetic field of 50 mT had almost no influence on the reflected light intensity.
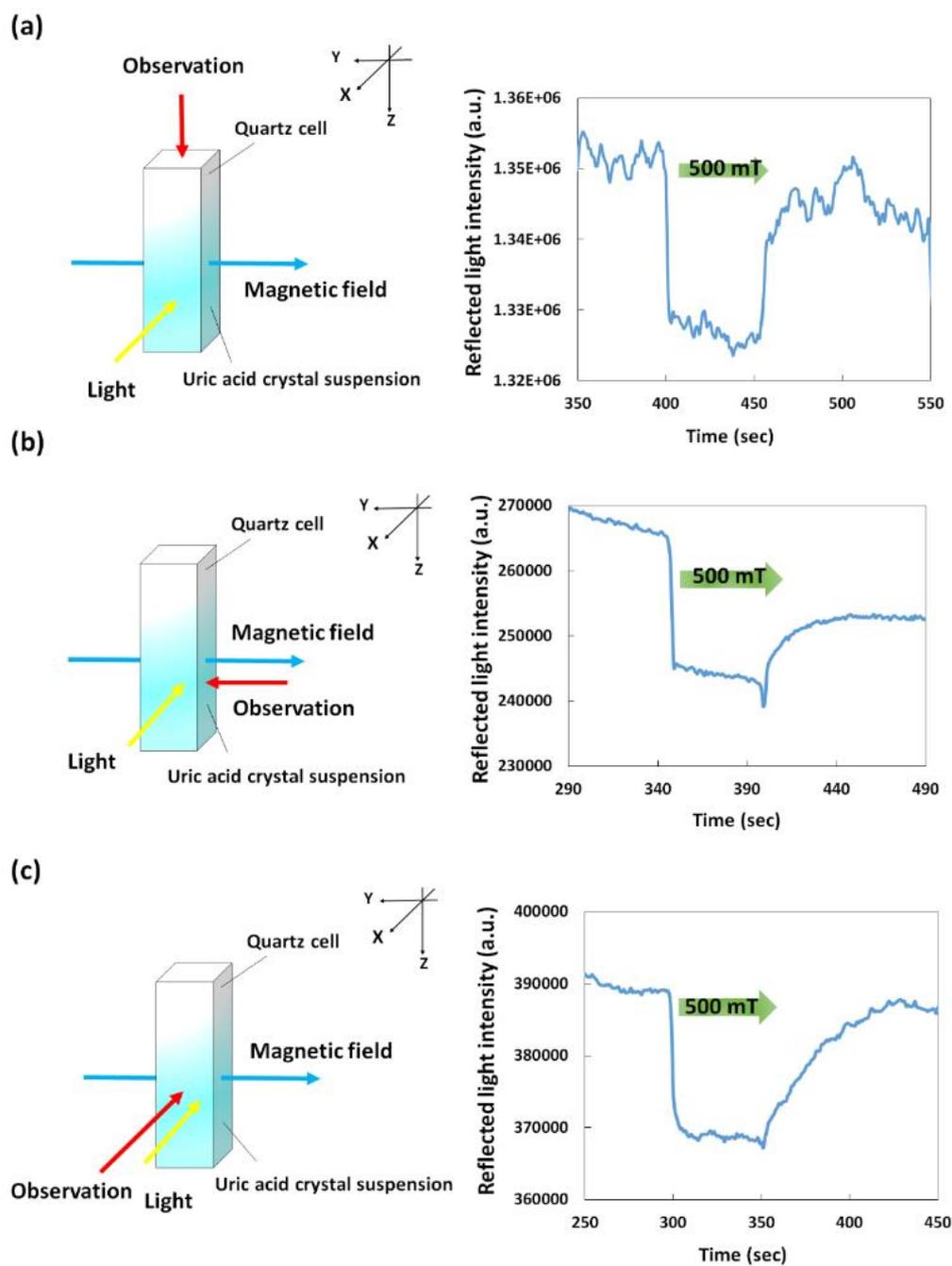
Fig. 3.9. Configuration for measurement of reflected light intensity (left) and time course of the reflected light intensity from uric acid crystals with and without magnetic field of 500 mT (right). (a) The conditions that magnetic direction is Y axis, light direction is X axis and observation direction is Z axis. (b) The conditions that magnetic direction and observation direction is Y axis and light direction is X axis. (c) The conditions that magnetic direction is Y axis and light direction and observation direction is X axis.
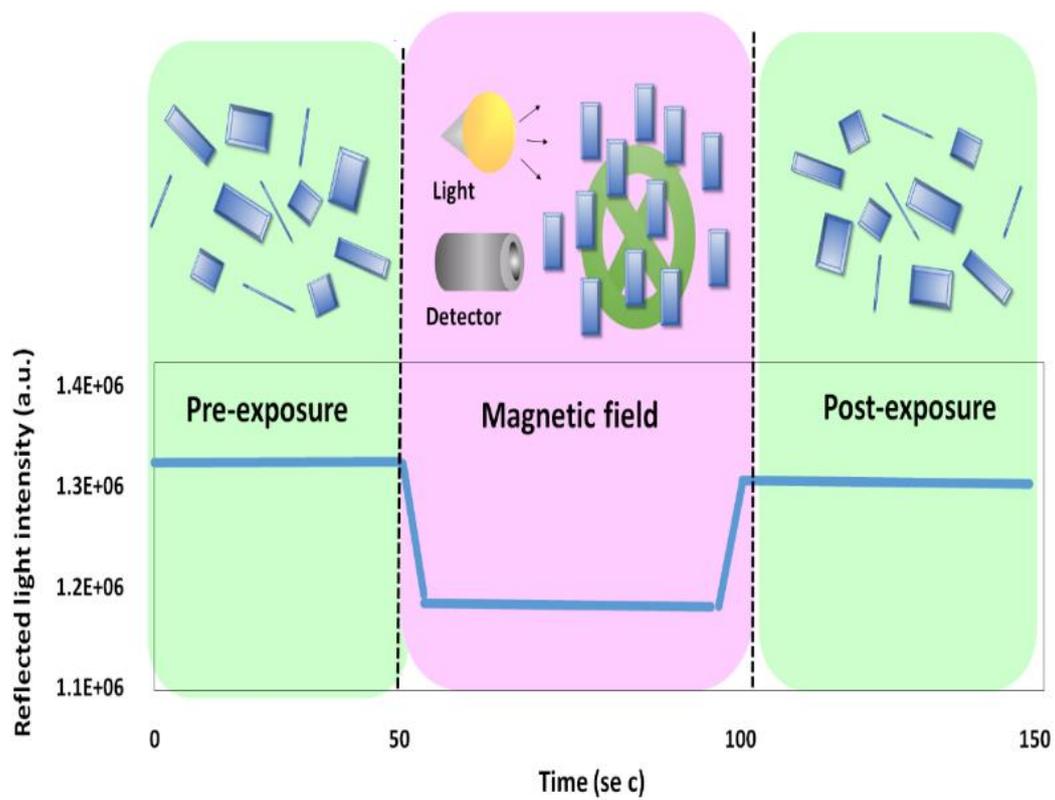
Fig. 3.10. The model of the uric acid crystals behavior in the reflected light intensity decrease.
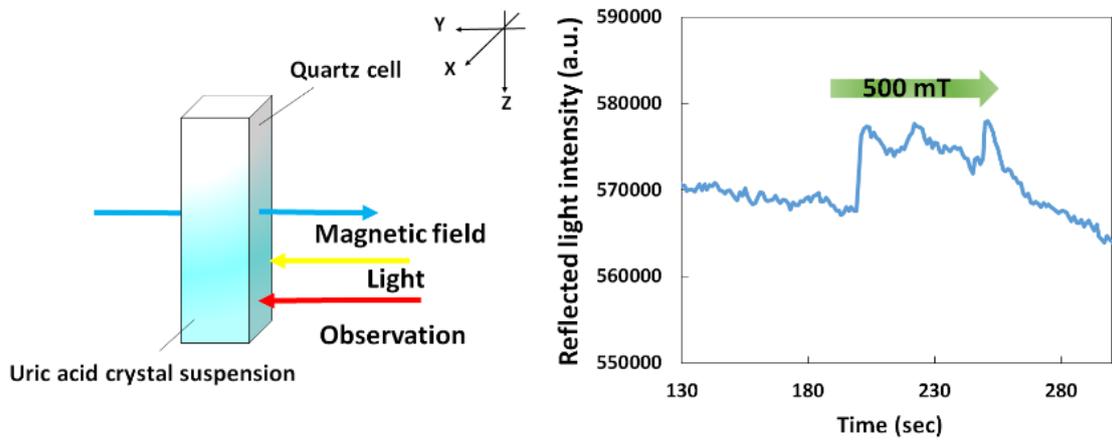
Fig. 3.11. Configuration for measurement of reflected light intensity under the conditions that magnetic direction, light direction and observation direction is Y axis (left) and time course of the reflected light intensity from MSU crystals with and without magnetic field of 500 mT (right).
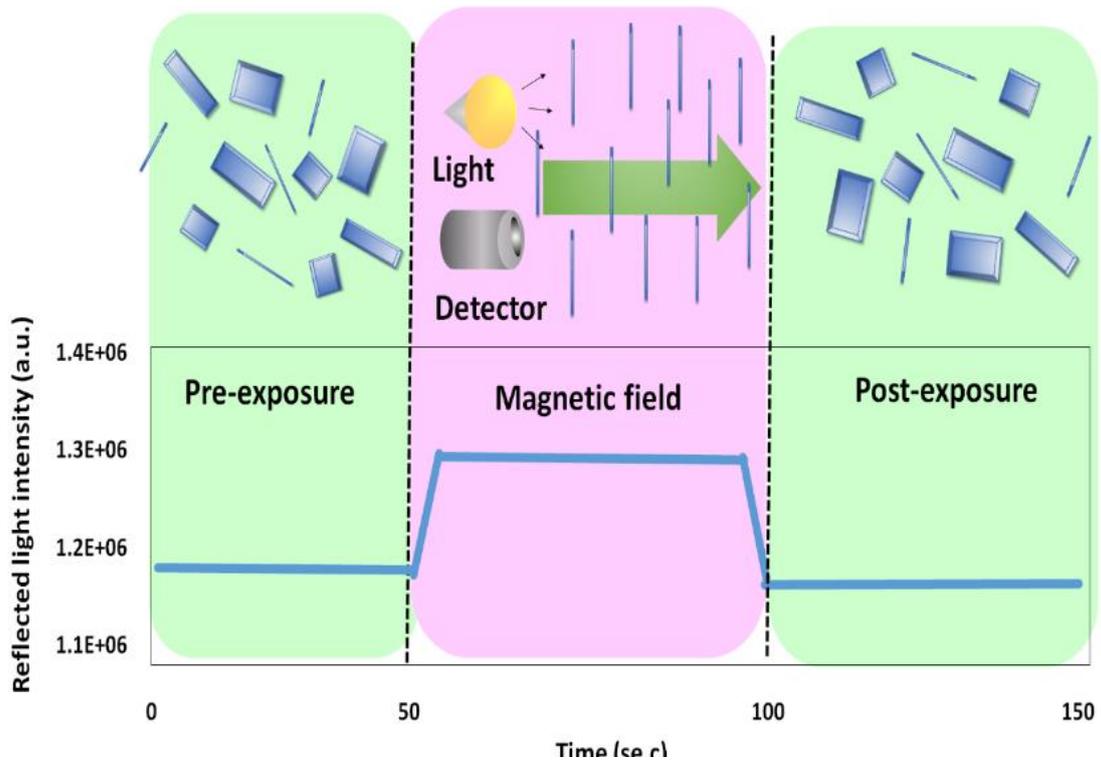
Fig. 3.12. The model of the uric acid crystals behavior in the reflected light intensity increase.
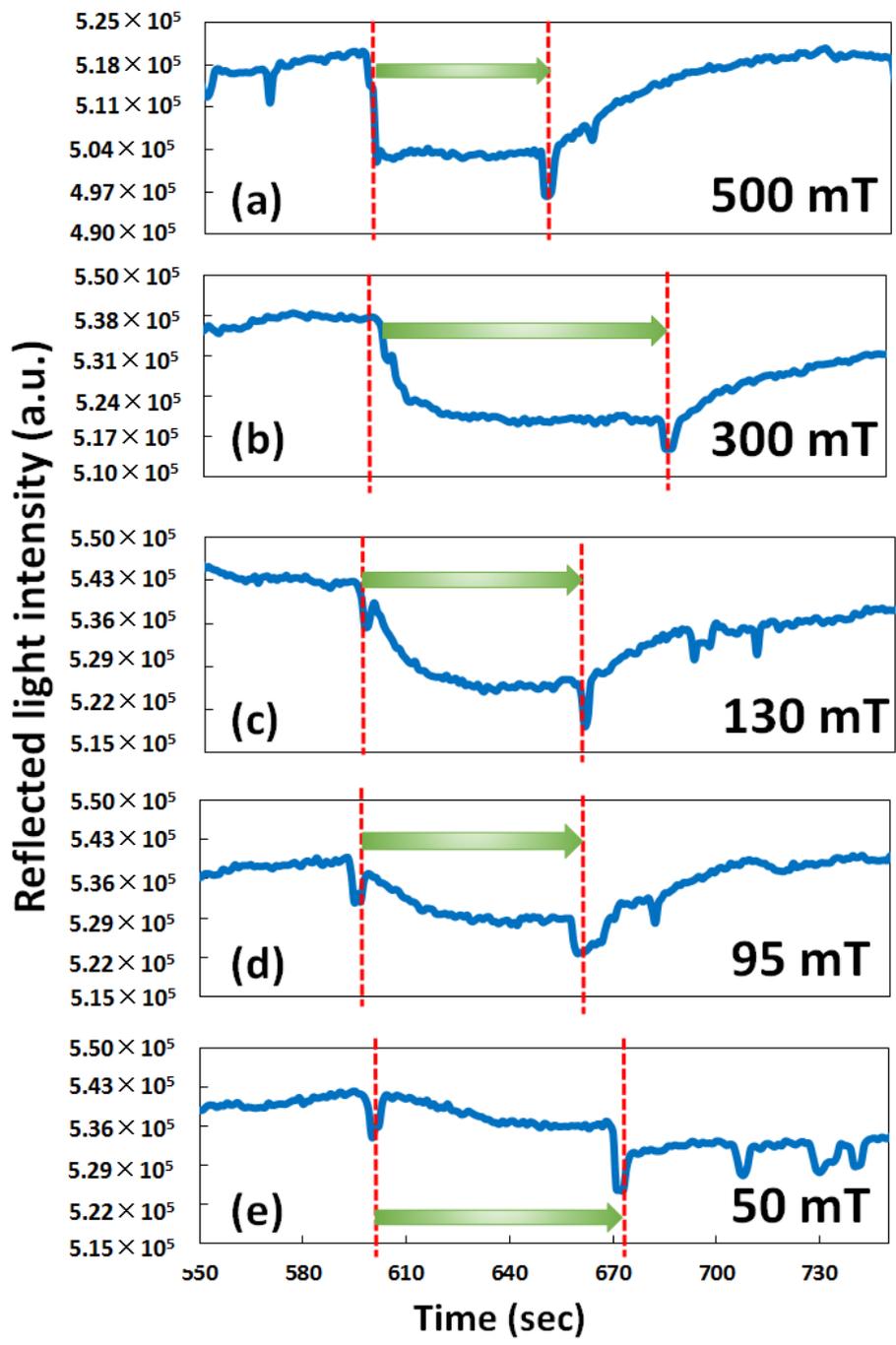
Fig. 3.13. (a)-(e) Time course of the reflected light intensity from uric acid crystals with and without magnetic field of 50, 95, 130, 300 and 500 mT under condition of Fig. 3.9(c).
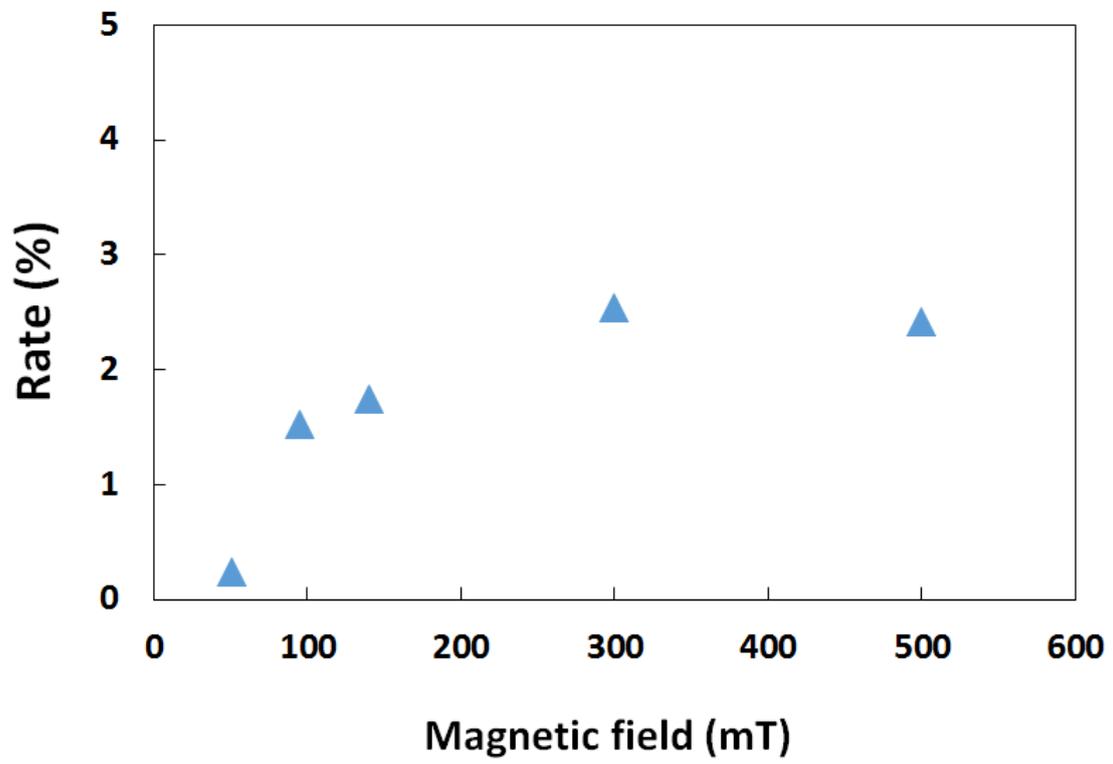
Fig. 3.14. Magnetic field dependence in the rate of change of the reflected light intensity.

Figure 3.15 shows a model of the two-stage orientation of the uric acid crystal. The (100) plane of the uric acid crystal was oriented perpendicular to the magnetic field when the magnetic field was applied, and the uric acid crystals finally oriented parallel to the magnetic field. This indicates that the uric acid crystal is most stable when the (100) plane of the crystal is parallel to the magnetic field. Therefore, the *a*-axis in the uric acid crystal is the axis of easiest magnetization. By Lenz's law, the magnetic moment occurs in the opposite direction to the magnetic field direction because the intramolecular electric current flows along the ring when the magnetic field is vertically applied with respect to the molecular plane. The ring rotates in the magnetic field, and the direction of rotation of the magnetic moment is perpendicular to the magnetic field because the magnetic moment is unstable. Figure 3.16 shows the uric acid crystal structure of the *a*-axis. It is suggested that the crystal is stable when a magnetic field is applied to the *a*-axis direction because the molecular plane of the uric acid crystals is inclined in the *b*- and *c*-axis directions of the uric acid crystal. The above experimental results are consistent with this explanation. Moreover, the second easiest axis of magnetization in the uric acid crystal is the *b* axis because the *b* axis rotated to be parallel to the magnetic field. The magnitude relationship of the magnetic susceptibilities is $\chi_c < \chi_b < \chi_a < 0$, if the magnetic susceptibilities of the *a*, *b*, and *c* axes are χ_a, χ_b, and χ_c, respectively (Figure 3.17).

It is believed that uric acid crystals undergo a two-stage orientation process because the crystal aligns itself in the direction of stability in two stages. In the first stage, when a magnetic field *B* is applied in the direction shown in Figure 3.18, the b-axis of the crystal on the cover glass becomes parallel to the magnetic direction. In the second stage, the crystal rotates around the c-axis so that the axis of the crystal becomes parallel to the direction of magnetic field (Figure 3.18). Furthermore, the gravity torque acts because the edge of the c-axis of the crystal makes contact with the cover glass. When the magnetic field *B* with magnetic torque T_M expressed with equation (3.5) is applied to a uric acid crystal, the crystal rotates in the direction where the magnetic energy is minimized. That is, it rotates to the direction where the axis of easy magnetization is parallel to the direction of the applied magnetic field.

$$T_{\mathrm{M}} = V\Delta\chi\frac{B^2}{2\mu_0}\sin(2\theta) \quad (3.5)$$

In the above equation, where μ_0 is the magnetic permeability in vacuum, θ is the angle between the magnetic field and the axis of easy magnetization, *V* is the volume of the

crystal, and $\Delta\chi$ is the magnetic susceptibility difference between the axis of easy magnetization and the axis of difficult magnetization. Furthermore, gravity torque T_g is expressed by equation (3.6).

$$T_g = -\rho g V \frac{\text{L}}{2}\cos\vartheta \tag{3.6}$$

Where ρ is the density, g is the acceleration of gravity, and L is the distance from the axis of rotation to the line of action. Moreover, viscosity torque T_{visc} is expressed by equation (3.7).

$$T_{visc} = -V\eta\alpha\frac{\mathrm{d}\theta}{\mathrm{dt}} \tag{3.7}$$

Where η is the viscosity and α is the drag coefficient. The flow is laminar and the Reynolds number is small. Therefore, in the equation of motion, the inertia term is not affected because the viscosity term is dominant. Hence,

$$T_M + T_g + T_{visc} = 0,$$

(3.8)

$$V\Delta\chi^2\frac{B^2}{2\mu_0}\sin(2\theta) - \rho g V\frac{\text{L}}{2}\cos\theta - \alpha\eta V\frac{d\vartheta}{dt} = 0 \tag{3.9}$$

the differential equation of equation (3.9) is solved for t and equation (3.10) is obtained.

$$t = \left(-\frac{2A\log(B - 2A\sin\theta)}{B^2 - 4A^2} - \frac{\log(\cos(\frac{\theta}{2}) - \sin(\frac{\theta}{2}))}{2A - B} - \frac{\log(\sin(\frac{\theta}{2}) - \cos(\frac{\theta}{2}))}{2A + B} \right)\eta\alpha$$

(3.10)

Here $A = \Delta\chi B^2/2\mu_0$ and $B = \rho g L/2$ are assumed.

Figure 3.19 shows the magnetic torque (B = 500 mT) and gravity torque that act upon a uric acid crystal with volume of 675 μm^3. The length, width, and height are 45, 15, and 1 μm, respectively. The maximum value of the magnetic torque that acts upon this crystal is $T_M = 3.1 \times 10^{-9}$ N·m and the maximum value of the gravity torque is $T_g = -4.3 \times 10^{-10}$ N·m. Figure 3.20 shows the entire torque that acts upon the uric acid crystal for a magnetic field of 500 mT. For angle θ between points A and B, the crystal does not rotate because the magnetic torque is weaker than the gravitational torque. For angle θ between points B and D, the crystal rotates because the magnetic torque is stronger than the gravitational torque. The crystal is in equilibrium at point D ($\theta = 90°$). The crystal acquires the second-stage rotation and attains the optimum angle θ if the magnetic torque exceeds the gravity torque. It is considered that the crystal fluctuates by Brownian motion to reach the optimum angle θ. Therefore, the crystal is observed to undergo two stages before attaining stability.

Figure 3.21 shows the rotation angle of the crystal over time. Figure 3.22 shows the magnetic torque acting upon the crystal. In 130 mT, when the magnetic torque is stronger than the gravity torque, $T_{total} = 8.7 \times 10^{-13}$ N·m at $\theta = 49°$. The crystal is subjected to Brownian motion in the solution. At 130 mT, the two-stage magnetic orientation is not seen because θ is smaller than 49°.

Next, we estimated the magnetic susceptibility of each component of the uric acid molecule. Many studies have suggested that it is possible to collate the diamagnetic susceptibility of a compound by summing the magnetic susceptibility near the atoms [15,16]. The contribution of internal and coupled electrons to diamagnetic susceptibility can be quantum mechanically computed [17-20]. Table 3.1 shows the summary of the magnetic susceptibility for the coupling scheme, and Table 3.2 shows the correction to the extra electron pair when double and triple bonds exist. The above agree with the calculation results of *Tillieu et al.* [19]. The diamagnetic susceptibility of each element in the X-direction, Y-direction, and Z-direction was estimated on the basis of the uric acid molecule. As a result, the calculated magnetic susceptibility of the X-element is 26 $\times 10^{-6}$ cm^3 mol^{-1}, of the Y-element is 32 $\times 10^{-6}$ cm^3 mol^{-1}, and of the Z-element is 95 $\times 10^{-6}$ cm^3 mol^{-1}.
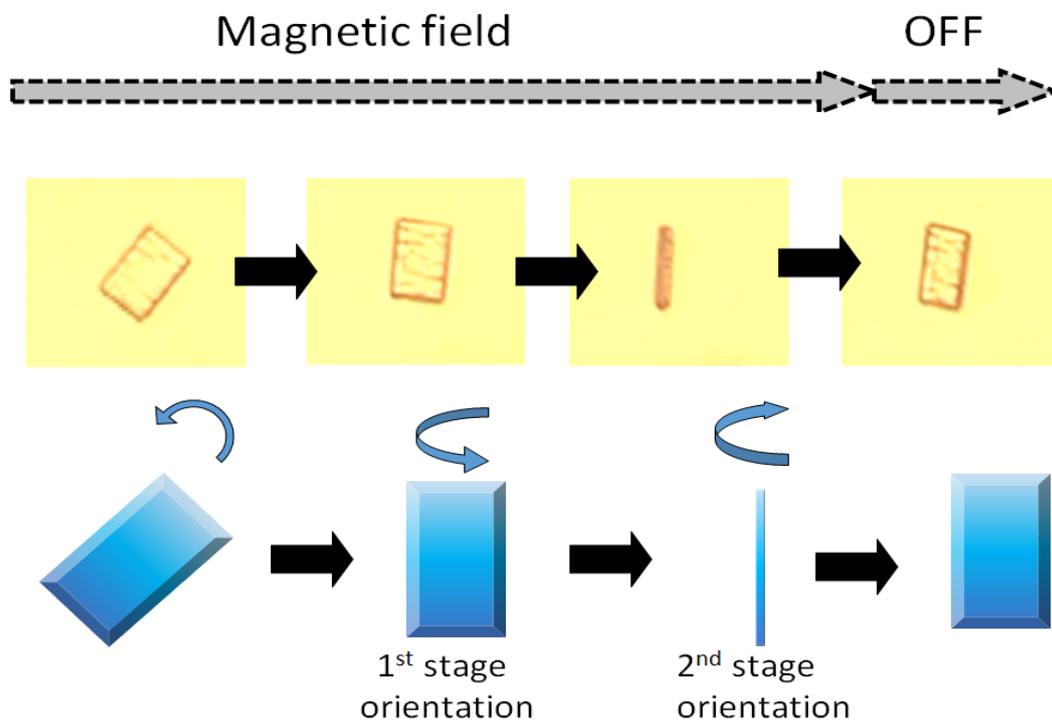
Fig. 3.15. Two stage magnetic orientation of uric acid crystal.
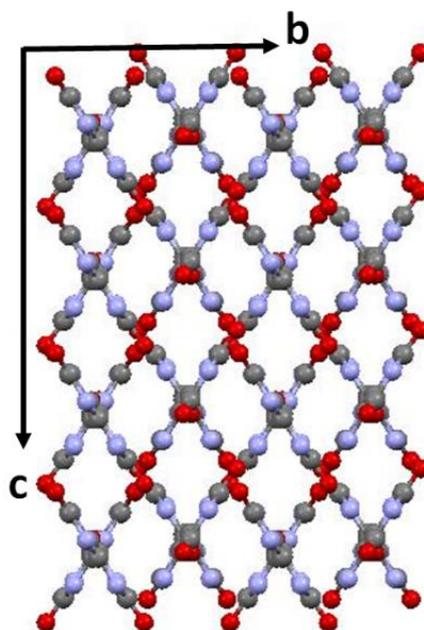
Fig. 3.16. Packing diagram of uric acid crystal viewed along the a-axis.

$$-\frac{B^2 V}{2\mu_0}\chi_1 \quad < \quad -\frac{B^2 V}{2\mu_0}\chi_2 \quad < -\frac{B^2 V}{2\mu_0}\chi_3$$
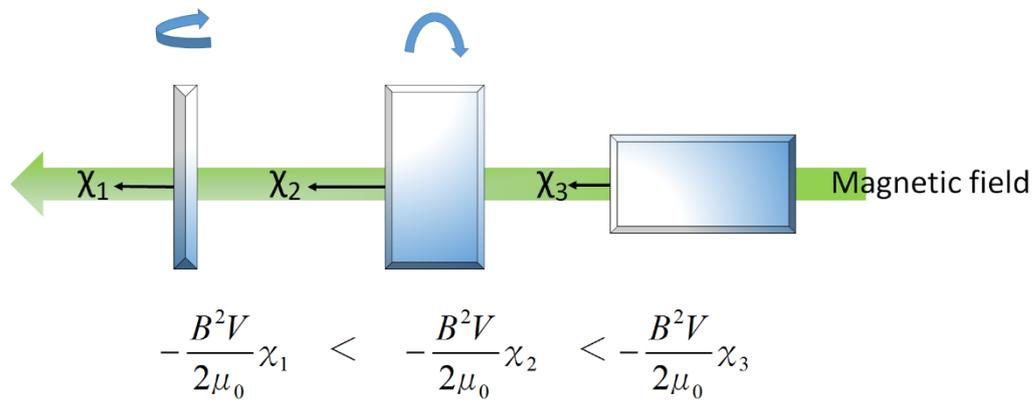
Fig. 3.17. A model to compare the diamagnetic anisotropic energy.
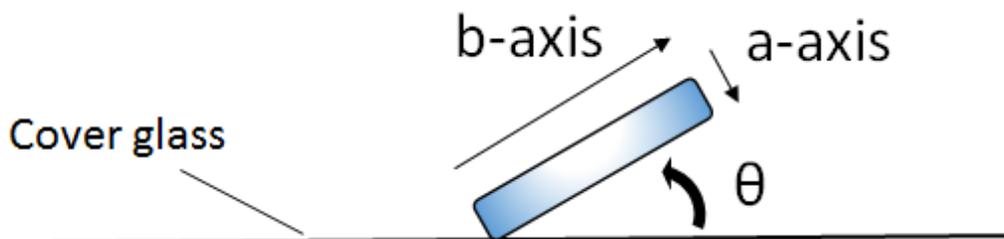
Fig. 3.18. Magnetic rotation in the second stage.
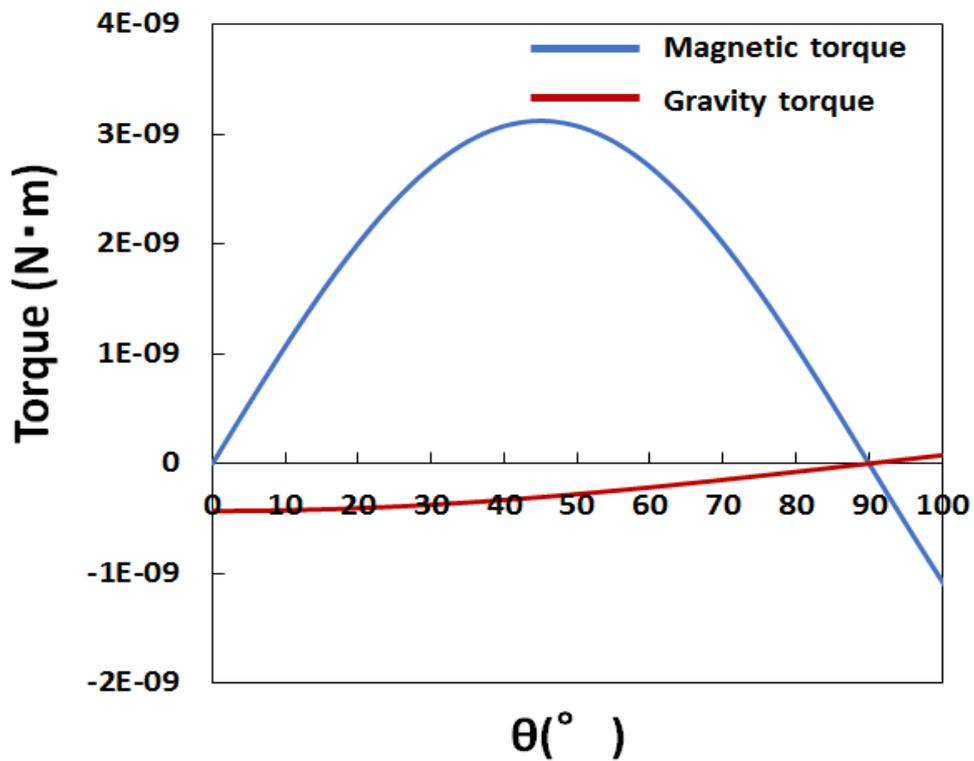
Fig. 3.19. The magnetic torque and gravity torque acting on the uric acid crystal for the angle (B=500 mT).
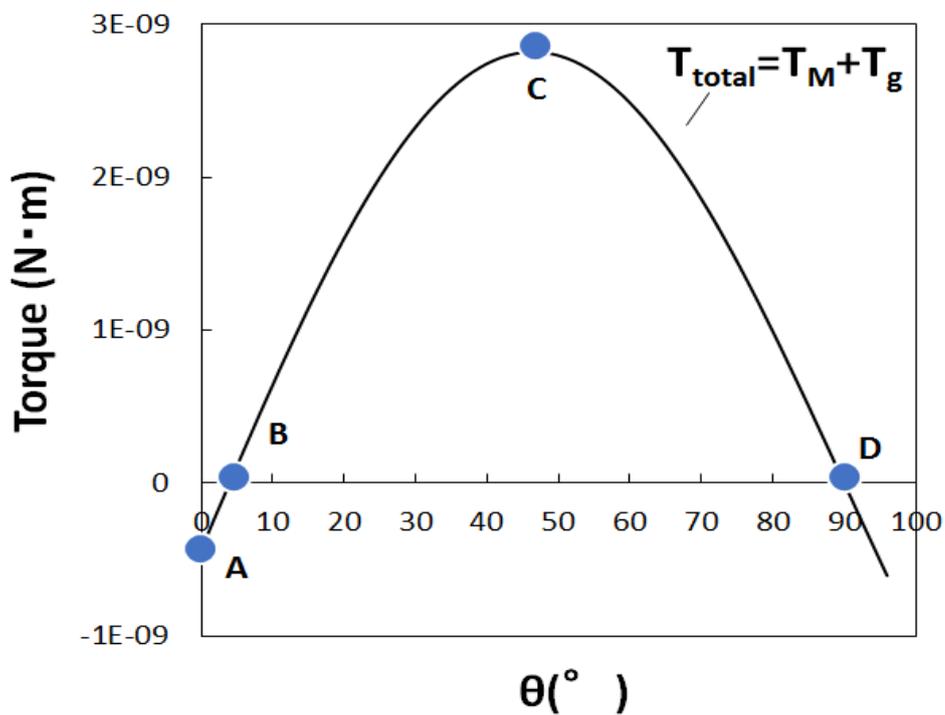
Fig. 3.20. The total torque acting on the uric acid crystal for the angle (B=500 mT).

60
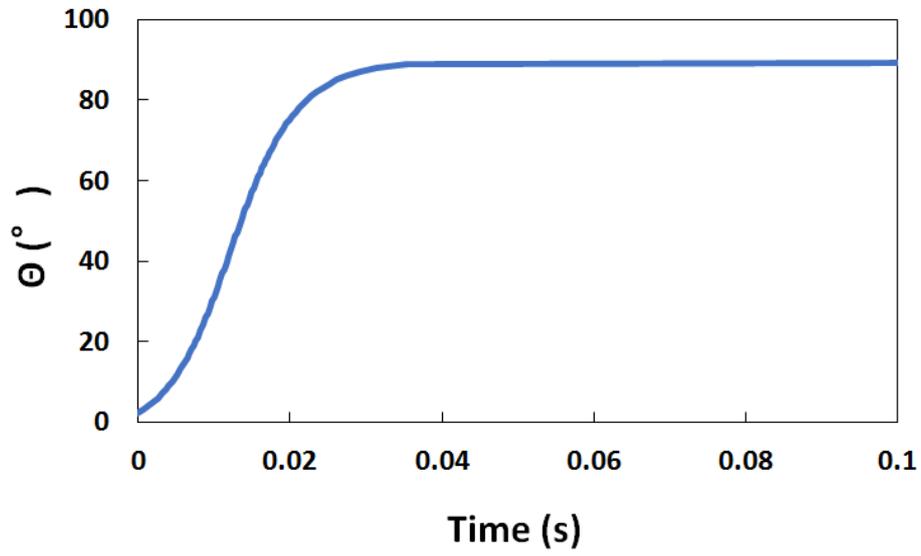
Fig. 3.21. The rotation angle of the crystal over time course. (B=500 mT).
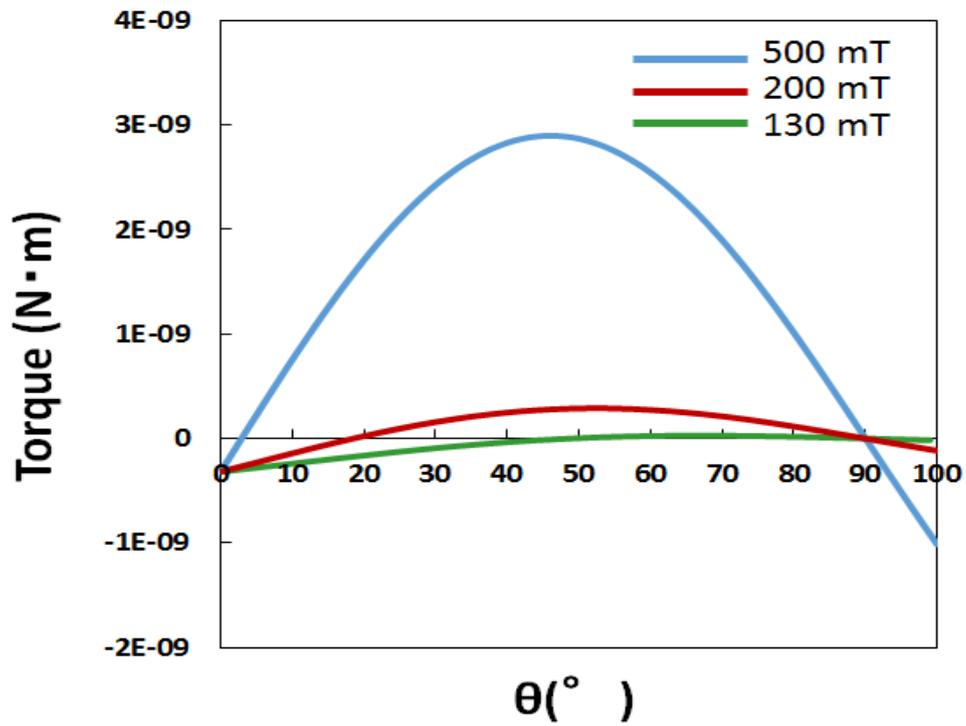
Fig. 3.22. The total torque acting on the uric acid crystal for the angle when the magnetic field is 500, 200 and 130 mT.

Next, we estimated the magnetic susceptibility of each components of uric acid molecule. Many researches have revealed that it is possible to assemble the diamagnetic susceptibility of the compound by the sum of the magnetic susceptibility in the vicinity of the atom [15,16]. Contribution of internal electron and coupled election to diamagnetic susceptibility is also computable quantum mechanically [17-20]. Table. 3.1 shows the summary of magnetic susceptibility concerning the coupling scheme, and Table. 3.2 shows the correction to an extra electron pair when the double bond and triple bond exist. These show the calculation result by *Tillieu, et al* [19]. The diamagnetic susceptibility of each element of X-direction, Y-direction and Z-direction was estimated based on uric acid molecule. As a result, the calculation is shown as follows: the magnetic susceptibility of X-element is 26×10^{-6} cm^3 mol^{-1}, Y-element is 32×10^{-6} cm^3 mol^{-1} and Z-element is 95×10^{-6} cm^3 mol^{-1}.

In general, in large crystals with aromatic rings, the ring current induced is large because large crystals have many aromatic rings. Therefore, large crystals tend to magnetically orient. However, Figure 3.8(a) shows that the angular velocity is large when the crystal size is small. It is considered that the influence of gravity causes friction between the cover glass and the crystal because it is easy to sink if the crystal is large contributes because it has sufficient magnetic field strength to cause magnetic orientation.

In the experiments under microscope, two-stage magnetic orientation was observed for magnetic fields <200 mT. However, orientation of crystals under a magnetic field of 130 mT is possible as a result of the magnetic energy. In the results of the reflected light intensity change experiment under a magnetic field of 130 mT, the crystals oriented because the reflected light increased, and a change of reflected light intensity was clearly observed. This experimental result of the reflected light intensity change is based on the estimate of the magnetic energy.

We estimated the diamagnetic susceptibility anisotropy of uric acid in Chapter 3.3.4. The value of the magnetic susceptibility anisotropy was -3.7×10^{-7}. In the horizontal and vertical directions to the molecular surface, it is generally accepted that the diamagnetic susceptibility is different if there is a planar structure, such as benzene, in the aromatic compound. Magnetic anisotropy is observed even when five atoms are uniplanar, such as ester bonds. The magnetic susceptibility anisotropy values are -54×10^{-6} for benzene, -8.8×10^{-6} [22] for the ester group, -4.5×10^{-6} [23] for the carboxyl group, and -5.3×10^{-6} [24] for the peptide group. Compared with these values, the diamagnetic susceptibility anisotropy of uric acid is large. Thus, the uric acid crystals are highly sensitive to millitesla magnetic fields.

Table. 3.1 Magnetic susceptibility of the bonding electron pair. [22]

Bond A-B	$-\chi$ mol$\times10^{-6}$/cm^3 mol^{-1}
N-H	3.63
C-N	2.37
C-C	2.38

Table. 3.2 Magnetic susceptibility of the electron pair in π bond. [22]

Bond	$-\chi$ mol$\times10^{-6}$/cm^3 mol^{-1}
C=C	3.42
C=O	3.05

3.4 Summary

Uric acid crystals were recrystallized from a saturated aqueous solution of uric acid powder. The obtained uric acid crystals had a rectangle shape. The orientation of the uric acid crystals under magnetic fields of several hundred millitesla was investigated. Using an electromagnet with a field strength of up to 500 mT, we were able to induce two stages of orientation in the crystals. First, the long axis of the uric acid crystals (*c* axis) oriented perpendicular to the magnetic field. Then, a second magnetic rotation occurred and the morphologically largest surface of the crystal oriented perpendicular to the magnetic field. This magnetic orientation behavior was observed for magnetic fields between 200 and 500 mT under a microscope. For an applied magnetic field of 130 mT, the crystals only underwent the first stage of orientation. Analysis of the angular velocity of uric acid crystals diamagnetically rotating under applied magnetic fields of 130–500 mT revealed that the angular velocity depended on the applied magnetic field, and the area and shape (aspect ratio) of the crystal. In reflected light intensity measurements, the reflected light intensity increased when the magnetic, light, and observation directions were parallel. This shows that the (100) plane of the uric acid crystal was perpendicular to the magnetic direction (i.e., the *a* axis of crystal was parallel to the magnetic direction). The change of the reflected light intensity was confirmed for magnetic fields ≥95 mT. This orientation behavior was consistent with the microscope measurements.

Reference

[1] C.Y. Park, "Kidney stones," Lancet, Vol. 351, pp. 1797 (1998).

[2] T. F. Yu and A.B. Gutman, "Uric acid nephrolithiasis in gout: predisposing factors," Ann. Intern. Med., Vol. 67, pp. 1138 (1967).

[3] B. Shekarriz and M.L. Stoller, "Uric acid nephrolithiasis, current concepts and controversies," J. Urol, Vol. 168, pp. 1307 (2002).

[4] A. P. Hall, P.E. Barry, T.R. Dawber, and P.M. McNamara, "Epidmiology of gout and hyperuricemia. A long-term population study," Am. J. Med., Vol. 42, pp. 27 (1967).

[5] H. Okabe and T. Hosoya," Clinical feature of urolitiasis in patients with gout," Hyperuricemia and gout, Vol. 8, pp. 47 (2000).

[6] E. L. Prien and E.L. Prien Jr, "Composition and structure of urinary stone," Am. J. Med., Vol. 45, pp. 654 (1968).

[7] F. L. Coo, A. Evan and E. Worceter,"Kidney stone disease," J. Clin. Invest. Vol. 115, pp. 2598, (2005).

[8] S. Yamaguchi, "Hyperuricemia as a risk factor for urolithiasis," Hyperuricemia and gout, Vol. 18, pp. 53 (2010).

[9] H. Ringertz, "The molecular and crystal structure of uric acid," Acta. Cryst., Vol. 20, pp. 397 (1966).

[10] C. Rinaudo and R. Boistelle, "The occurrence of uric acids and the growth morphology of the anhydrous monoclinic modification: $C_5H_4N_4O_3$," J. Cryst. Growth. Vol. 49, pp. 569 (1980).

[11 Ryan E. Sours , Dorothy A. Fink , and Jennifer A. Swift "Dyeing Uric Acid Crystals with Methylene Blue," J. Am. Chem. Soc. Vol. 124, No. 29, pp. 8630 (2002).

[12] M. G. Simic and S. V. jovanovic, "Antioxidation Mechanisms of Uric Acid," J. Am. Chem. Soc., Vol. 11, pp. 5778 (1989).

[13] L. Pauling," The Diamagnetic Anisotropy of Aromatic Molecules," J. Chem. Phys. Vol. 4, pp. 673 (1936).

[14] A. Weiss and H. Witte, Magnetochemie Grundlagen und Anwendungen, trans. M. Sorai, (Tokyo: Misuzu Shobo (1980).

[15] P. Pascal, Ann. Chim. Phys. 19. 5 (1910).

[16] A. Pacault, Rev. sci. Paris. 86. 38 (1948).

[17] J. Tillieu, Ann. Phys. (Paris) 2, 471, 631 (1957).

[18] J. Tillieu, and J. Guy, C. R. Acad. Sci. Paris 239, 1203, 1283 (1954); 240, 1402 (1955); 242, 1279, 1436 (1956).

[19] J. Bauder, J. Tillieu and J. Guy, C. R. Acad. Sci. Paris 244, 1756 (1957); 244, 2920 (1957).

[20] R. Gans, and B. Mrowka, *Konigsberger Gelehrte Gesellschaft Nachr*. 12, 1 (1935).

[21] A. Pacault, J. Hoarau and A. Marchand, Adv. Chem. Phys. 3, 171 (1961).

[22] D. L. Worcester, "Structural origins diamagnetic anisotropy in proteins," Proc. Natl. Acad. Sci. USA, Vol. 75, pp. 5475 (1978).

[23] L. Pauling "Diamagnetic anisotropy of the peptide group," Proc. Natl. Acad. Sci. USA, Vol. 76, pp. 2293 (1797).

[24] K. S. Krishnan, B. C. Guha and S. Banerjee, Philos. Trans. R. Soc. London Ser. Vol. A 231, pp. 235 (1933).

4

Magnetic Rotation of Monosodium Urate Crystal

4.1 Introduction

Diseases in the human body that are caused by crystals such as uric acid crystals and calcium oxalate crystals have become a serious problem in everyday life. Uric acid is known as the substance that is responsible for gout [1-2]. Gout is a severe inflammatory arthritic disease that develops when high accumulations of uric acid crystallize [3-5]. The agent of gout is a monosodium urate (MSU) crystal, which is a compound formed from uric acid and sodium from the patient's blood [6]. The shapes of these MSU crystals are needle-like and frequently cause severe pain for the patient. Similarly, urinary tract stone disease is also caused by crystals, and is categorized in terms of compounds that form the crystals, such as calcium oxalate, calcium phosphate, and uric acid. Gout and hyperuricemia are linked to the formation of urinary tract calculi [7-8]. In our previous study, we reported that uric acid crystals that were rectangular in shape show distinct magnetic orientations under magnetic fields. Therefore, it is believed that the needle-like MSU crystals, which are composed of the same component as uric acid crystals, will also have magnetic orientations induced by their magnetic anisotropy. This Chapter focused on the magnetic behavior of the MSU crystal which is responsible for gout.

4.2 Experiment Section

4.2.1 Materials

The monosodium urate (MSU) crystals that cause gout are monohydrate, and they were examined by the X-ray diffraction method of Mandel et al [9]. MSU crystals are needle-shaped triclinic crystals 5–50 μm in length, 5–7 μm in width, and 1–3 μm thick. The unit cell dimensions are a=10.88 Å, b=9.53 Å, c=3.56 Å, α=95.3°, β=99.47°, and γ = 97.17° [9]. It is elongated in the c-axis [9-16]. The sodium ion exists in layers because the uric acid anions are held together by hydrogen bonding in the crystal (Figure 4.1). Therefore, MSU crystals are negatively charged in aqueous solution because sodium ions dissociate from the urate ion (Figure 4.2) [9-11]. The flat side face of the needle-shaped crystals is reported to be the (010) surface by optical and X-ray, and the other side faces correspond to the (100) and (1−10) surfaces [9-11]. A representative MSU crystal is shown in Figure 4.3. The urate ion twists 7.7° out of the (1−10) plane. This twist is presumably required for the urate anions to form these three sets of hydrogen bonds while maintaining the octahedral geometry of the Na ion [9-11].

We prepared MSU crystals by dissolving uric acid powder (Wako, 216-00222, 98% purity) in a solution of sodium hydroxide (0.025 mol/L) at high temperature. Figure 4 shows a photograph of the artificially obtained MSU crystals. The crystals were thin needle-like shaped with a small surface area, as shown in Figure 4.4.
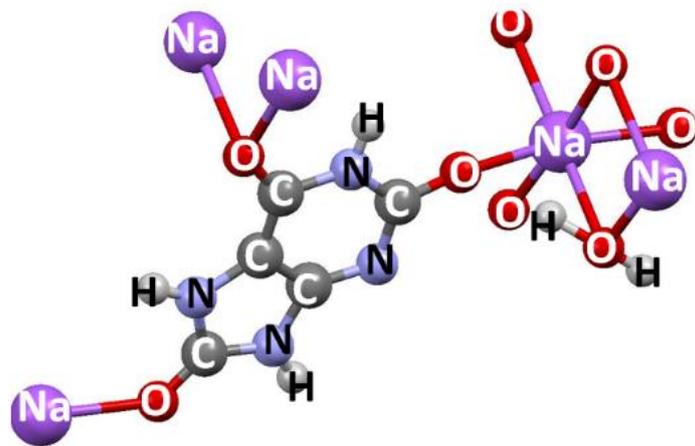
Fig. 4.1. Monosodium urate molecule.
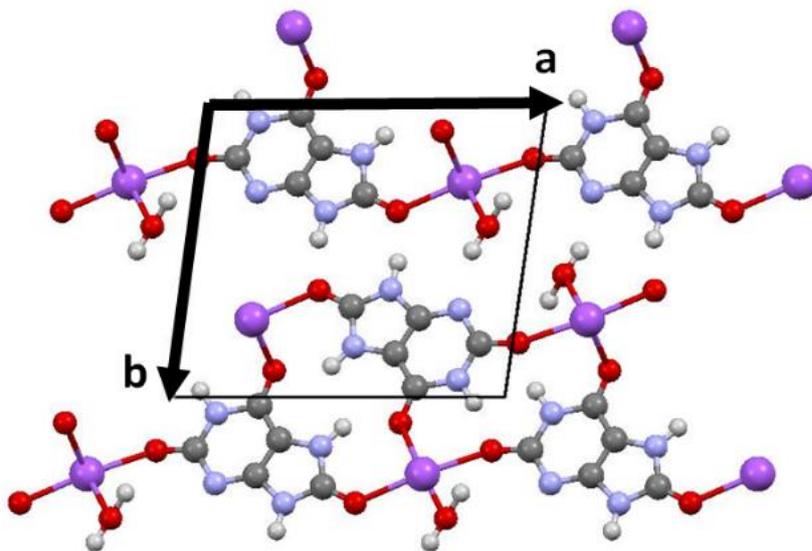
Fig. 4.2. Crystal structures of monosodium urate crystal.
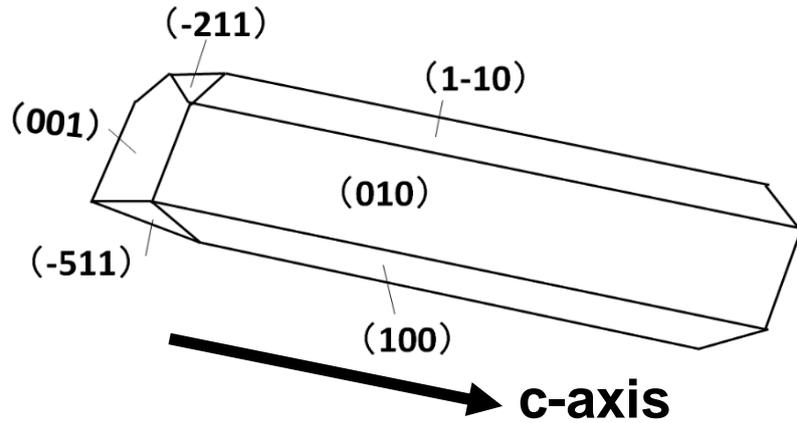
Fig. 4.3. A model of monosodium urate crystal.
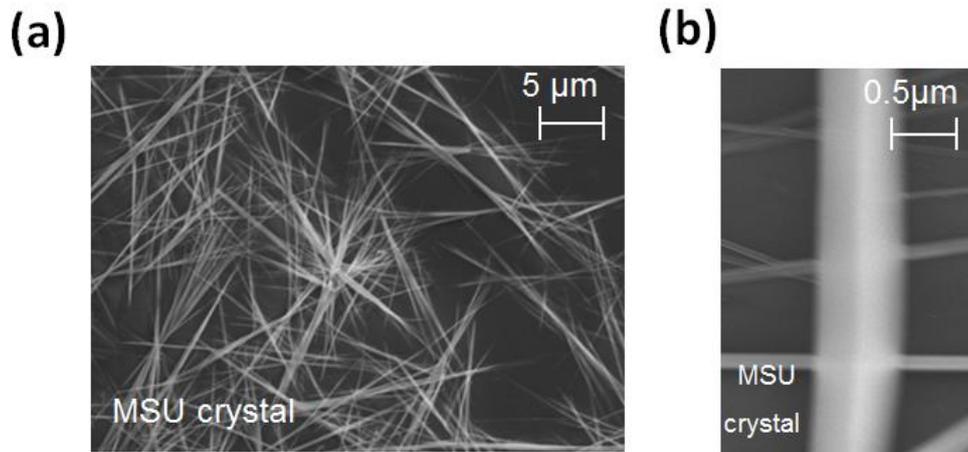
Fig. 4.4. (a) A scanning electron microscope (SEM) image of MSU crystals. (b) A SEM image of the left image scaled up ten times.

4.2.2 Measurements

We transferred the MSU crystals to a microchamber, which consisted of a cover glass window (18×18 mm^2, 0.12–0.17 mm thick) and a rubber sheet (Figure 3.1(a)). The microchamber was positioned in a CCD microscope, which was placed in an electromagnet with a magnetic field strength of up to 500 mT to observe the behavior of the crystals (Figure 3.1(b)). We measured the reflected light intensity using the same experimental system as that shown in Figure 3.1(c). Spectroscopic measurement of the reflected light was carried out in a fiber-optic measurement system. The light source used was a halogen lamp, which provided a continuous stream of light. The magnetic field, light source, and fiber-optic measurement system were orthogonal.

4.3　Results and Discussion

4.3.1　The Size of the Crystals

Various stages exist in arthritis, although gout arthritis occurs because of MSU crystals. Continuing lithemia is assumed to be a cause, and various factors are involved in the process of precipitating the MSU crystals. From the 1970s to the 1990s, studies were conducted *in vivo*, and the factors affecting the crystallization of MSU were investigated. The production and size of MSU crystals are different according to the mass ratio, temperature, and final pH. MSU is in a supersaturated state under physiological conditions (pH 7.4, 37 °C, 7.0 mg/dL). However, the crystal does not immediately precipitate if the crystal becomes supersaturated, but the crystal precipitates after a metastable supersaturated state. Here, the size of the MSU crystals depended on the preparation of the sample.

The MSU crystals were precipitated by dissolving uric acid powder in aqueous sodium hydroxide (0.025 mol/L). The MSU crystals were obtained by standing the solution for more than a day at 4 °C after natural cooling of the solution containing completely dissolved uric acid powder. The obtained MSU crystals were needle-shaped. However, the crystal size was different depending on the experimental procedure used to obtain the sample. Figure 4.5(a) (left) shows a photograph of the MSU crystals when 1 mL of aqueous sodium hydroxide was used to dissolve 3.75 mg of uric acid. We chose about 100 crystals and measured their length, and the distribution is shown in Figure 4.5(a) (right). In a similar way, Figure 4.5(b)–(e) show the length distributions of MSU crystals when 1 mL of aqueous sodium hydroxide was used to dissolve 3.00, 2.50, 2.00, and 1.50 mg of uric acid, respectively.

Figure 4.6 shows a photograph of the precipitated crystals when 1 mL of aqueous sodium hydroxide was used to dissolve 4.3 mg of uric acid. Because the concentration of dissolved uric acid was high, the crystals aggregated and a single crystal could not be obtained. The time taken for the crystals to precipitate was long when the dissolved concentration was small. The MSU crystals required more than 1 week to precipitate when the dissolved concentration was 1.5 mg/mL. However, the MSU crystals precipitated in about a day when the dissolved concentration was 3.0 mg/mL. In addition, the lower the concentration of dissolved uric acid, the longer the obtained crystals. However, the widths of the crystals were almost unchanged compared with the crystal length. The MSU crystals grew in the *c*-axis direction. The mean length of the crystals changed depending on the concentration of dissolved uric acid, although there

were large variations in the crystal lengths for the same dissolved uric acid concentration.

McGill [17] reported that biological substances affect crystal growth in vitro of uric acid concentration   and result in small crystals with uniform size. Figure 3.7 shows the MSU crystals obtained when a solution containing 0.1 mL of blood serum and 10 mL of aqueous sodium hydroxide was used to dissolve 30 mg uric acid. The blood serum was calf serum (Biowest, SO400). The obtained MSU crystals had an average length of 12 µm with a standard deviation (SD) of 1.6 µm. Unlike the crystals described above, the MSU crystals containing serum were uniform crystals with no variation in size. Figure 3.8 shows the mean crystal length for each concentration of uric acid.

(e)
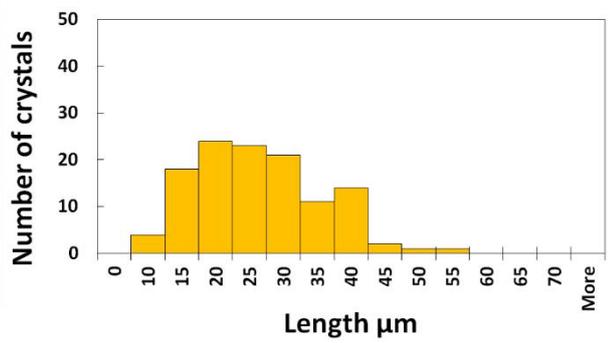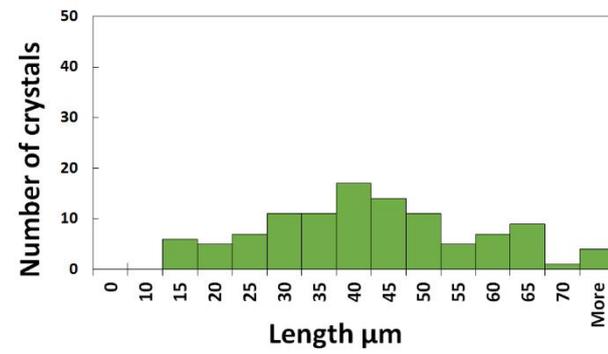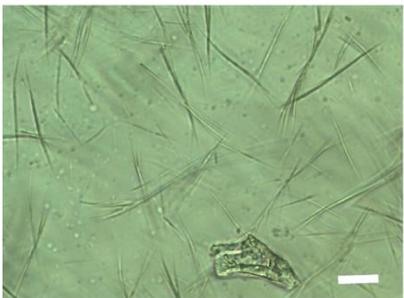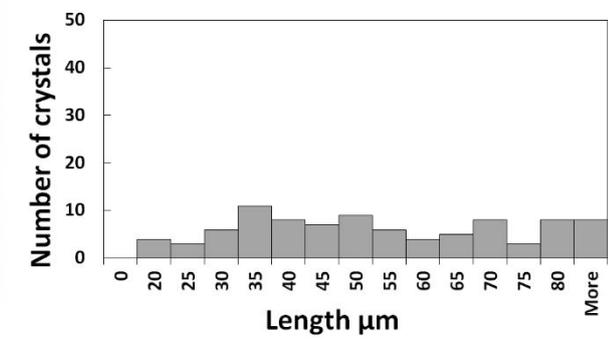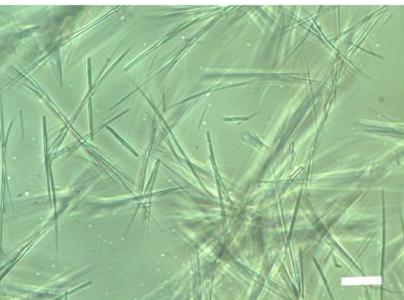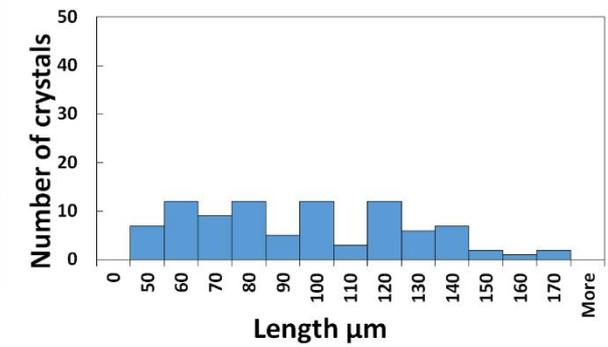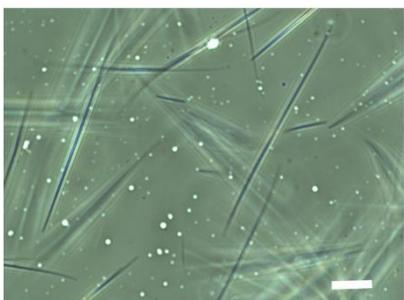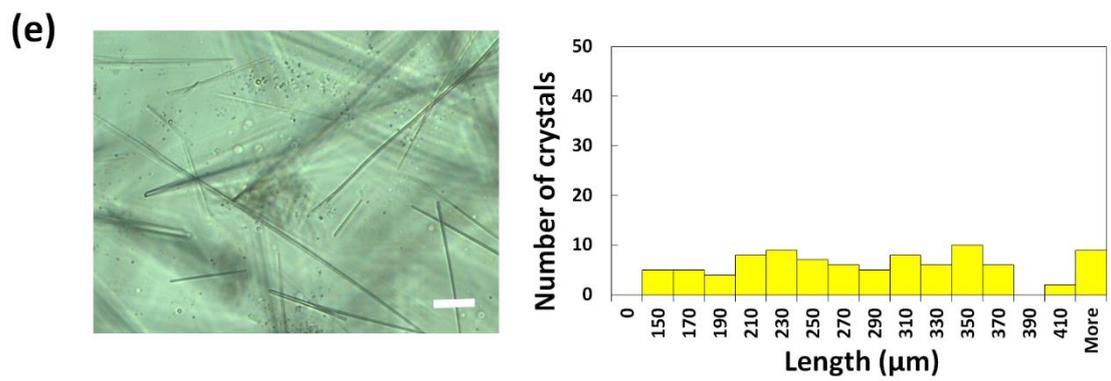
Fig. 4.5. (a)- (e) Microscope image of MSU crystals (left) and length distribution of crystals (right). Bar, 18μm.
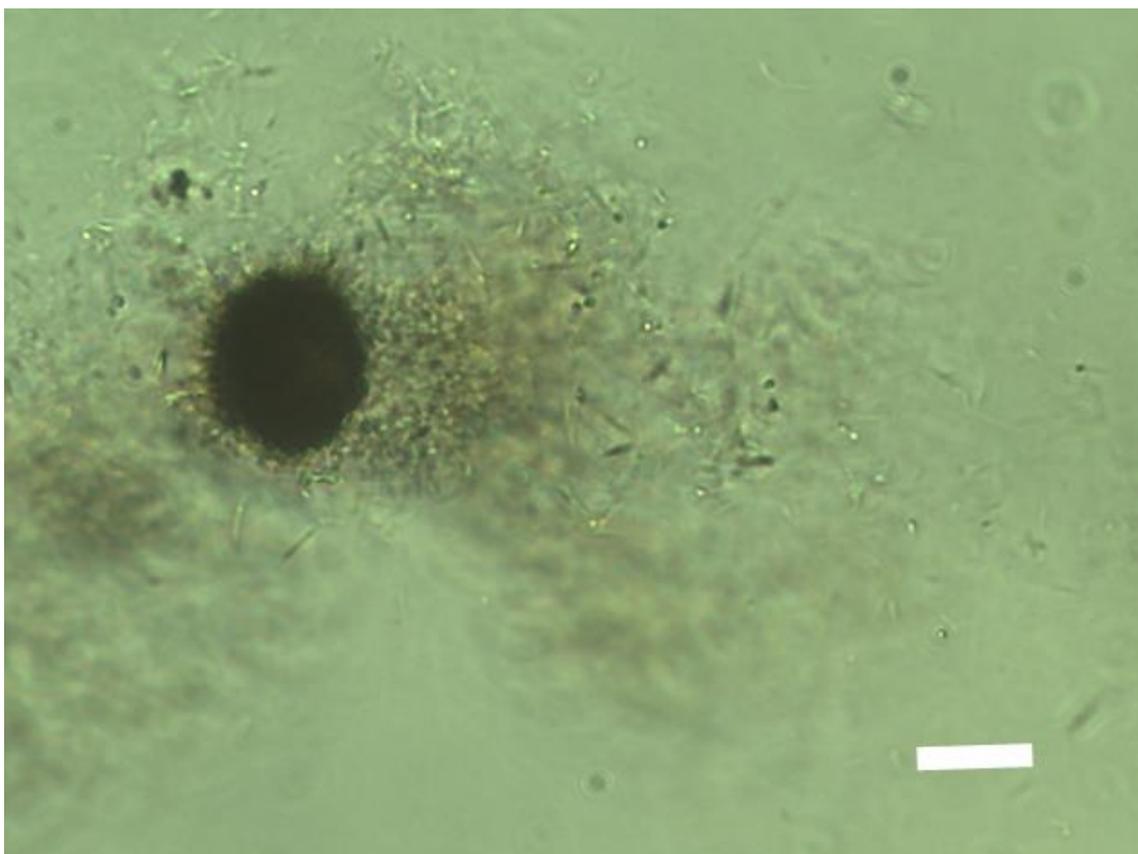
Fig. 4.6. Microscope image of MSU crystals in high concentration. Bar, 18μm.

(a)
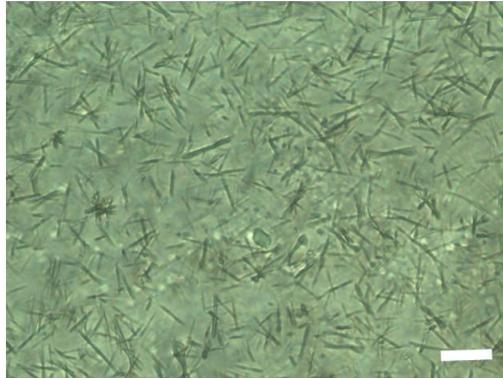
(b)
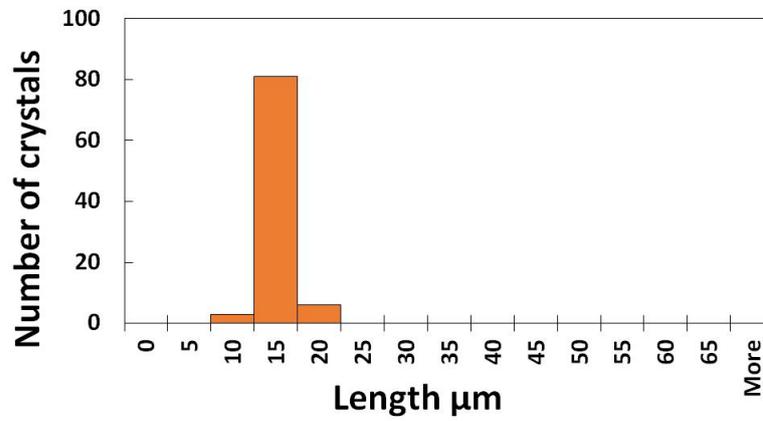
Fig. 4.7. (a) Microscope image of MSU crystals that added serum. (b) Length distribution of crystals. Bar, 18µm.
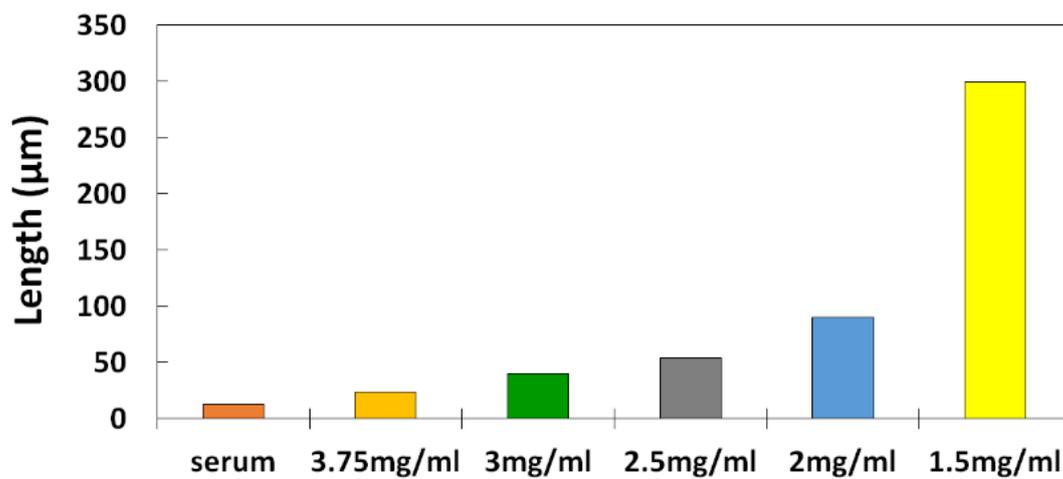
Fig. 4.8. The mean length of crystals precipitated for each concentration.

4.3.2 *Magnetic Susceptibility Measurements Using a SQUID*

The MSU crystals formed by combination of sodium ions and uric acid. Uric acid is known to be a diamagnetic material, but there are no reports about the magnetic susceptibility of MSU crystals. To determine the magnetic susceptibility of MSU crystals, we measured the magnetic susceptibility using a superconducting quantum interference device (SQUID). The sample was filled in a capsule, as shown in Figure 4.9, and fixed in a straw. This SQUID has a coil with a Josephson junction. When a sample is placed in the magnetic field in the device, the sample is magnetized, causing changes in the density of the magnetic flux that passes through the coil. Measurement of the variance makes it possible to calculate the magnetic susceptibility by measuring the magnetization to the magnetic field of the material. Figure 4.10 shows the relationship between the magnetic moment and the magnetic field strength. The magnetic field strength was varied up to 500 mT. The magnetic moment was negative, which confirms that the MSU crystals are a diamagnetic material. The magnetic moment decreased as the magnetic field increased. Figure 4.11 shows the relationship between the magnetic moment and temperature. The magnetic field was fixed at 500 mT, and the temperature was varied from 0 to 300 K. The magnetic moment showed marginal temperature dependence, although the changes were almost negligible compared with those of electromagnetic materials. Figure 4.11 shows that the magnetic moment rapidly increased from 40 to 50 K, and then rapidly decreased after 70 K. This was caused by the oxygen remaining in the capsule. Oxygen is paramagnetic and shows magnetism at around 50 K. Thus, it was believed that oxygen was still present because the sample did not completely fill the capsule.
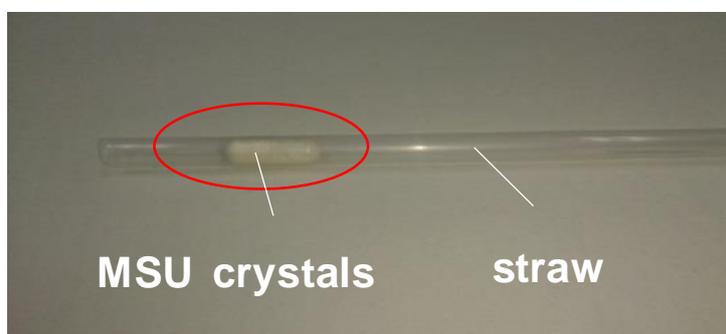
Fig. 4.9. Measurement sample.
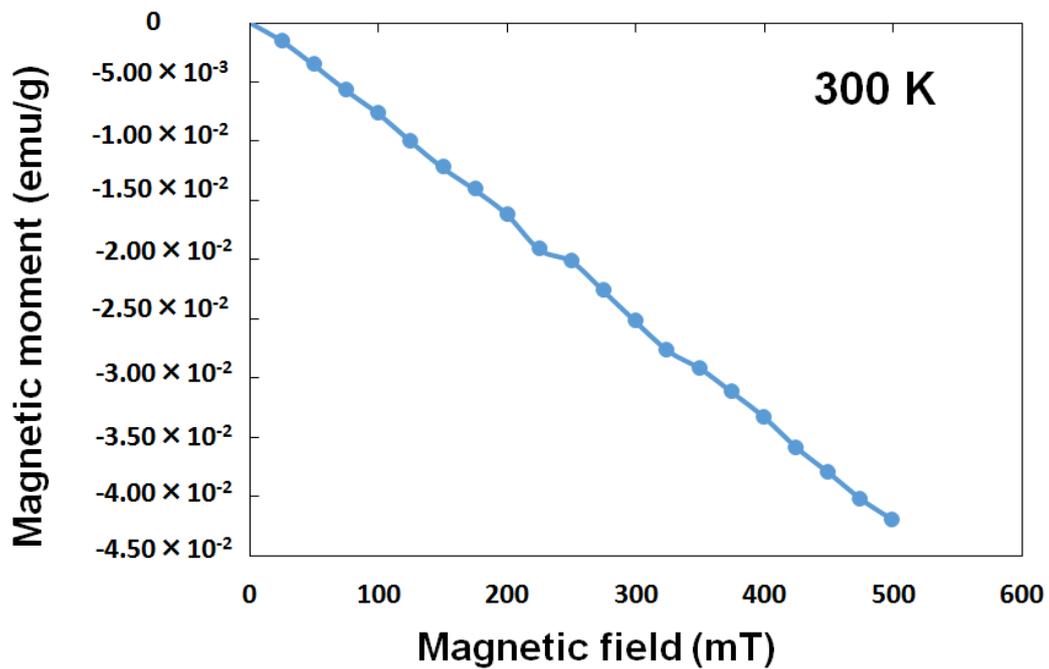
Fig. 4.10. Magnetic susceptibility of the MSU crystal to the magnetic field dependence.
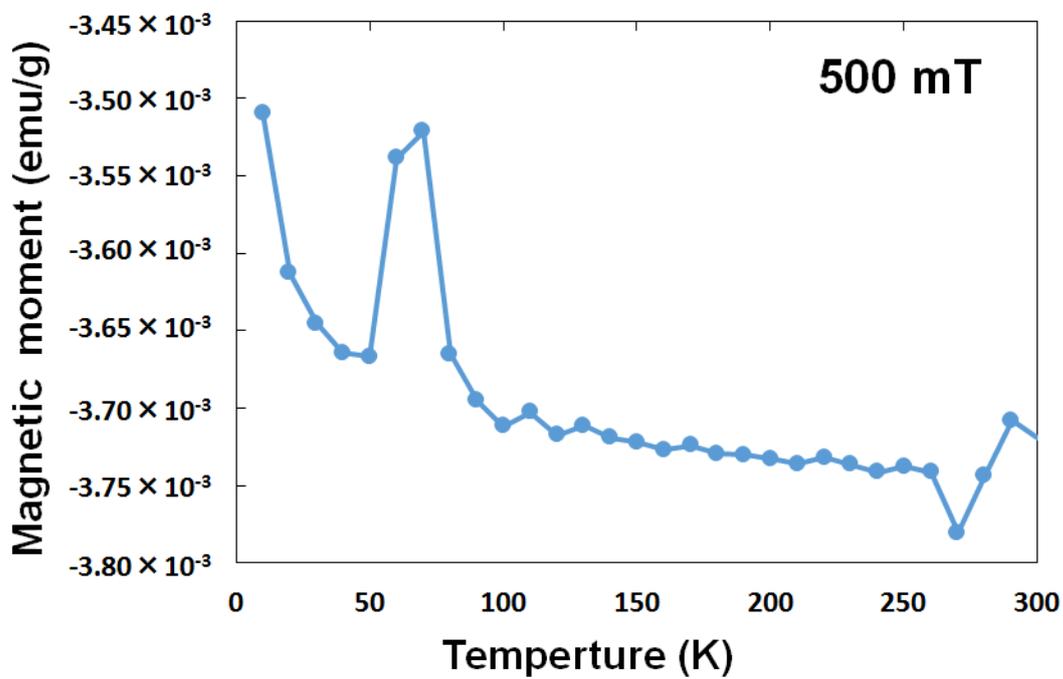
Fig. 4.11. Magnetic susceptibility of the MSU crystal to the temperature dependence.

4.3.3 *Microscope Observation of the Magnetic Orientation*

Figure 4.12 shows a photograph of MSU crystals prepared by dissolving 30 mg uric acid powder (98% purity) in 8.0 mL sodium hydroxide (0.025 mol/L) (*i.e.*, a uric acid concentration of 3.75 mg/mL) under a magnetic field strength of 500 mT. The crystals rotated following the magnetic field direction when a magnetic field was applied to MSU crystals in random directions.

Figure 4.13 shows the relationship between angular velocity and the length of the crystal, and indicates that the longer the length of the crystal, the smaller the angular velocity. Figure 4.14 shows the relationship between the angular velocity and the magnetic field strength when the length of the crystal was 12 μm, and indicates that the smaller the magnetic field, the smaller the angular velocity. Figure 4.12 shows that the crystal is oriented in the magnetic field direction, but the long axis of the crystal is not oriented completely vertical to the magnetic field direction but is slightly inclined. We supposed that the long direction of the crystal attempted to orient diagonal to the magnetic field direction, but the rotation was limited by friction with the cover glass because of the large size of the crystal. As mentioned in Chapter 4.3.1, we precipitated small and uniform crystals by adding blood serum, and confirmed the detailed orientation behavior. The long axis of the crystal was not vertical but slightly inclined to the magnetic field direction. The angle between the length direction and the vertical direction of the image was defined as θ. Figure 4.16(a)–(f) shows the angular distribution of the crystal under magnetic fields of 500, 400, 300, 200, 100, and 50 mT. The crystal was oriented $\pm23°$ from the mean under the magnetic field of 500 mT. The crystal angular distribution showed a large variance when the magnetic field strength was small. Thus, the rotation of the crystal was not limited by friction with the cover glass and the length of the crystal was oriented to the magnetic field direction. Figure 4.17 shows the relationship between the mean angle of the MSU crystal and the magnetic field strength. The crystal rotated to a direction of about 20° under magnetic fields of 400 and 500 mT. For magnetic fields between 100 and 300 mT, the crystal rotated to a direction of about 30°.The MSU crystal was clearly oriented with the magnetic field for magnetic fields of 100–500 mT. However, in a magnetic field of 50 mT, the crystal showed no change.

Ambient

Magnetic field 500 mT
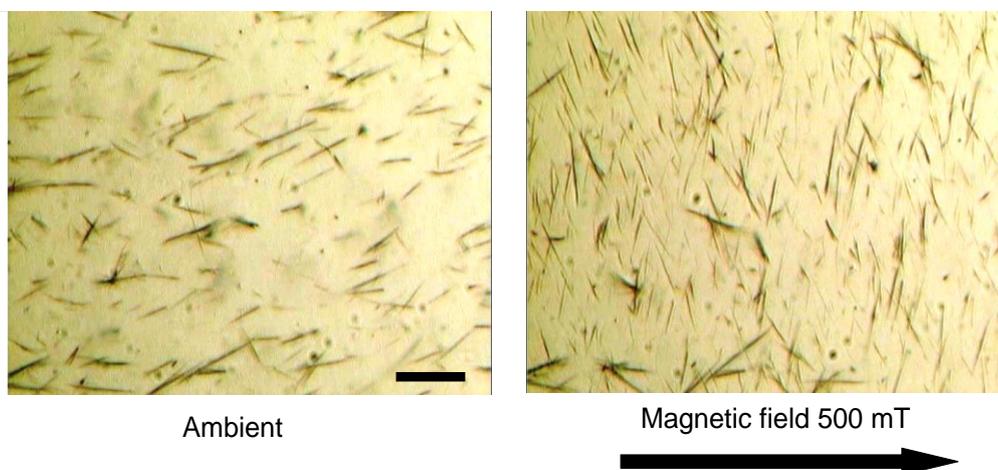
Fig. 4.12. Microscopic images showing the diamagnetic orientation in MSU crystals under the ambient fields and magnetic field of 500 mT.
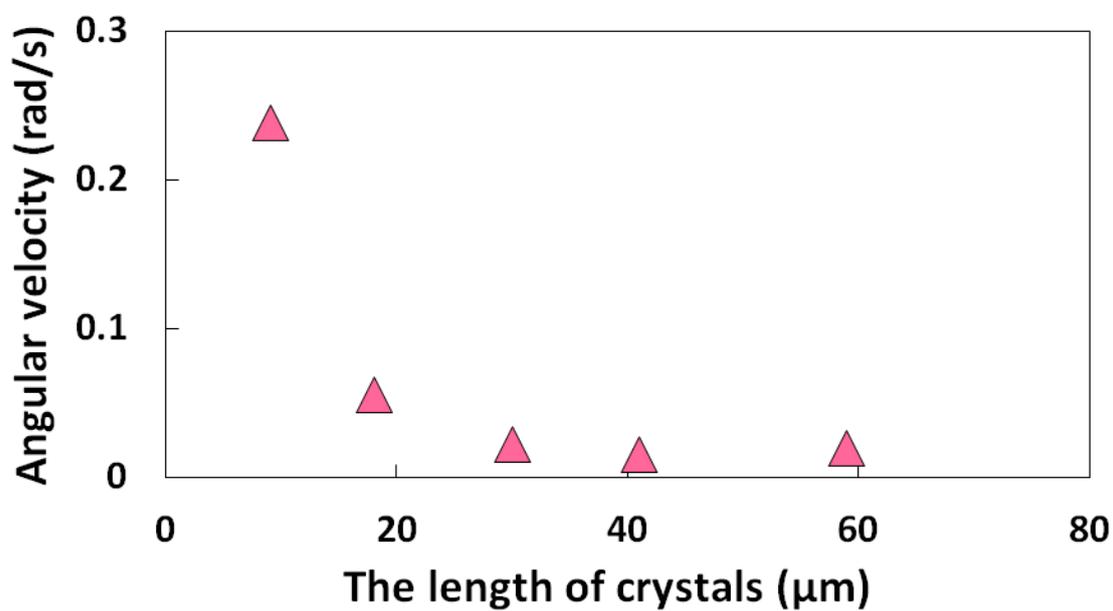

Fig. 4.13. The angular velocity with respect to the length of the crystal.
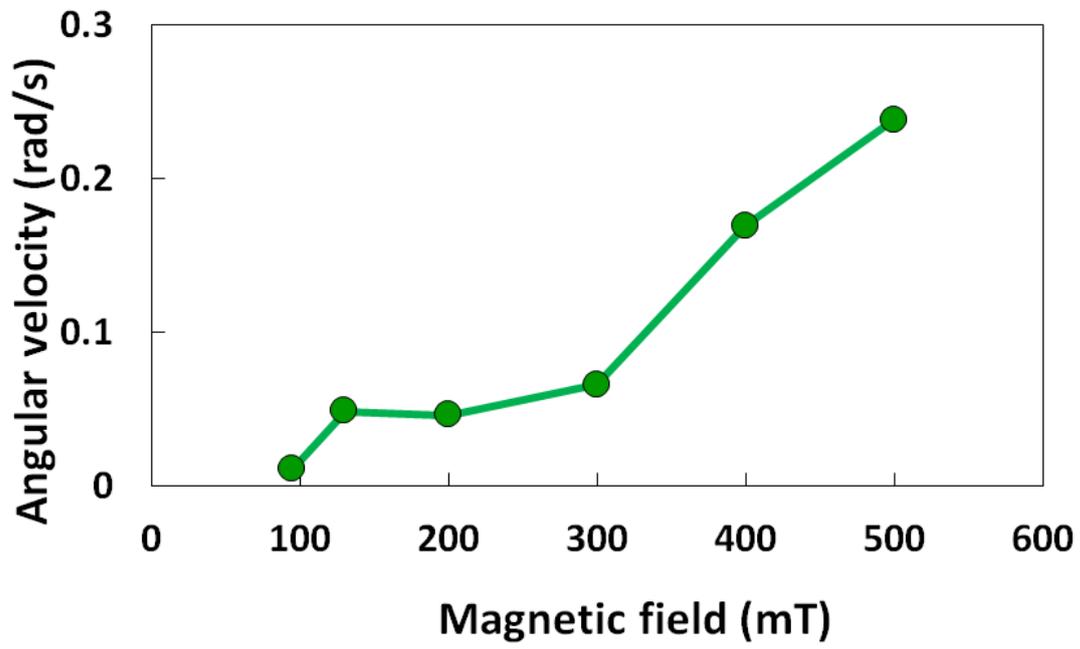
Fig. 4.14. The angular velocity with respect to the magnetic field.
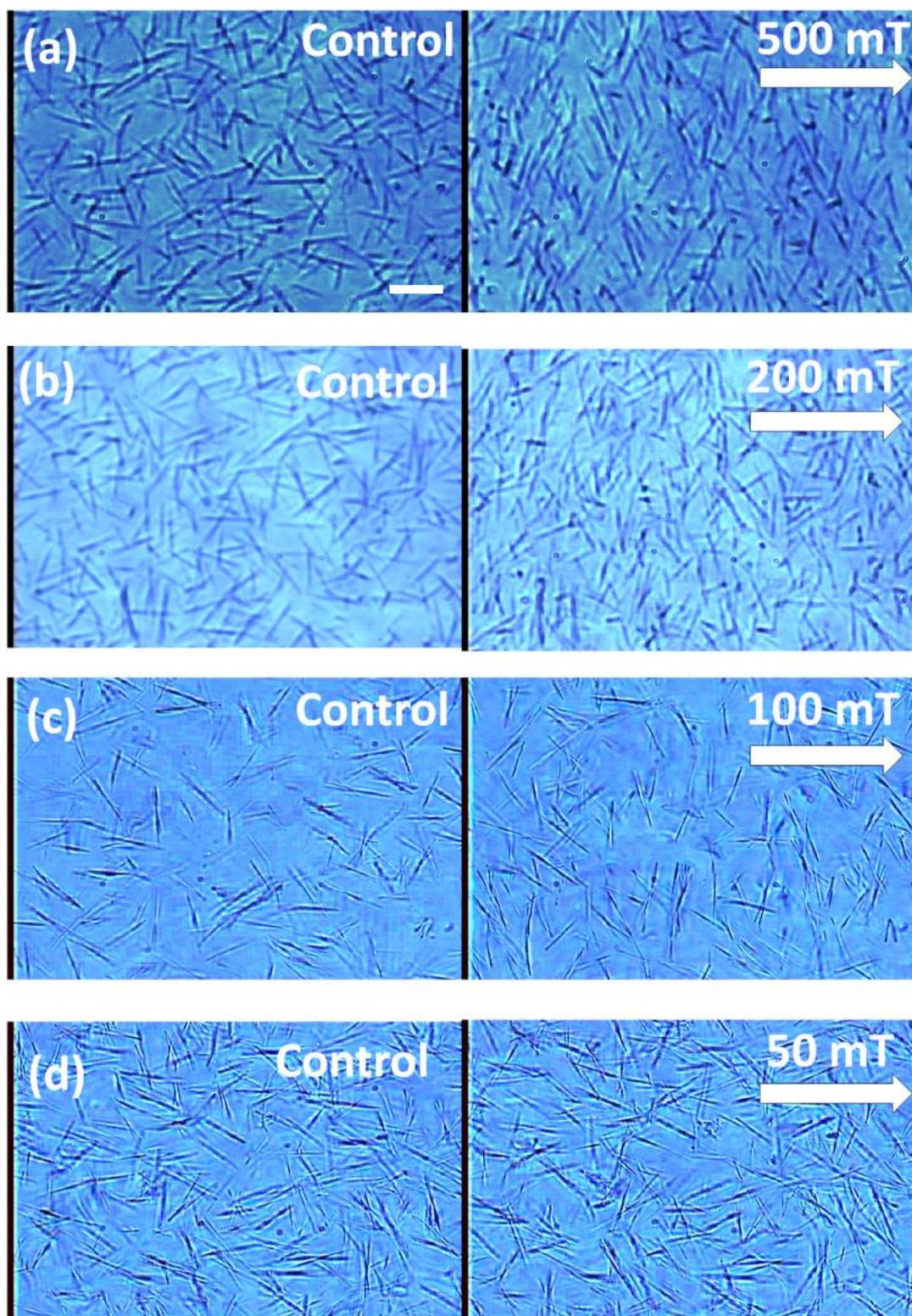
Fig. 4.15. (a)-(d) Microscopic images showing the magnetic orientation of regular size MSU crystals under magnetic fields of 50, 100 200 and 500 mT. Bar, 10 µm.
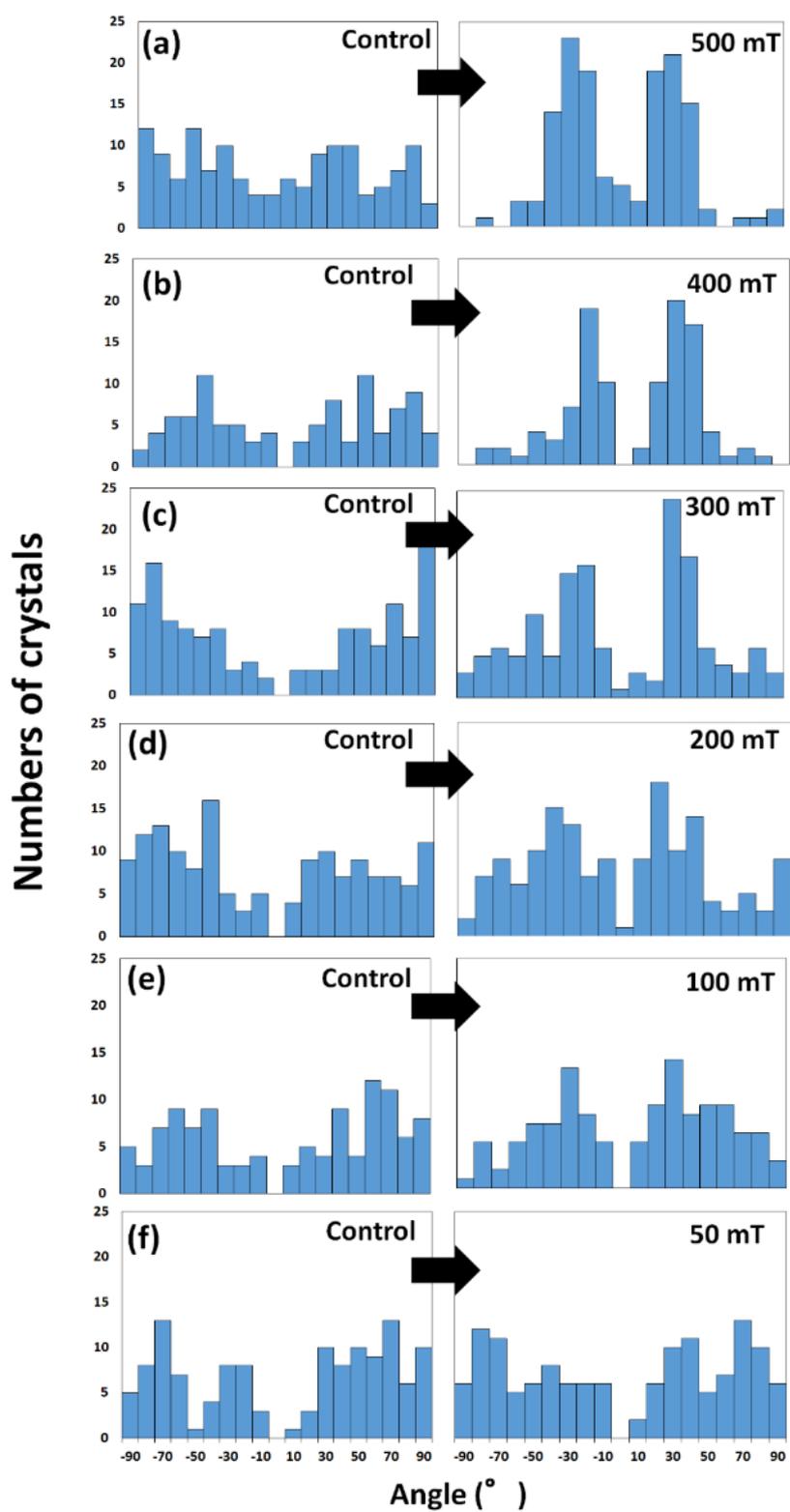
Fig. 4.16. (a)-(f) Orientational angle distributions under magnetic fields of 50, 100 200, 300, 400 and 500 mT.
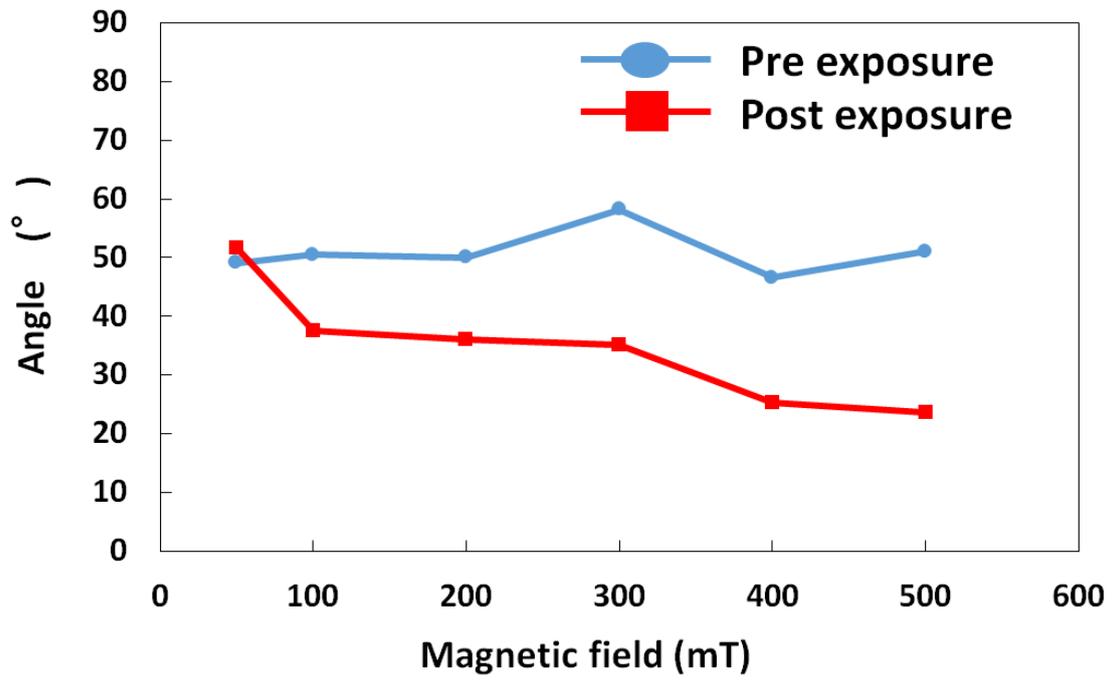
Fig. 4.17. The mean angle with and without magnetic field for each magnetic field.

4.3.4 *Magnetic Orientation and Reflected Light Intensity Changes*

Next, to verify magnetic orientation a high sensitivity on a widespread basis, we measured the reflected light over a time course change from the suspension of floating of MSU crystals. Figure 4.18 shows configuration for measurement system of reflected light intensity. The reflected light intensity was continuously measured both with and without applied magnetic fields of several hundred mT, as shown in Figure. 4.19(a)-(f). The results clearly show that the reflected light intensity increased under magnetic fields of between 100 mT and 500 mT when the magnetic field was switched on, and that it gradually decreased as the magnetic field was switched off. In a case of 500 mT, the light intensity increased 1.3 % from free exposure, and it decreased 2.2 % with post exposure. Additionally, the light intensity decreased as the magnetic field decreased. When the magnetic field was 95 mT, the light intensity increased 0.2 % from free exposure, and it decreased 0.1 % at post exposure. Figure 4.20 shows the change in the ratio of light intensity to the magnetic field. It increases as the magnetic field increases. We were able to detect the magnetic orientations of these needle-like MSU crystals quantitatively.

This indicates that the uric acid molecule that the forms part of the MSU crystal was diamagnetism and that the MSU crystal contain neither paramagnetic nor ferromagnetic. It can be concluded that the crystal orientation is induced by the diamagnetic anisotropy of these crystals.
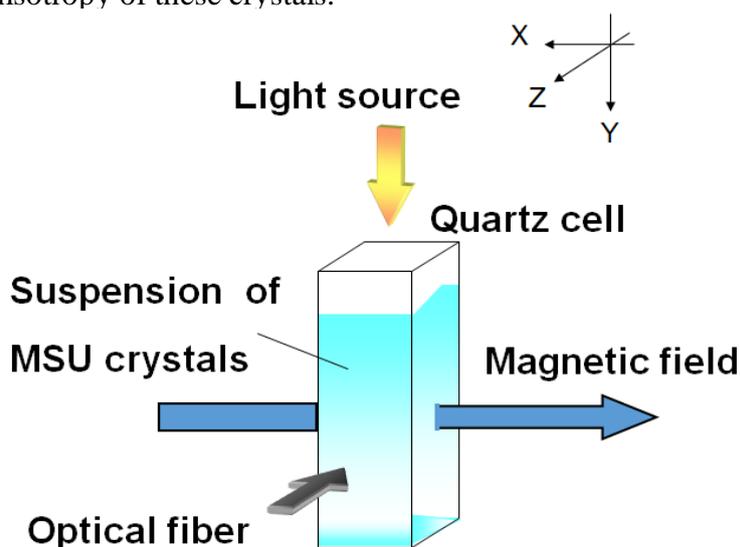

Fig. 4.18 Measurement system
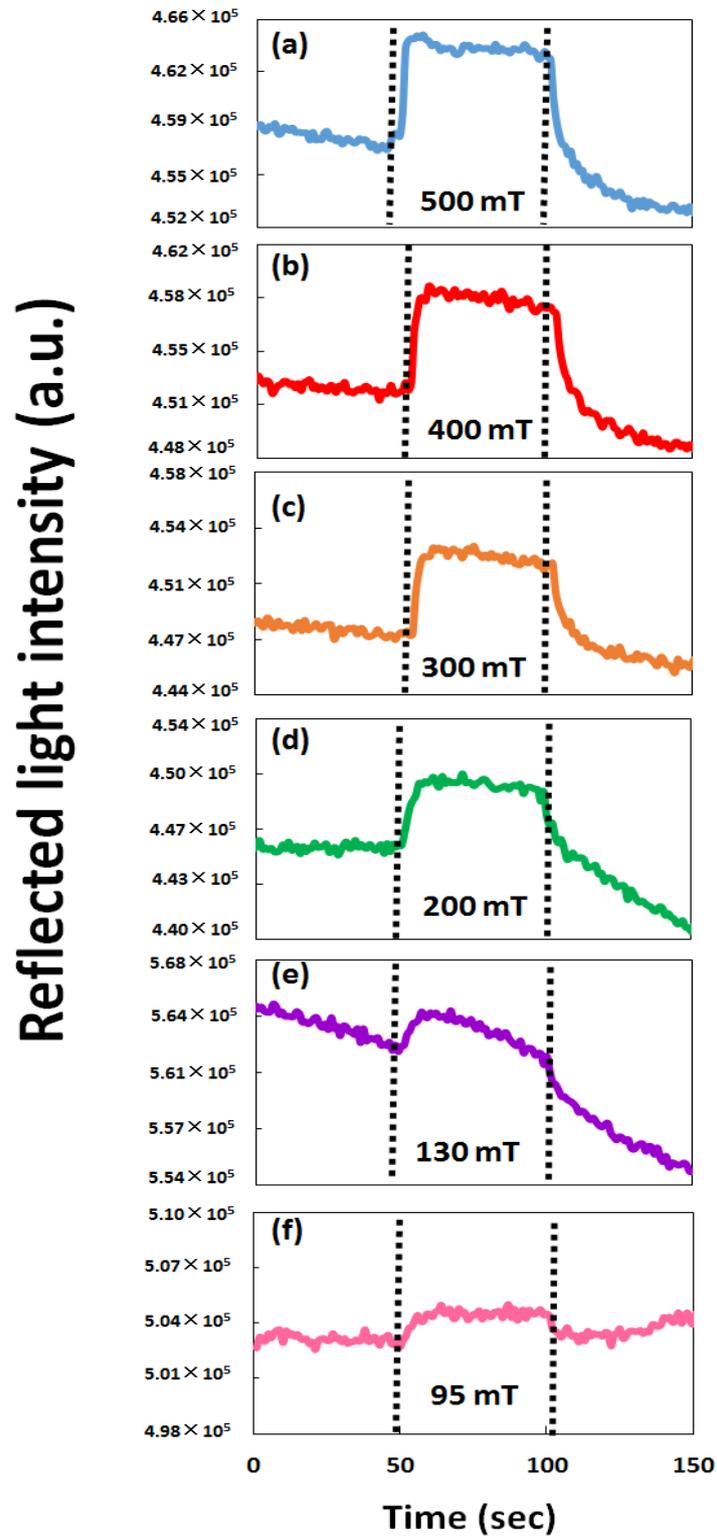
Fig. 4.19(a)-(f) Time course of the reflected light intensity from MSU crystals with and without magnetic field of 100, 130, 200 300 400 and 500 mT.
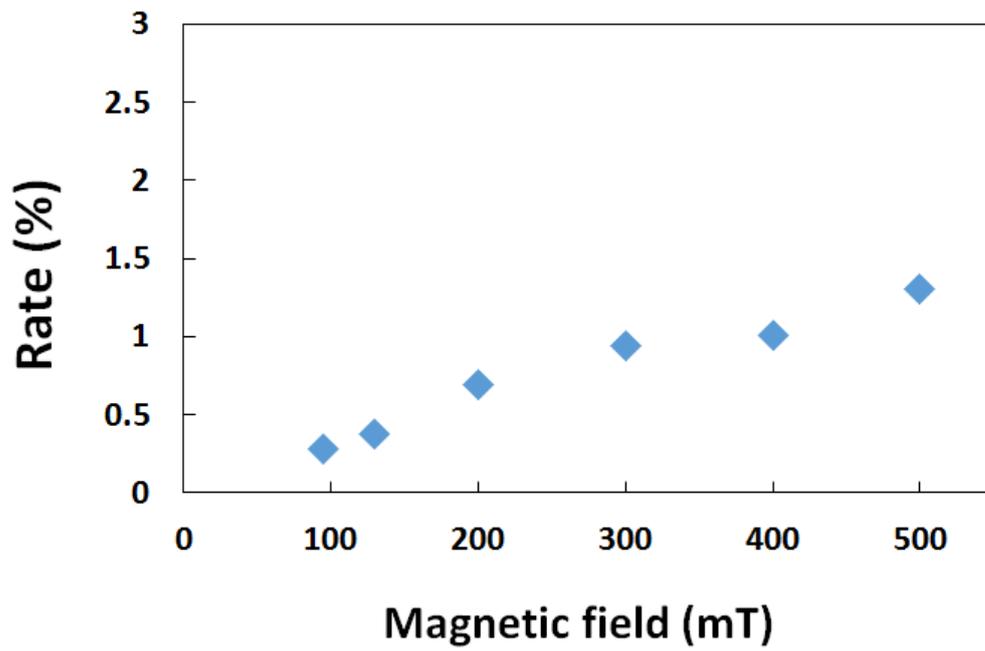
Fig. 4.20. Magnetic field dependence in the rate of change of the reflected light intensity.

4.3.5 Rotational Behaviors and Reflected Light Intensity Changes

In the above experiments, the magnetic effect of the MSU crystals was investigated using microscope observations. However, the crystals were sealed in a microchamber, which was consisted of a cover glass window and a rubber sheet. Therefore, the three-dimensional behavior of the crystals was limited. To investigate the three-dimensional orientation behavior, we performed light intensity measurements by varying the light, magnetic field, and observation directions.

We observed the floating MSU crystals in the quartz cell using the CCD microscope as shown in Figure 4. 21(a). Figure 4. 21(b) shows the photograph of MSU crystals in the quartz cell when the magnetic field of 500 mT is applied. The gravity direction is Z axis, and magnetic direction is Y axis. The c-axis of the MSU crystal was clearly rotted to the Y axis around X axis. As the result of angular distribution of the crystal under magnetic fields, the crystal was oriented $\pm 15^{\circ}$ from the mean under the magnetic field of 500 mT.

According to the literature [9-11], the large flat side face of the MSU crystals can be assigned by optical and X-ray as the (010) plane, which is the reflecting plane. The illuminated MSU crystals are oriented in a definite direction according to magnetic torque by applying a magnetic field. The reflected light intensity of the crystal changed depending on the orientation. The reflected light intensity was highest when the reflecting plane was facing the observation direction. In contrast, the reflected intensity was lowest when the reflecting plane was not facing the observation direction. We measured the change in the reflected light intensity from the suspension of floating MSU crystals. The reflected light intensity was continuously measured both with and without an applied magnetic field of 500 mT. The orientation behavior of the MSU crystals was estimated by varying the irradiation and observation directions, and the reflected light intensity was measured for a total of 15 directions.

Figures 4.22(a), 4.23–4.26(a) and (c), 4.29(a), 4.28–4.29(a) and (c), and 4.30(a) show the configurations used for the measurement of the reflected light. The obtained MSU crystal suspension was transferred to an optical cell ($1.0 \times 1.0 \times 4.5$ mm^3). Spectroscopic measurement of the reflected light was carried out in a fiber-optic measurement system. The magnetic field was generated by an electromagnet, which is shown in Figure 3.3. The light source used was a halogen lamp, which provided a continuous stream of light. The magnetic field, light source, and fiber-optic measurement system were orthogonal. Y axis is applied magnetic field direction, and Z axis is gravity direction. Figures 4.22(b), 4.23–4.26(b) and (d), 4.29(b), 4.28–4.29(b)

and (d), and 4.30(b) show the reflected light intensity of MSU crystals with and without an applied magnetic field of 500 mT. Figures 4.22(c), 4.23–4.26(e), 4.27(c), 4.28–4.29(e), and 4.30(c) show the model of the MSU crystal in the optical cell.

The direction of the magnetic field was set to the Y axis. Figure 4.22(b) shows that the reflected light intensity was decreased when the magnetic field, light, and observation direction were parallel. The reflected light intensity should be high if the (010) plane is vertical to the magnetic field. Therefore, the (010) plane was not vertical to the magnetic field direction in Figure 4.22(b). In addition, the experimental systems shown in Figures 4.23(b) and (d), and 4.24(b) and (d) resulted in relatively low reflected light intensity. The reflected light intensity is high when the (010) plane is vertical to the magnetic field and tilted around the Z axis. Therefore, it was not oriented in this direction in these systems. The experimental systems shown in Figures 4.25(b) and (d), and 4.26(b) and (d) resulted in relatively low reflected light intensity. The reflected light intensity is high when the (010) plane is tilted toward the light incidence and observation directions. Figure 4.27(b) shows that the reflected light intensity was high when the light and observation directions were parallel to the Y axis. Therefore, the (010) plane was parallel to the magnetic field direction. Figures 4.28(b) and (d), and 4.29(b) and (d) show that the reflected light intensity was high when the magnetic field, light, and observation directions were orthogonal. This means that the long axis of the crystal was not perfectly parallel to the Z axis, the (010) surface was parallel to the magnetic field, and the crystal was tilted around the Y axis. Figure 4.30(b) shows that the reflected light intensity was decreased when the light direction was parallel to the observation direction (Z axis). The crystal was tilted around the Z axis, as shown in Figures 4.30(e) and 4.29(e). However, this shows that it was only slightly tilted. For the MSU crystals, the (010) plane of the crystal was oriented parallel to the magnetic field direction. Moreover, the length direction (c axis) of the crystal oriented to slightly tilt around the Y-axis direction. Thus, we determined the orientation behavior of the MSU crystal from measurement of reflected light intensity.

In Figure 4.23, despite being measured from the same axis, there are differences in the change of reflected light intensity because the detecting fiber was fixed to a mirror in Figure 4.22(a) and (c). The change of the reflected light intensity was about half when not fixed to a mirror. The same is true in Figures 4.25, 4.27, and 4.28. In Figures 4.24 and 4.29, compared with the reflected light intensity measured from the top of the cell, the reflected light intensity measured from the bottom of the cell is very small. It is considered that the detection range of the fiber narrowed because MSU crystals precipitated on the bottom of the cell.

Figure 4.31 shows the orientation behavior of the MSU crystals was inferred from the results of reflected light intensity change measurement. Combining these results with the microscope observations, the *c* axis of the crystal inclination was ±15° to *Y* axis around the *Z* axis, the (010) plane was perpendicular to the *X* axis, and tilted to *X* axis around the *Y* axis. From the above discussion, the MSU crystals were found to be oriented in three dimensions (Figure 4.32).
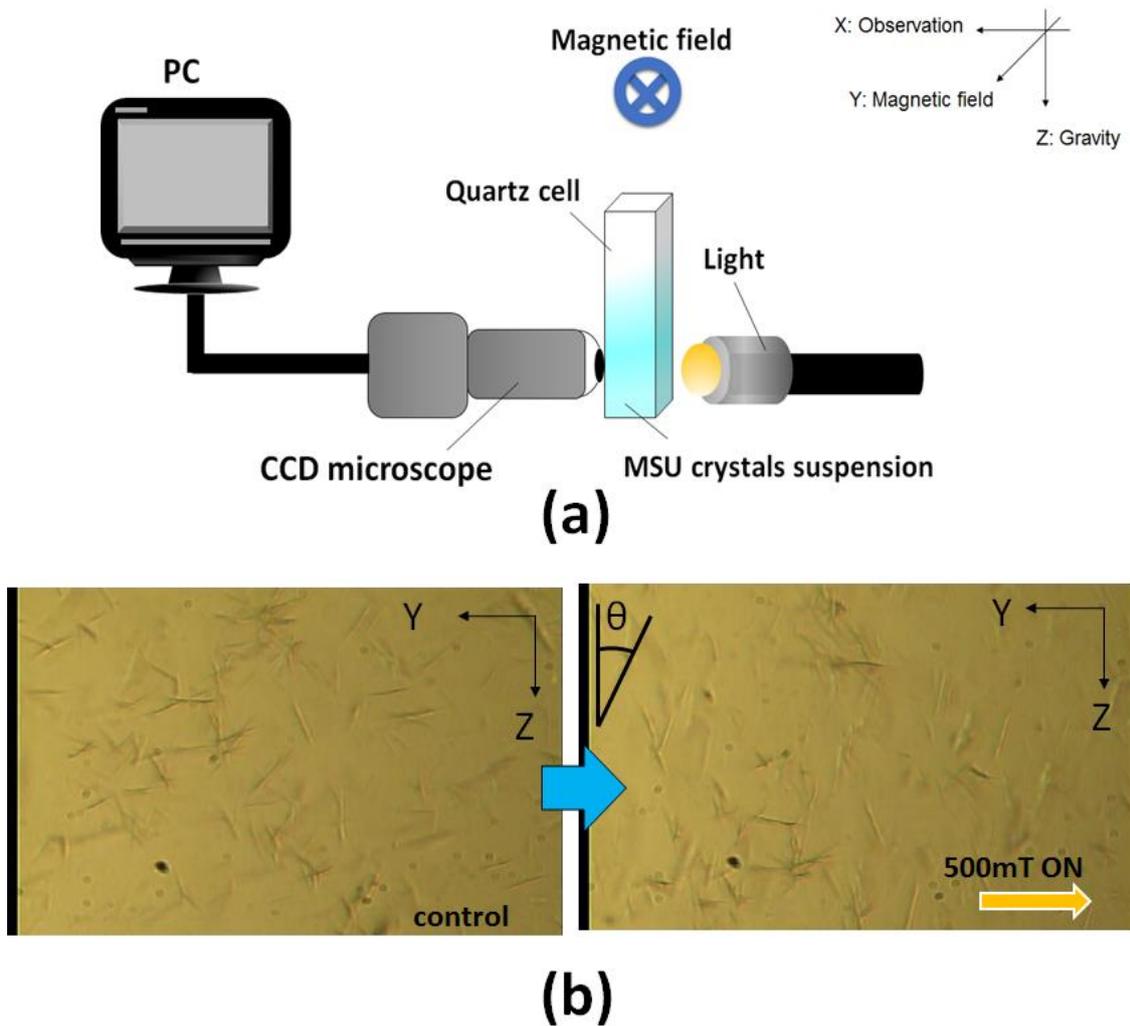

Fig. 4.21 (a) A diagram of measurement system (b) A photograph of floating MSU crystal in quartz cell with and without magnetic field.
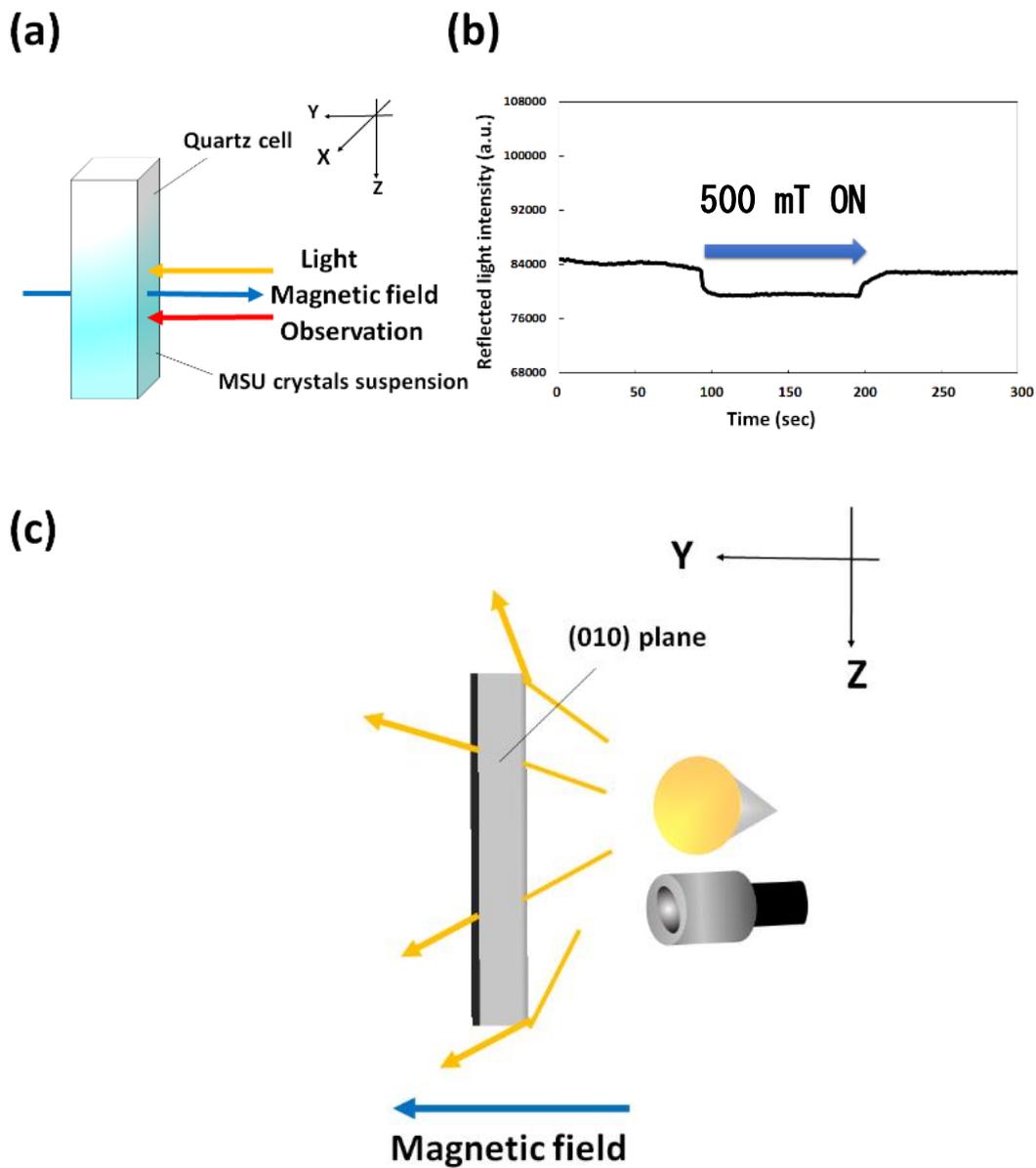
Fig. 4.22. (a) Configuration for measurement of reflected light intensity under the conditions that magnetic direction, light direction and observation direction is Y axis. (b) Time course of the reflected light intensity from MSU crystals with and without magnetic field of 500 mT. (c) The correct model of MSU crystal behavior under condition.
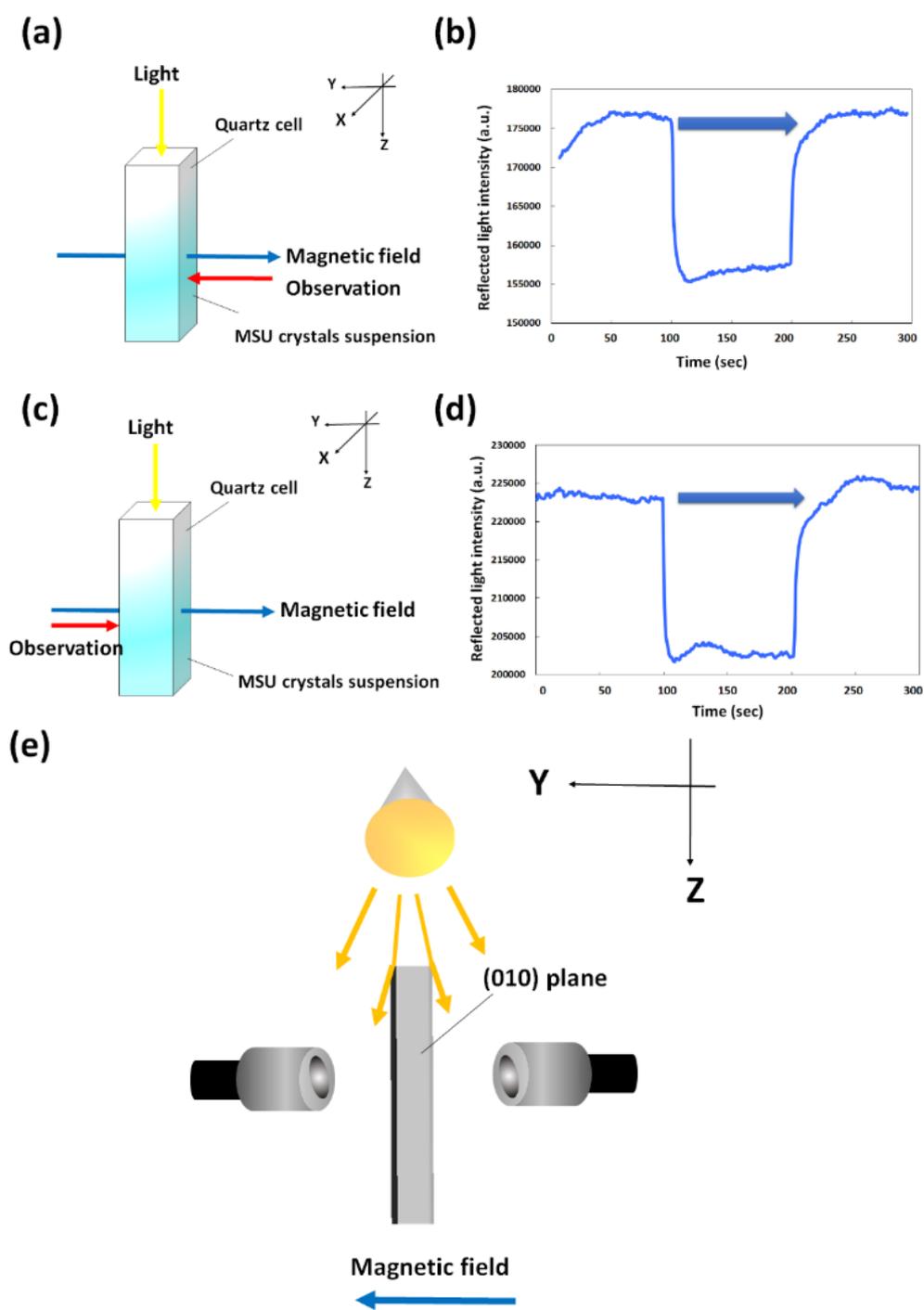
Fig. 4.23. (a) Configuration for measurement of reflected light intensity under the conditions that magnetic direction, light direction and observation direction is Y axis. (b) Time course of the reflected light intensity from MSU crystals with and without magnetic field of 500 mT. (c) The correct model of MSU crystal behavior under condition.
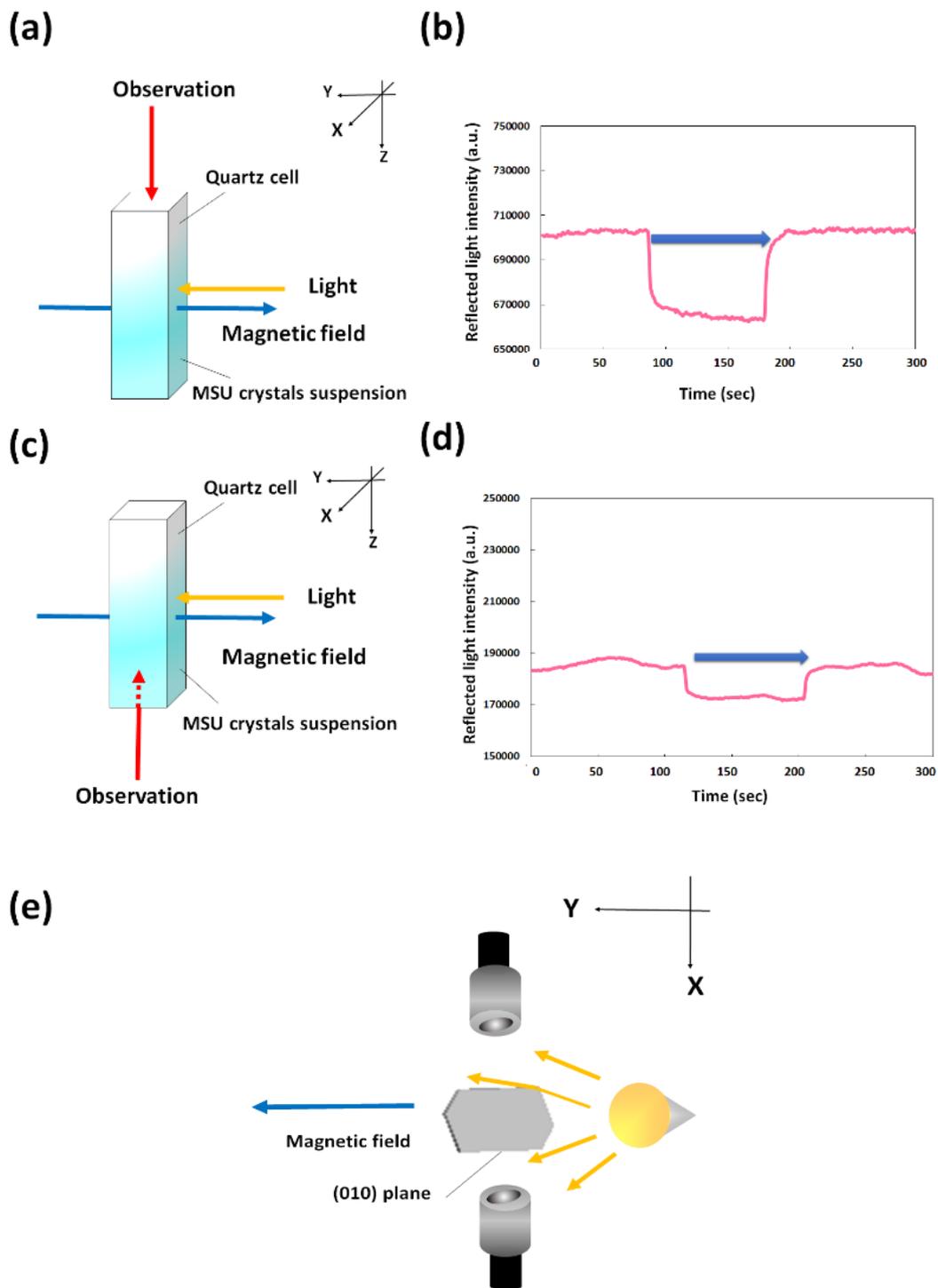
Fig. 4.24. (a)(c) Configuration for measurement of reflected light intensity under the conditions that magnetic direction, and light direction is Y axis and observation direction is Z axis. (b)(d) Time course of the reflected light intensity from MSU crystals with and without magnetic field of 500 mT. (e) The correct model of MSU crystal behavior under condition.
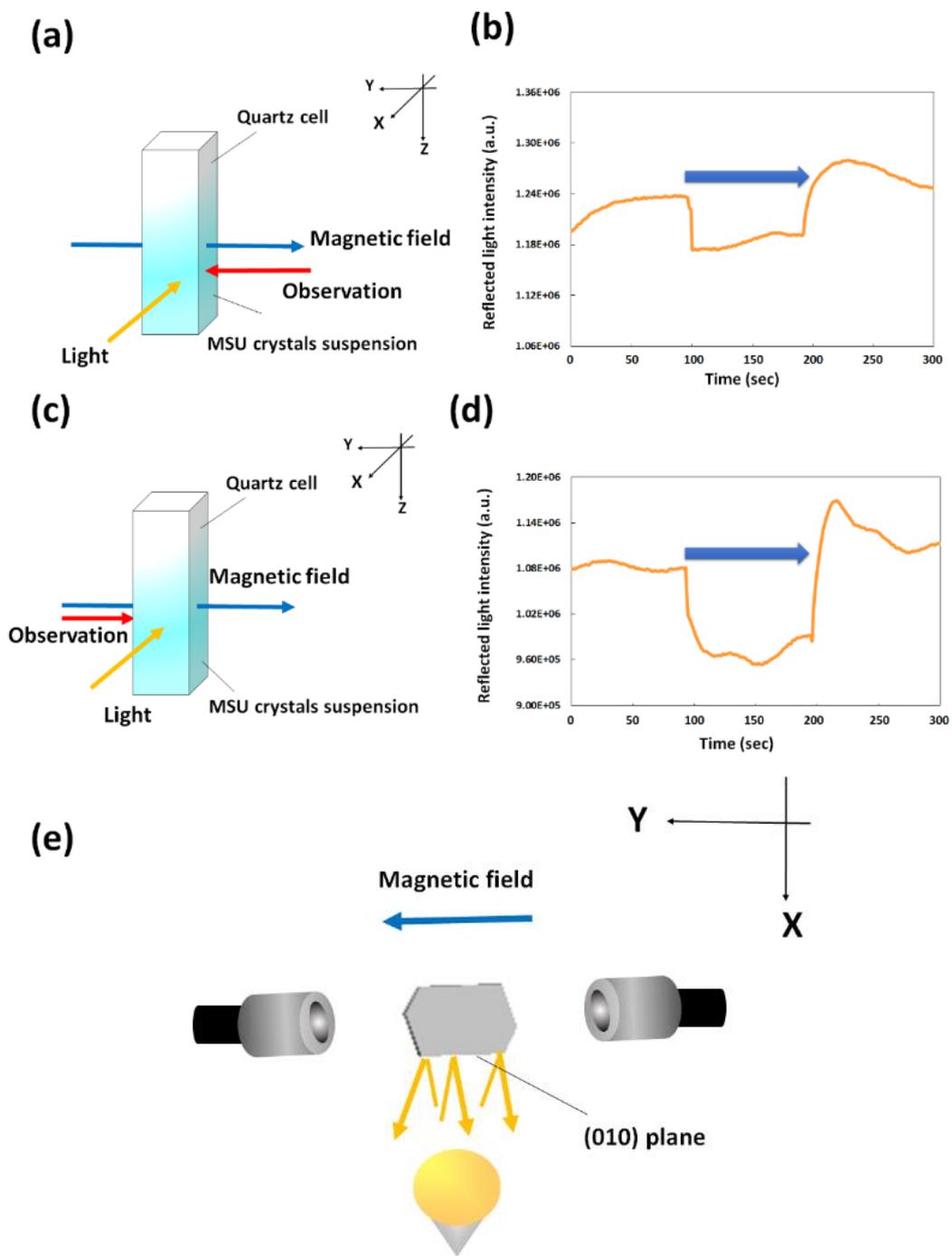
Fig. 4.25. (a)(c) Configuration for measurement of reflected light intensity under the conditions that magnetic direction and observation direction is Y axis and light direction is X axis. (b)(d) Time course of the reflected light intensity from MSU crystals with and without magnetic field of 500 mT. (e) The correct model of MSU crystal behavior under condition.
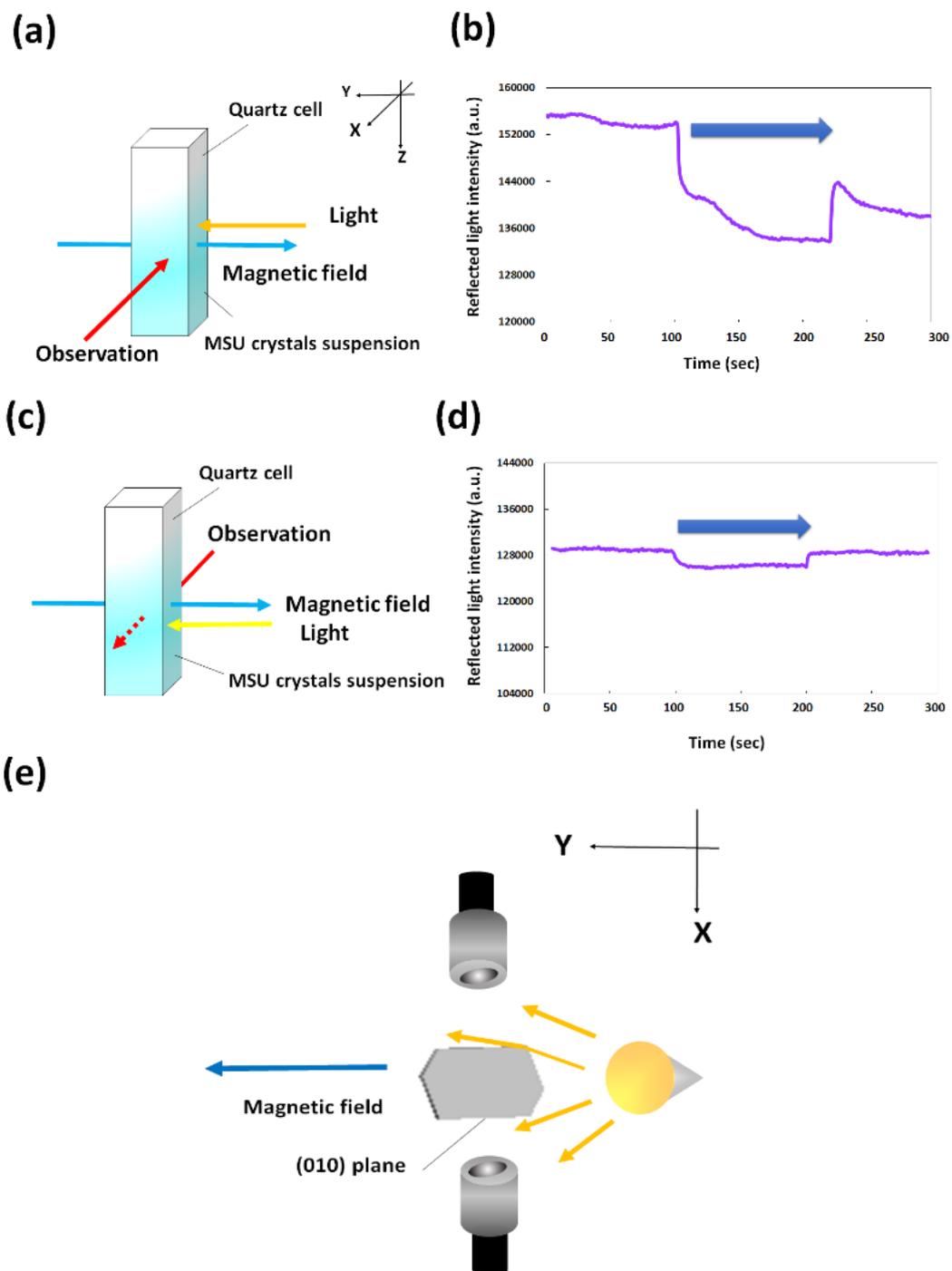
Fig. 4.26. (a)(c) Configuration for measurement of reflected light intensity under the conditions that magnetic direction and light direction is Y axis and observation direction is X axis. (b)(d) Time course of the reflected light intensity from MSU crystals with and without magnetic field of 500 mT. (e) The correct model of MSU crystal behavior under condition.
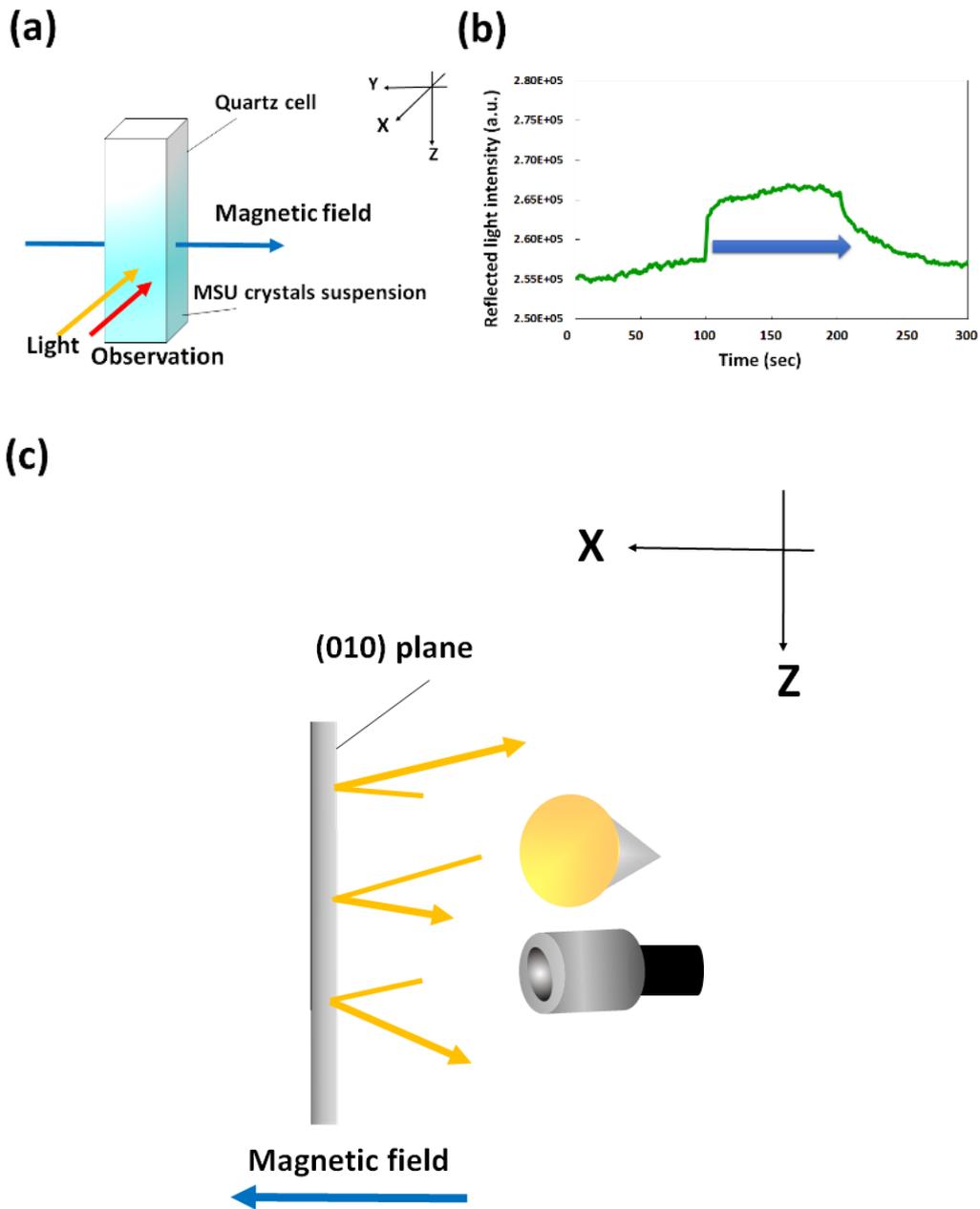
Fig. 4.27. (a) Configuration for measurement of reflected light intensity under the conditions that magnetic direction is Y axis and observation direction and light direction is X axis. (b) Time course of the reflected light intensity from MSU crystals with and without magnetic field of 500 mT. (c) The correct model of MSU crystal behavior under condition.
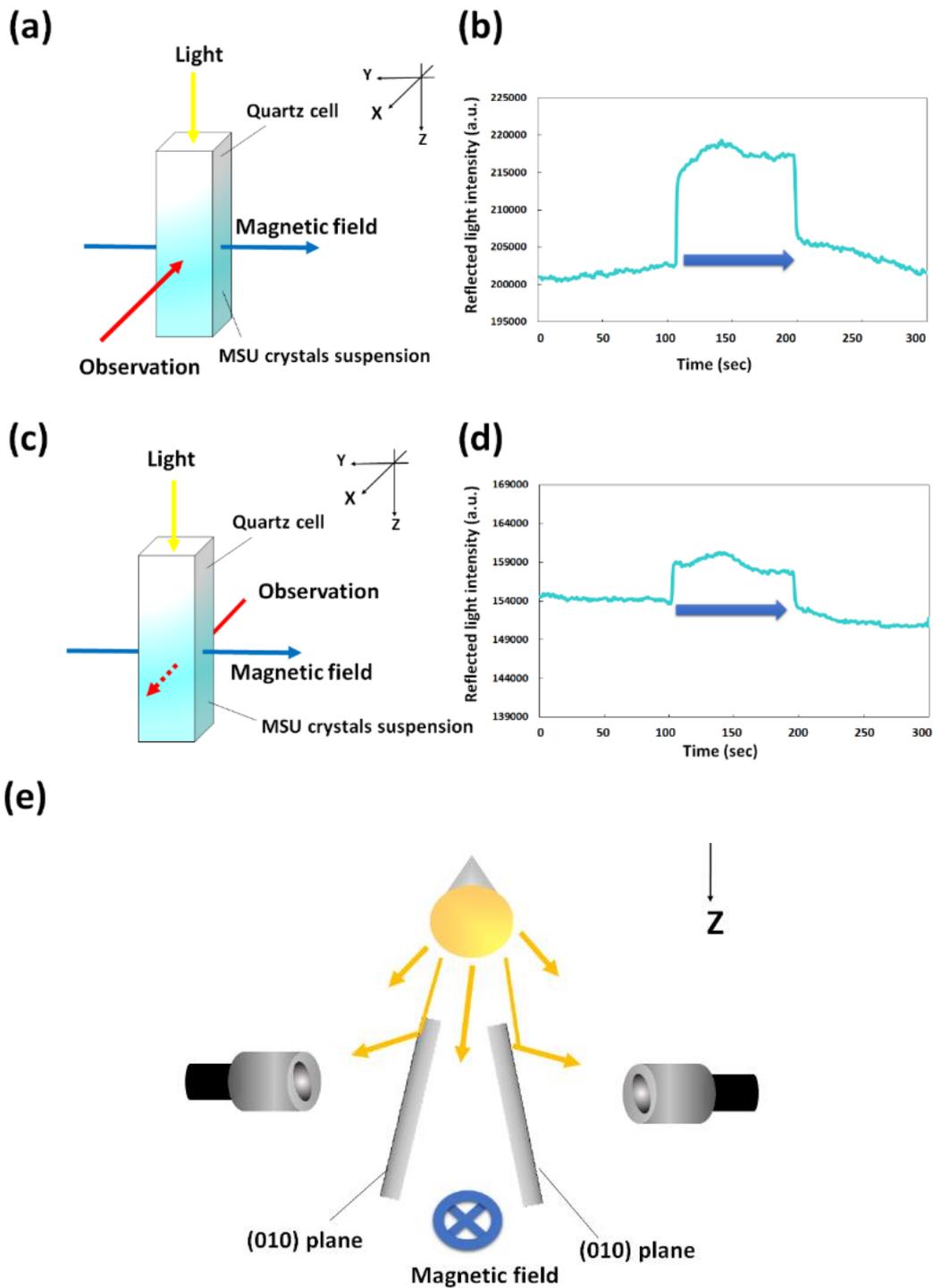
Fig. 4.28. (a)(c) Configuration for measurement of reflected light intensity under the conditions that magnetic direction is Y axis, light direction is Z axis and observation direction is X axis. (b)(d) Time course of the reflected light intensity from MSU crystals with and without magnetic field of 500 mT. (e) The correct model of MSU crystal behavior under condition.
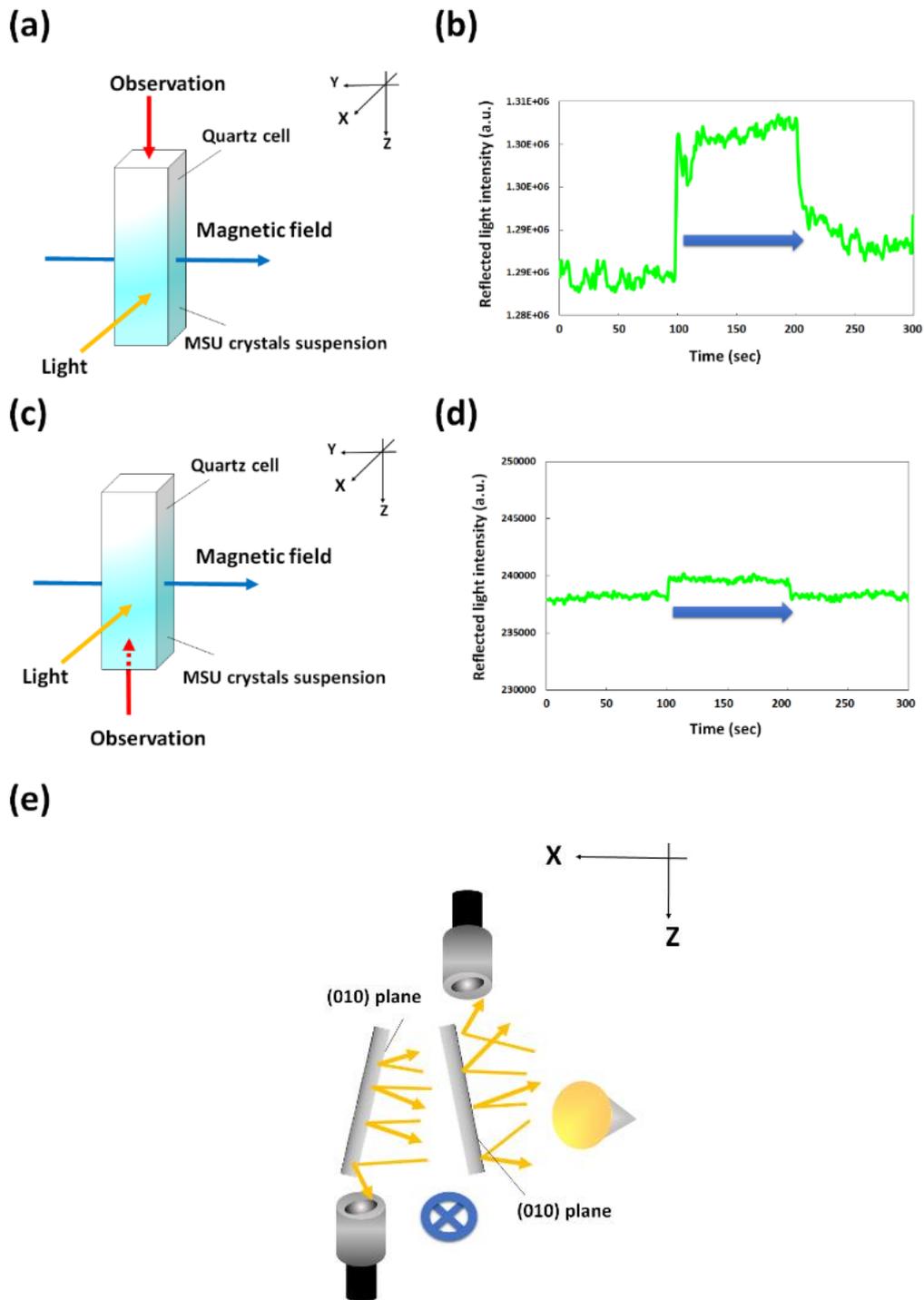
Fig. 4.29. (a)(c) Configuration for measurement of reflected light intensity under the conditions that magnetic direction is Y axis, light direction is X axis and observation direction is Z axis. (b)(d) Time course of the reflected light intensity from MSU crystals with and without magnetic field of 500 mT. (e) The correct model of MSU crystal behavior under condition.
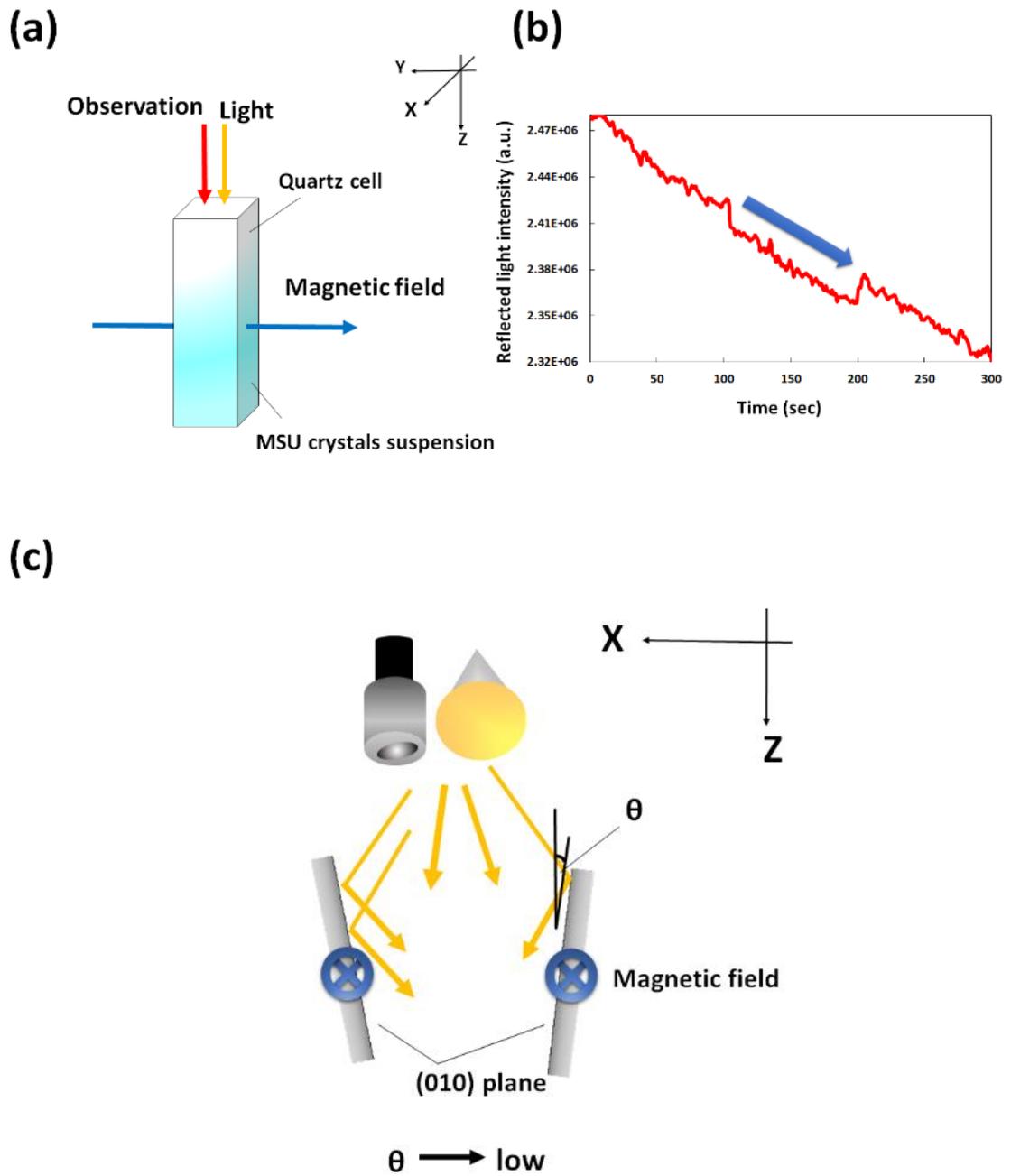
Fig. 4.30. (a) Configuration for measurement of reflected light intensity under the conditions that magnetic direction is Y axis and observation direction and light direction is Z axis. (b) Time course of the reflected light intensity from MSU crystals with and without magnetic field of 500 mT. (c) The correct model of MSU crystal behavior under condition.
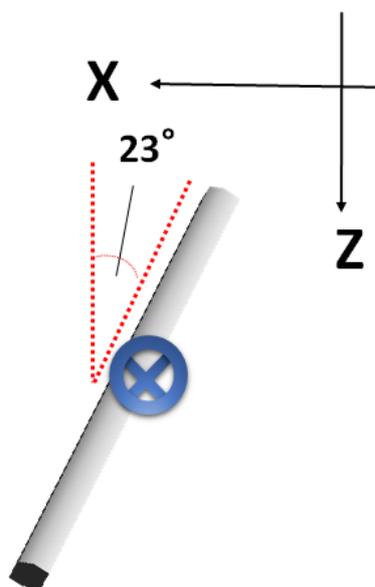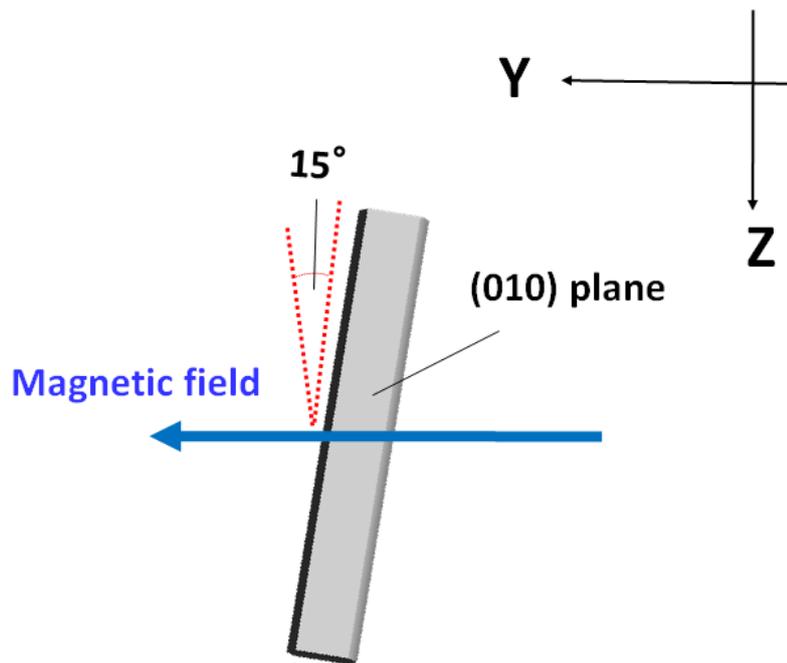
Fig. 4.31. The magnetic orientation behavior of MSU crystals was inferred from the results of reflected light intensity change measurement.
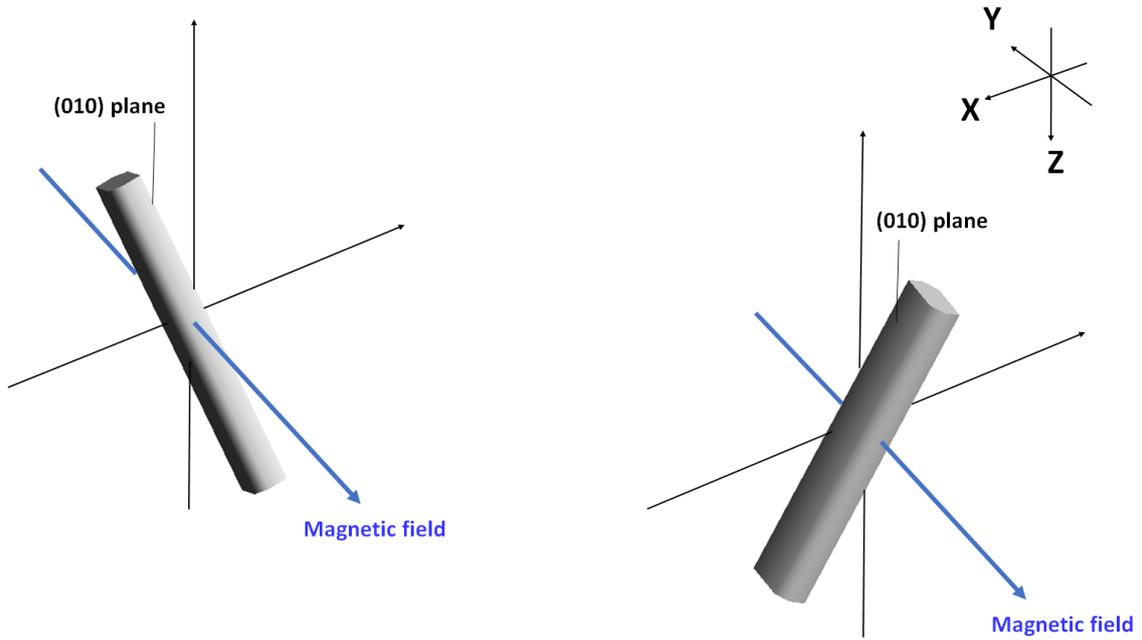
Fig. 4.32. The magnetic orientation of MSU crystal in three dimensional. Y axis: applied magnetic field direction. Z axis: gravity direction.

4.3.6　Reflected Light Intensity in the Near-infrared Region

　　The human body less absorbs light in near-infrared region. The degree of absorption and scattering varies according to the light wavelength and the living body. In particular, near-infrared light is absorbed by hemoglobin, a component of blood, and the degree of absorption varies when oxygen is attached to hemoglobin. Near-infrared spectroscopy (NIRS) is a technique of measuring the concentration of oxygenated and deoxygenated hemoglobin by measuring the degree by near-infrared radiation absorption. Optical measurement of a living tissue is performed by using a near infrared light at a wavelength of 700–900 nm. Visible light at 400–700 nm is strongly absorbed by the hemoglobin and other living body constituents. Because water absorbs light with wavelength longer than that of near infrared light, the light at more than 900 nm cannot penetrate in vivo. In contrast, near-infrared light at 600-800nm can easily penetrate into the body, and penetrates the tissue about 10 times deeper than the case of visible light. Therefore, near-infrared radiation is used for noninvasive probing of tissues because it can give information about deep tissues.

　　We investigated a method to detect the existence of MSU crystals inside the body in a noninvasive way using a magnetic field and light by exploiting the response of MSU crystals to a magnetic field. We measured the wavelength dependency of the reflected light intensity of MSU crystals (Figure 4.33). The reflected light intensity was the strongest when the wavelength was about 700 nm. Furthermore, the longer the wavelength of the light, the weaker the light intensity. The reflected light intensity was measured for light wavelengths of 700–750 nm (near-infrared light), and the measurements are shown in Figure 4.34. For 300 and 500 mT magnetic fields, the reflected light intensity changed about 4.3%. The reflected light intensity changed about 2.5% at 130 mT and about 1.7% at 95 mT. However, the reflected light intensity changed about 0.6% at 50 mT.
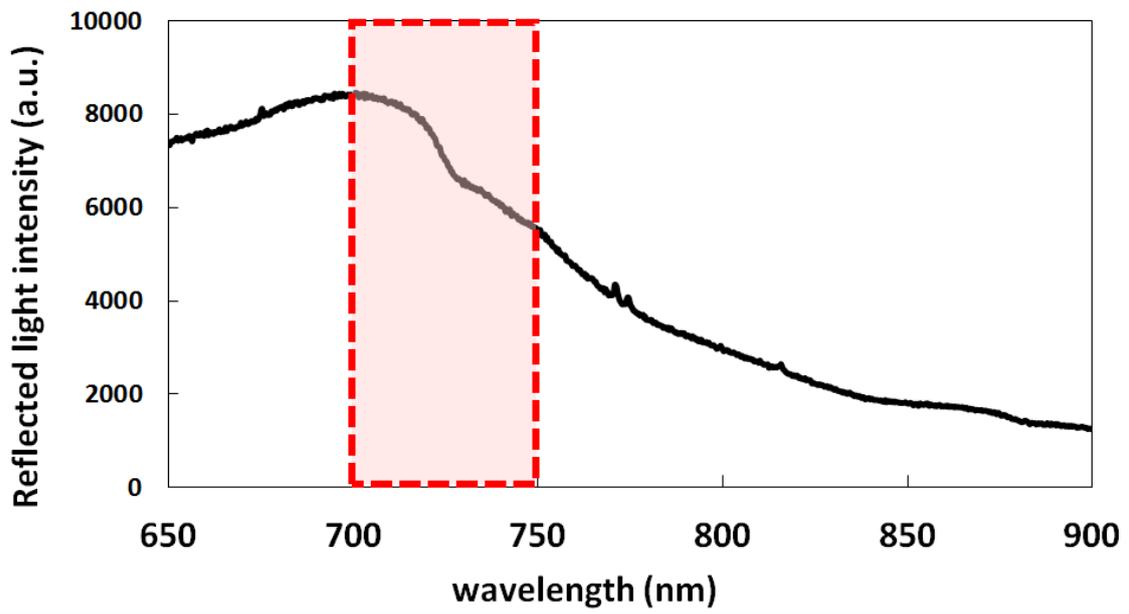
Fig. 4.33. The reflected light intensity to wavelength dependence.
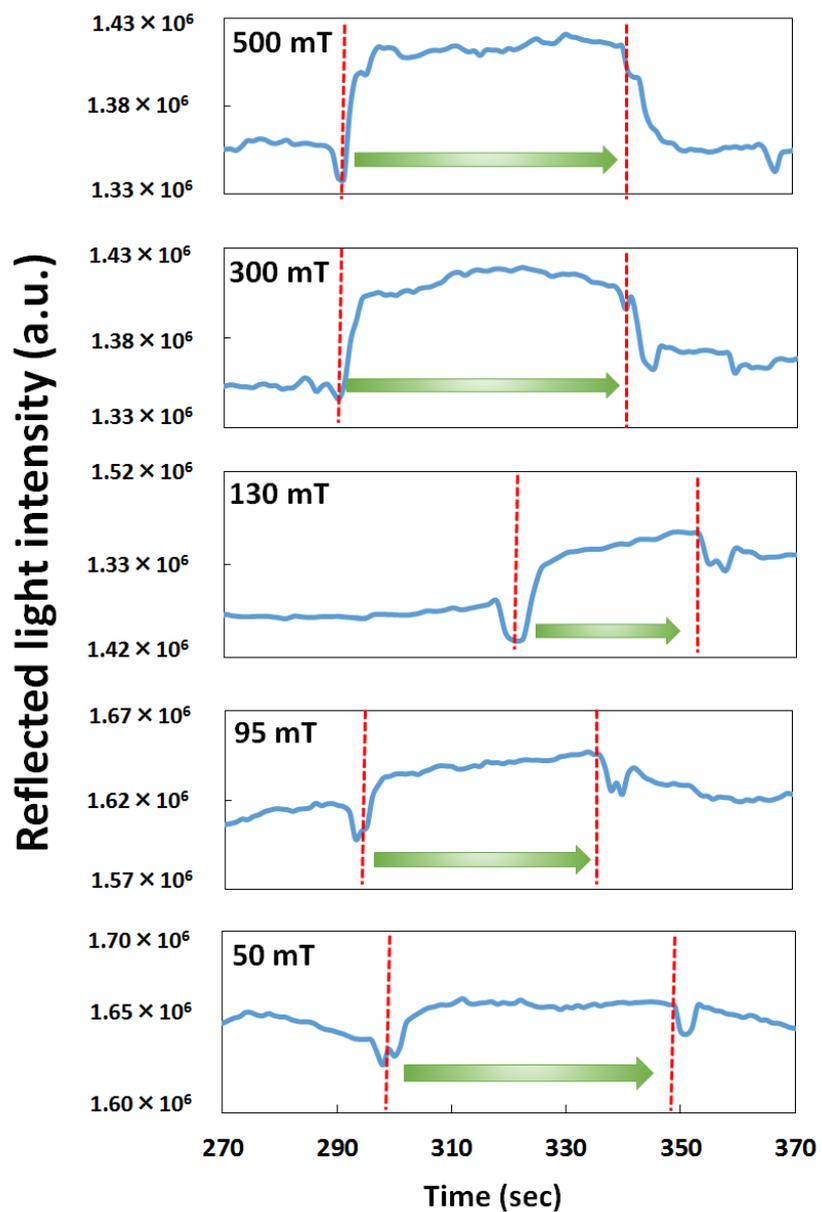
Fig. 4.34. Time course of the reflected light intensity between 700 and 750 nm from MSU crystals with and without magnetic field of 50, 95, 130, 300 and 500 mT under condition of Fig. 4.27(a).

It has been reported that small uniform MSU crystals form *in vitro* if serum or synovial fluid is added [17]. This study reported that serum and synovial fluid was obtained from patients with gout, and the obtained mean crystal lengths with serum and synovial fluid were 35 μm (SD: 12 μm) and 36 μm (SD: 10 μm), respectively [17]. It has been reported that the native mean crystal (i.e., formed *in vivo*) length is 11 μm (SD: 3 μm) [17]. In our study, we precipitated MSU crystals using calf serum *in vitro*. The obtained mean crystal length was 12 um (SD: 1.6 μm). Thus, using calf serum, the crystal size approaches the size of native crystals.

In microscope measurements, magnetic orientation occurred so that the *c* axis of the crystal was orthogonal to the *Z* axis. However, in reflected light intensity measurements, the *c* axis of the crystal was orthogonal to the *Y* axis. It is speculated that movement in the *z* axis was limited because the MSU crystals were sealed with a rubber sheet and cover glass in the microscope measurement.

In Chapter 4.3.2, we measured the magnetic moment using a SQUID. The obtained magnetic moment of MSU crystals was -4.2×10^{-2} emu/g when the magnetic field was 500 mT at room temperature (300 K). The bulk susceptibility of diamagnetic MSU crystal can be determined from the measured magnetic moment. At room temperature, the bulk susceptibility of the MSU crystal was -16×10^{-6}. In general, water, diamond and graphite are considered to show large bulk diamagnetic susceptibility, and these values are -9.1×10^{-6} for water -22×10^{-6} for diamond and -14×10^{-6} for graphite [18-20]. The diamagnetic susceptibility of the MSU crystals has comparable level magnetic susceptibility compared with diamond and graphite, and about 10 times smaller than water.

Uric acid is a heterocyclic compound, consisting of condensed pyrimidine and imidazole rings. The molecules in MSU crystals are arranged in laminae by hydrogen bonding, with sodium ions in between the laminae. For aromatic molecules, when a magnetic field is applied perpendicular to the surface of the aromatic molecules, circulating currents are induced by delocalized π electrons in the aromatic rings. Energetically unstable aromatic rings orient parallel to the magnetic field to become stable. MSU crystals have been analyzed by Mandel *et al*. using X-ray diffractometry [9]. The surface of aromatic ring of Monosodium urate molecules are inclined with respect to c-axis at an angle of approximately 110°. That is, when a magnetic field is applied it, the surface of the aromatic rings since parallel to the magnetic field directions, c-axis is inclined about 20° with respect to the perpendicular direction to the direction of the magnetic field direction (Figure 3.35). Moreover monosodium urate molecules are twisted at 7.7° to the direction of (1-10) plane according to the literature [9-11]. In

other words, this aromatic rings are inclined 14 ° with respect to the c-axis. This inclination contributes to a result of observing the MSU crystals suspended in the solution by a CCD microscope inclined the mean ± 15 °. Therefore, theoretical prediction and experimental values was relatively good agreement. That is, MSU molecules are twisted three-dimensionally against the crystal shape. It is speculated that the reason for that the c-axis of the crystal was inclined around the Y axis and X axis is contributed to this twisting. It is considered that MSU crystals have a twisted orientation because the aromatic rings in the urate ions orient perpendicular to the direction of the magnetic field. The above mentioned results are based on these principles and support the experimental outcome of the three-dimensional orientation. From the analysis results of reflected light intensity changes in Chapter 4.3.5, the MSU crystal is most stable when (100) plane of crystal is parallel to the magnetic direction because (010) plane of the crystal was clearly perpendicular to the magnetic direction. If magnetic field is parallel (100) plane of crystal, the c-axis of crystals is inclined around the Y axis and X axis. This is consist with the result of CCD microscope measurement and reflected light intensity changes in Chapter 4.3.5.

In addition, under near-infrared light with a wavelength of 700–750 nm, MSU crystals with a size of approximately 12 μm showed a 1.7% change in their light intensity in a magnetic field with intensity strength of >95 mT. MSU crystals that accumulate in the human body are about 12 μm in size, and they mostly precipitate in the fingers and toes, which are lower in temperature than the rest of the body. Because the finger and toe joints in which the crystals precipitate are short, attenuation by distance in a direct-current magnetic field is small. Furthermore, because near-infrared light passes through the human body, diagnosis of gout using near-infrared radiation can be performed noninvasively from outside the body. Therefore, it should be possible to detect the existence of uric acid crystals in the actual diagnosis of gout by combining a magnetic field with the strength of a permanent magnet and near-infrared light.
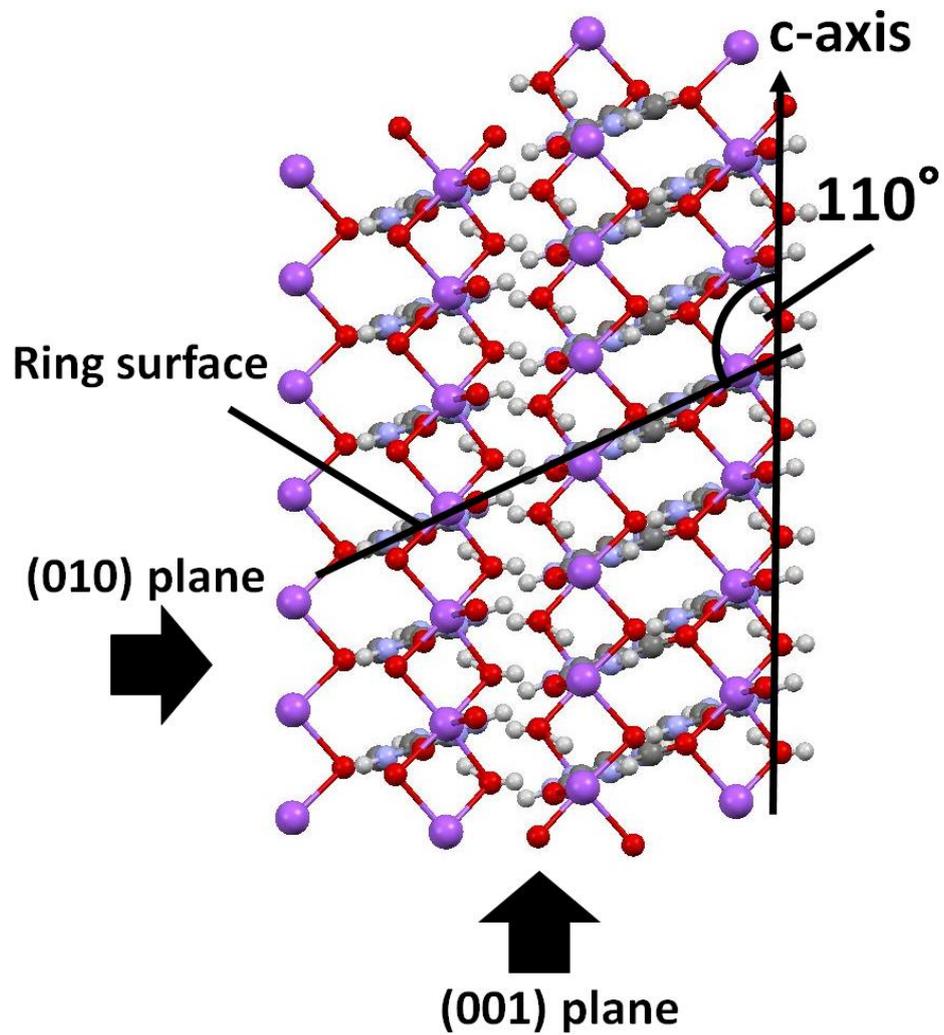
Fig. 4.35. Packing diagram of MSU crystal viewed along the a-axis.

4.4 Summary

We precipitated needle-shaped monosodium urate (MSU) crystals. The MSU crystal size changed by adjusting the concentration of the sample. We obtained small and uniform MSU crystals by adding calf serum, and these crystals were close to the size of crystals obtained from gout patients. The orientation of MSU crystals under magnetic fields of several hundred millitesla was examined. The magnetic orientations of MSU crystals under magnetic fields of 500 mT were determined. In the microscope measurement, the *c* axis of the crystals was inclined with respect to the magnetic direction. Analysis of the inclination angle of the crystals under an applied magnetic field of 500 mT revealed that the mean inclination angle was ±23° when the direction was perpendicular to the applied magnetics direction. Reflected light intensity measurements revealed that the (010) plane of the crystal was parallel to the magnetic direction. If the *Y* axis is defined as the magnetic direction, the *X* axis is perpendicular to the magnetic direction, and the *Z* axis is perpendicular to the *XY* plane, the *c* axis of the crystal tilted around the *Y* axis. The MSU crystals were found to be oriented in three dimensions. The inclination of the crystal under an applied magnetic field contributes to the inclination of the molecular structure of the crystal and the angle nearly conforms to the inclination angle of the molecular structure. Moreover, for a crystal about 12 μm long, the crystal responded to magnetic fields >95 mT.

Reference

[1] A. P. Hall, P. E. Barry, T. R. Dawber, and P. M. McNamara, "Epidemiology of gout and hyperuricemia: A long-term population study" Am. J. Med. Vol. 42, pp. 27 (1967).

[2] A. T. Eggebeen, "Gout: an update," Am. Fam. Physician. Vol. 76, No. 6, pp. 801 (2007).

[3] E. W. Campion, R. J. Glynn, and L. O. DeLabry, "Asymptomatic hyperuricemia. Risks and consequences in the Normative Aging Study." Am. J. Med. Vol. 82, pp. 421 (1987).

[4] I. A. Prior, T. J. Welby, T. Ostbye, C. E. Salmond, and Y. M. Stokes,"Migration and gout: the Tokelau Island migrant study", Am. J. Med. Vol. 295, pp. 457 (1987).

[5] N. Schlesinger, "Diagnosing and treating gout: a review to aid primary care physicians," Postgrad Med. Vol. 122, No. 2, pp. 157 (2010).

[6] L. X. Chen, H. R. Schumacher, "Gout: an evidence-based review." J. Clin. Rheumatol. Vol. 14 (5 Suppl), pp. S55 (2008).

[7] R. Terkeltaub, "Update on gout: new therapeutic strategies and options". Nature Reviews Rheumatology, Vol. 6, No. 1, pp. 30 (2010).

[8] A. K. Tausche, T. L. Jansen, H. E. Schröder, S. R. Bornstein, M. Aringer and U. Müller-Ladner, "Gout--current diagnosis and treatment". Dtsch. Arztebl. Int. Vol. 106 (34–35), pp. 549 (2009).

[9] N. S. Mandel and G. S. Mandel, "Monosodium urate monohydrate, the gout culprit," J. Am. Chem. Soc. Vol. 98, pp. 2319 (1976).

[10] M. C. Perrin and J. A. Swift, "Step kinetics on monosodium urate monohydrate single crystal surfaces: an in situ AFM study" CrystEngComm, Vol. 14, pp. 1709 (2012).

[11] M. C. Perrin, M. A. Dobish, E. V. Keuren and J. A. Swift, "Monosodium urate monohydrate crystallization," CrystEngComm. Vol. 13, pp. 1111 (2011).

[12] C. Y. Lam Erwin and G. H. Nancollas, "The crystallization and issolution of sodium urate," J. Cryst. Growth, Vol. 53, pp. 215 (1981).

[13] C. Rinaudo and R. Boistelle, "Theoretical and experimental growth morphologies of sodium urate crystals," J. Cryst. Growth, Vol. 57, pp. 432 (1982).

[14] N. S. Mandel and G. S. Mandel, "Monosodium urate monohydrate, the gout culprit," J. Am. Chem. Soc., Vol. 98, pp. 2319 (1976).

[15] A. G. Fam, H. R. J. Schumacher, G. Clayburne, M. Sieck, N. S. Mandel, P. T. Cheng and K. P. Pritzker, "A comparison of five preparations of synthetic monosodium urate monohydrate, crystals" J. Rheumatology, Vol. 19, pp. 780 (1992).

[16] D. J Jr. McCarty and J. S. Faires,"A comparison of the duration of local anti-inflammatory effect of several adrenocorticosteroid esters-a bioassay technique." Curr. Ther. Res. Clin. Exp. Vol. 5, pp. 284 (1963).

[17] N. W. McGill, A. Hayes, and P.A. Dieppe, "Morphological evidence for biological control of urate crystal formation in vivo and in vitro." Scand. J. Rheumatol. Vol. 21, No. 5, pp. 215 (1992).

[18] G. P. Arrighini, M. Maestro, and R. Moccia, "Magnetic Properties of Polyatomic Molecules: Magnetic Susceptibility of H2O, NH3, CH4, H2O2," J. Chem. Phys. Vol. 49, No. 2, pp. 882 (1968).

[19] J. Heremans, C. H. Olk and D. T. Morelli, "Magnetic Susceptibility of Carbon Structures," Phys. Rev. B Vol. 49, No. 21, pp. 15122 (1994).

[20] N. Ganguli and K.S. Krishnan, "The Magnetic and Other Properties of the Free Electrons in Graphite." Proceedings of the Royal Society. Vol. 177, No. 969, pp. 168 (1941).

5

Conclusions and Future Plans

5.1   Conclusions

A great deal of research on the magnetic properties of materials is underway, concerning both basic characteristics and applications. Many research targets are, however, paramagnetic or ferromagnetic substances, based on their electronic spin properties. In contrast, several materials in the natural world and *in vivo* are diamagnetic. In diamagnetic materials, magnetism is intra-molecularly induced by an external magnetic field. However, because only a weak magnetism is induced, diamagnetic materials had been treated as non-magnetic substances under low magnetic fields at the terrestrial magnetism level, and research did not sufficiently investigate their properties at sub-tesla magnetic fields.

Various research began in the 1990s regarding the influence of a magnetic field on diamagnetic materials, such as fiber molecules, like collagen and actin, and red blood cells in substances in the body, and regarding various magnetic phenomena, such as the magnetic field orientation phenomenon, which works to arrange diamagnetic materials in a constant direction in magnetic fields on the order of 10 T. During this research trend, knowledge of the characteristics and magnetic orientation conditions of diamagnetic materials and quantities such as a threshold at which these materials are rotated with respect to magnetic field lines was still insufficient.

It has been reported recently that the optical reflection phenomenon from a crystal board changes remarkably and that control and quenching of this optical reflection occur in magnetic fields of more than 0.26 T when a guanine crystal from biological, that is, diamagnetic, material is observed in a dark visual field. Guanine is formed by the molecule $C_5H_5N_5O$ and is one of the four materials (adenine, cytosine, guanine, and thymine) that are key to the double-helical structure of DNA. Adenine and guanine have a structure called a purine base, and uric acid is generated as a result of purine. The present study focused on uric acid, one of the diamagnetic materials, and aimed at the clarification of the millitesla magnetic field effect on the uric-acid-content crystallite

that causes gout and urinary tract stones.

Uric acid is an organic compound with the molecular formula $C_5H_4N_4O_3$. Its crystals are one of the causes of urinary tract stones, a disease caused by crystallite accumulation in the human body. Uric acid crystals grow in layers on the (100) plane. Crystallization behavior was observed with a microscope when the magnetic field was applied to uric acid crystals with an electromagnet that could generate up to 500 mT. As a result, although the crystals were in random order, the lengths of the crystals were aligned in parallel to the magnetic field after the magnetic field was applied, and it was rotated so that the (100) plane of the crystals was oriented vertically to the magnetic field. That is, it was revealed that uric acid crystals are oriented with respect to the magnetic field by a two-stage rotational movement. It was thought that the diamagnetic energy state would be the most stable under a magnetic field because the absolute value of the normal direction of the magnetic susceptibility of the largest area of uric acid crystals [(100) plane] is the smallest. Uric acid crystals in a monoclinic system have three orthogonal magnetic axes with different magnetic susceptibilities. Therefore, the susceptibility anisotropy of urate crystals was predicted from these results. It was potentially possible to control the magnetic crystal by changing the direction of magnetic field by making use of this property.

Next, the magnetic field effect on monosodium urate (MSU) crystals was examined. MSU crystals, which are a combination of uric acid and sodium, are known to cause gouty arthritis. An MSU crystal is a needle crystal in the triclinic system, and it has an elongated structure along the c-axis. In this study, a MSU crystal was artificially precipitated, and its behavior in an applied magnetic field was observed under a microscope. It was observed that the MSU crystal rotated following the direction of the magnetic field lines. It turned out that the rotation speed became slow, depending on the magnetic field strength. The MSU crystal was not oriented completely perpendicularly to the magnetic field, but was rather inclined toward the magnetic direction. When the vertical direction was assumed to be the initial side encountered by the applied magnetic field, analysis demonstrated that the crystal was inclined $\pm23^\circ$ on average under a magnetic field of 500 mT.

The (010) plane—the largest plane of an MSU crystal—is known to be a reflecting plane. Taking advantage of this property, light was irradiated to the crystal turbid solution that had been put in the optical cell. When a magnetic field was applied to this system, the light changed its intensity by aligning the crystal in a constant direction. The orientation behavior of crystals floating on cells was observed by measuring the reflected light intensity at various combinations of magnetic field,

incident light intensity, and direction of observation. As a result, it was revealed that the MSU crystals were oriented three-dimensionally. Moreover, the threshold magnetic response of MSU crystals (of approximately 12 μm) was 95 mT, as shown by the light-change intensity (1.7 %) obtained from the crystal light-reflection measurements in the suspension. That is, MSU crystals were shown to react with high sensitivity to the magnetic field in terms of the order of the permanent magnet.

In the present study, the magnetic field orientation phenomenon of uric acid crystals and MSU crystals accumulated *in vivo* under a magnetic field with intensity on the order of 100 mT was determined *in vitro*. Results revealed that, using this characteristic, magnetic control of crystals is possible by changing the direction of the magnetic field.

5.2   Future Plans

Gouty arthritis is caused by hyperuricemia, but it can develop even when control of the serum urate level is maintained. Therefore, diagnostics not based on the serum urate level are desired to determine effective methods and durations of therapy. To recognize and identify the symptom, the methods include examinations by polarizing microscopes, X-rays, DECT, MRIs, or ultrasonography. However, because they are for diagnosis, each of them has a problem, such as not meeting the need for early diagnosis; hence, no satisfactory method has yet been established. Since the light intensity in MSU crystals shows a highly sensitive response to the magnetic field, it is believed that non-invasive and simplified gout diagnosis may be possible with a magnetic sensor using near-infrared light.

Near-infrared light is known to transmit well through a living body. In recent years, near-infrared spectroscopy has attracted attention as a rapid and non-destructive analytical procedure. It has also been used as a new method of chemical analysis in the food industry for measuring the compositions of fruits, vegetables, and fish, or for quality control of processed foods. In the medical field, this technology is attracting attention as a means of visualizing deeper parts of the body, which is done by monitoring from the body surface the fluorescence produced by the near-infrared fluorescent agent, which is excited by near-infrared light and delivered to the deep parts of the body. This technology has been applied in sentinel lymph-node surgery in breast cancer or malignant melanoma, hepatocellular cancer surgery, heart bypass surgery, and other surgeries. The advantages of using near-infrared light are: it eliminates the need for radiological protection equipment; there is no exposure to radiation; and it allows for easy and convenient repeated use.

We measured the magnetic effect of the dissolution process of MSU crystal suspension in preparation for gout treatment using a magnetic field. The treatment of gout involves chemical medicines, such as uricosuric, and a urinary alkalizer. The urinary alkalizer is dispensed to return the acidic pH of the urine of gout patients to a normal level. However, excess intake of such medicines is reported to lead to side effects. Moreover, an overdose of these medicines increases the risk of urinary stones. In this study, MSU crystals were dissolved by adding an alkaline solution to turbid MSU crystal liquid. The dissolution was performed by applying a magnetic field using an electromagnet, and the solution was removed before the crystals were completely dissolved in order to measure the turbidity of the solution by measuring the transmitted light. The results demonstrate that application of a magnetic field of 500 mT to the

MSU crystal suspension increased the dissolution rate by ~1.2 times compared to that of the MSU crystal suspension placed in an ambient field (Figure. 5.1). This phenomenon is considered to be caused by accelerated dissolving due to the increased permeation of the alkali solution by the magnetic field orientation, which depends on the diamagnetic susceptibility. The above results indicate the effectiveness of combining a magnetic field and drug in gout treatment. If MSU crystals, which cause gout, can be controlled in a magnetic field, it is possible to treat gout with magnetic fields, as in physical therapies such as the electrical treatment of low-back pain in orthopedics (Figure. 5.2). In other words, it is possible to non-invasively treat gout.

The health effects of a magnetostatic field on the human body have so far been reported to be comparatively low or negligible. However, in experiments involving cell-size matter, magnetic-field effects have been recognized, including magnetic-field orientation of fibrin in blood coagulation, deflection of blood-cell flow in blood vessels, and in vivo chemical reactions. In epidemiological studies with operators, patients, and volunteers, exposure to magnetostatic fields of up to 8 T resulted in dizziness, nausea, and minimal changes in blood pressure and heart rate, depending on the amount of exposure. However, these effects are within the range of physiological variations, and no evidence has been reported that shows that the magnetostatic field affects the cardiovascular system or other physiological specificities, such as serum proteins or hormones; furthermore, no temperature changes are caused in the human body. However, there has also been a report claiming that applying a 60 mT permanent magnet to the epiphysis and vicinal organs of a mouse enhances the mouse's immune functions. Although orientation in intra-vital substances does not threaten the life of the body, there is a possibility that in vivo chemical reaction time or nerve conduction velocity changes. Thus, the effects of magnetic fields on living organisms still remain unresolved.

From the above-mentioned facts, the possibility of inexpensive and convenient gout therapy was demonstrated, which uses a magnetic field on the order of 100 mT and the marked diamagnetic susceptibility anisotropy, without using intense magnetic fields of several tens of tesla, and a broad range of applications is expected. In micro/nanoscience, the use of diamagnetic field orientation for structural control of in vivo organic crystals in gout therapy is considered to further benefit the nation's health by fusing nanoscience and medical technology.
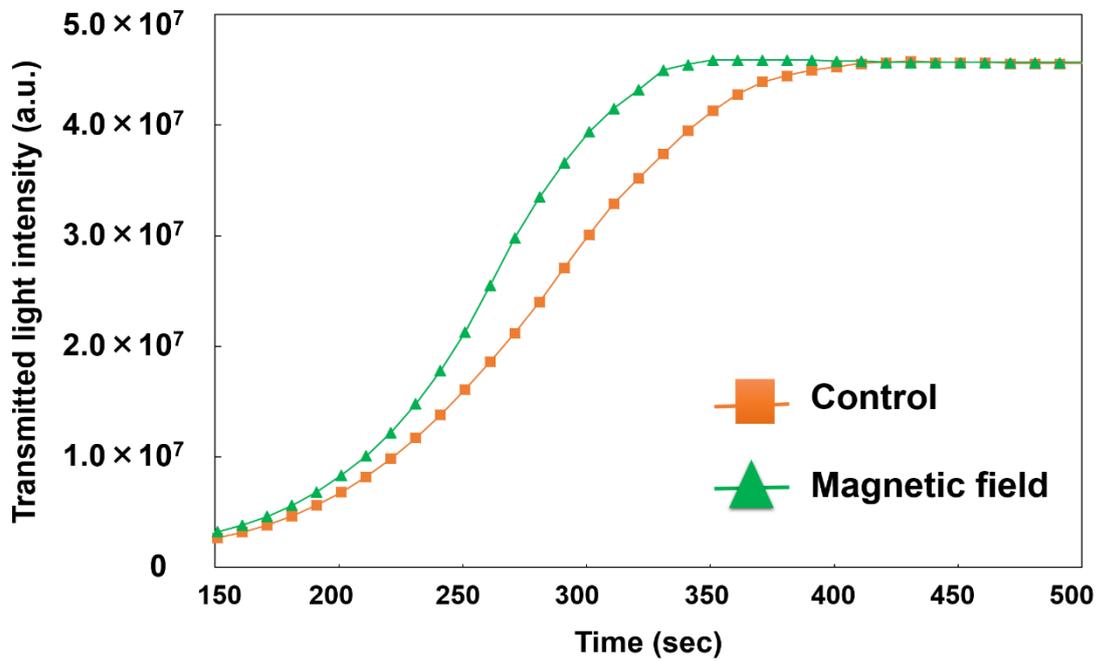
Fig. 5.1. Time course of the transmitted light intensity in the presence (500 mT) and absence of a magnetic field in the dissolution process following the addition of an alkali solution.
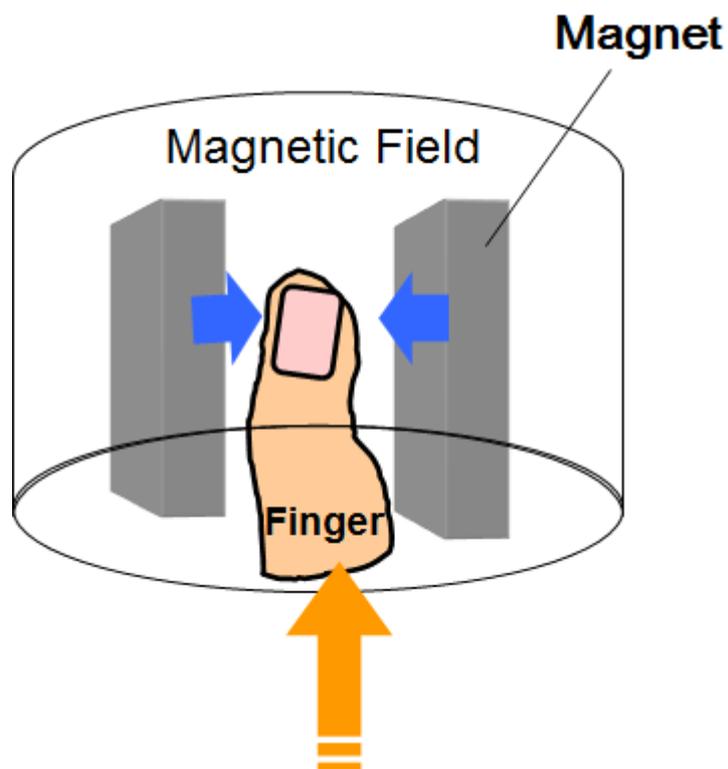

Fig. 5.2. A new therapeutic method for the treatment of gout.

114

Publication

Journal

(1) Two-stage magnetic orientation of uric acid crystals as gout initiators
Y. Takeuchi, Y. Miyashita, Y. Mizukawa, M. Iwasaka
Applied Physics Letters, **104**, 024109 (2014).

(2) Magnetic Rotation of Monosodium Urate and Urinary Tract Stones for Clinical Treatment Applications
Yuka Takeuchi, Yoko Sugawara, Tadashi Sugawara, Masakazu Iwasaka
IEEE Transactions on Magnetics, **50** (11), 6101204 (2014).

(3) Effects of magnetic fields on dissolution of arthritis causing crystals
Y. Takeuchi and M. Iwasaka
Journal of Applied Physics **117** 17D152.

Proceeding

(1) Magnetic rotations of uric acid crystals and uranic crystals by static magnetic fields of up to 500 mT
Y. Takeuchi, Y. Mizukawa and M. Iwasaka
35th Annual International Conference of the IEEE Engineering in Medicine and Biology Society (EMBC2013), Conf. Proc. IEEE Eng Med Biol Soc. 2013:3261-4, Osaka, Japan, July 3-7 (2013).

Acknowledgments

公表論文

(1) Magnetic Rotation of Monosodium Urate and Urinary Tract Stones for Clinical Treatment Applications

<u>Yuka Takeuchi</u>, Yoko Sugawara, Tadashi Sugawara, Masakazu Iwasaka

IEEE Transactions on Magnetics, **50** (11), 6101204 (2014).

(2) Two-stage magnetic orientation of uric acid crystals as gout initiators

<u>Y. Takeuchi</u>, Y. Miyashita, Y. Mizukawa, M. Iwasaka

Applied Physics Letters, **104**, 024109 (2014).

Magnetic Rotation of Monosodium Urate and Urinary Tract Stones for Clinical Treatment Applications

Yuka Takeuchi[1,2], Yoko Sugawara[3], Tadashi Sugawara[4], and Masakazu Iwasaka[2,5,6]

[1]Graduate School of Advanced Science of Matter, Hiroshima University, Hiroshima 739-8527, Japan
[2]Chiba University, Chiba 263-8522, Japan
[3]School of Science, Kitasato University, Kanagawa 252-0373, Japan
[4]Faculty of Science, Kanagawa University, Kanagawa 259-1293, Japan
[5]Research Institute for Nanodevice and Bio System, Hiroshima University, Hiroshima 739-8527, Japan
[6]Japan Science and Technology Agency, PRESTO, Saitama 332-0012, Japan

In recent years, diseases such as gout and urinary tract calculi, caused by crystals *in vivo*, are rapidly increasing due to excess intake of alcohol, salt, and so forth. Crystals causing gout are compounds of uric acid with sodium in the blood, which are called monosodium urate (MSU) crystals. On the other hand, urinary tract calculus is caused by calcium oxalate crystal. In this paper, we focused on the behaviors of MSU crystals and oxalic acid crystals under magnetic fields of several hundreds of mT (Tesla), and developed a method for new medical treatments by using a magnetic field. MSU crystals and oxalic acid crystals were prepared by a recrystallization from the aqueous solution. We observed these crystals using a charge-coupled device microscope under horizontal magnetic fields (maximum of 500 mT). While the magnetic fields were applied, the MSU crystals were oriented by the magnetic fields. In addition, oxalic acid crystals were oriented perpendicularly to the magnetic field. The dynamic rotation of MSU crystal was observed quantitatively by measuring the time course of the lightscattering intensities of the MSU suspension. The results show that the diamagnetic anisotropy in the MSU crystals controlled the rotational responses. As a possible medical application, a remote control of the MSU crystals and oxalic acid crystals in living body by the magnetic fields is proposed.

Index Terms—Diamagnetic material, gout, magnetic orientation, monosodium urate crystal, oxalic acid crystal, uric acid.

I. INTRODUCTION

DISEASES in the human body that are caused by crystals such as uric acid crystals and calcium oxalate crystals have become a serious problem in everyday life. Uric acid is known as the substance that is responsible for gout. Gout is a severe inflammatory arthritic disease that develops when high accumulations of uric acid crystallize. The agent of gout is a monosodium urate (MSU) crystal, which is a compound formed from uric acid and sodium from the patient's blood. These MSU crystals are needle-like and frequently cause severe pain for the patient. Similarly, urinary tract stone disease is also caused by crystals, and is categorized in terms of compounds that form the crystals, such as calcium oxalate, calcium phosphate, and uric acid [1]. In general, urinary tract stone disease is caused for many people by the calcium oxalate crystal. Gout and hyperuricemia are associated with the formation of urinary tract calculi [2]–[9], and an approach to control the formation of these crystals is necessary. Because chemical medicines or excess water intake have the possibility of side effects, physical stimulation methods such as those using magnetic fields are candidates for new medical treatments for gout as a substitute for pharmaceutical dosage [10]–[12]. In our previous study, we reported that uric acid crystals which were rectangular in shape show distinct magnetic orientations under magnetic fields in the 130–500 mT

range [13]. Therefore, it is believed that the needle-like MSU crystals, which are composed of the same component as uric acid crystals, will also have magnetic orientations induced by their magnetic anisotropy.

This paper focuses on the magnetic behavior of two kinds of disease-related crystals: the MSU crystal, which is responsible for gout, and the oxalic acid crystal, which is responsible for urinary tract stones. These crystals were artificially synthesized and were then exposed to magnetic fields of several hundreds of millitesla to control the crystal alignment direction.

II. METHODS

We prepared the MSU crystal by dissolving the uric acid powder (98% purity, 33 mg) with a solution of sodium hydroxide (0.025 mol/l, 8.0 ml) at high temperature. The MSU crystals were obtained to static standing for over a day at 4 °C after natural cooling to this solution. The oxalic acid crystal was extracted using the difference in solubility at the point of completely dissolution, when heating the oxalic acid dihydrate solution (99.5% purity, 2.0 g) in 10 ml of distilled water.

We observed these crystals which were transferred into a microchamber which was consisted of a cover glass window (18 × 18 mm, 0.12–0.17 mm thick) and a rubber sheet [Fig. 1(a)]. It was positioned on a charge-coupled device (CCD) microscope, which was placed in an electromagnet with a maximum field of 500 mT to observe the behavior of the crystals. The magnetic field was directed horizontally. Fig. 1(b) shows configuration for measurement of reflection light. Spectroscopic measurement of reflection light was carried out in the fiber-optic measurement system. The magnetic field was generated by an electromagnet that is shown in Fig. 1(a).

(a)

(b)
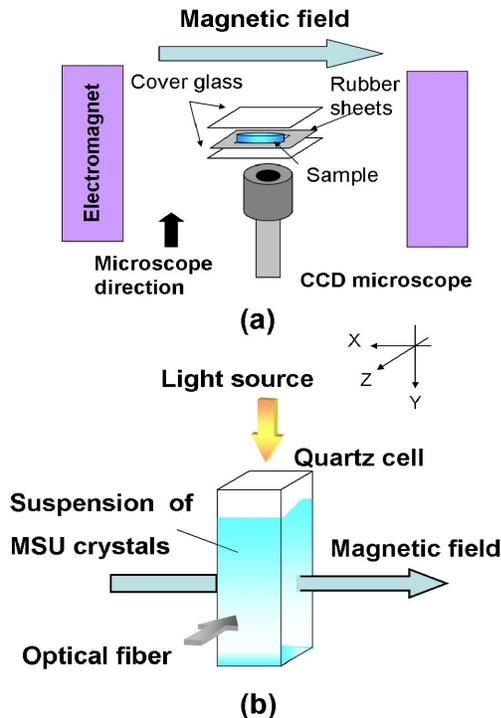
Fig. 1. (a) Experimental system for observation of the magnetic rotation of MSU crystals and oxalic acid crystals. (b) Configuration for measurement of reflected light.

The used light source was halogen lamp which provided a continuous. The magnetic field, the light source, and fiber-optic were orthogonal.

III. RESULTS AND DISCUSSION

We artificially obtained the MSU crystals as shown in Fig. 2(a). The crystals are slender needle-like with a slight surface, as shown in Fig. 2(b).

Fig. 2(c) shows a photograph of the MSU crystals under a magnetic field of 500 mT. The MSU crystals obtained were about 15 μm long with less than 1 μm width. When the magnetic field was applied to the MSU crystals which were turned in random directions, the crystals oriented their needle (long) axis to be perpendicular to the applied magnetic field by degrees. The microscopic image was taken after the crystals were exposed to the magnetic field for 5 min. The MSU crystals suspended in the solution were easy to raise for orientation, while the crystals that had sunk were harder to rotate because they had stuck to the cover glass.

Fig. 2(d) shows the microscopic image of the recrystallized oxalic acid. It was speculated that the cuboids shapes were the oxalic acid crystals. The oxalic acid crystals showed a tendency to orient perpendicular to the applied magnetic field of 500 mT because of the diamagnetic susceptibility anisotropy in the oxalic acid crystals. In the case of the MSU crystals, the viscosity of the surrounding water and friction between the crystals and the cover glass surface limited the diamagnetic rotation of the crystals.

Next, to verify magnetic orientation a high sensitivity on a widespread basis [14], we measured the reflected light over
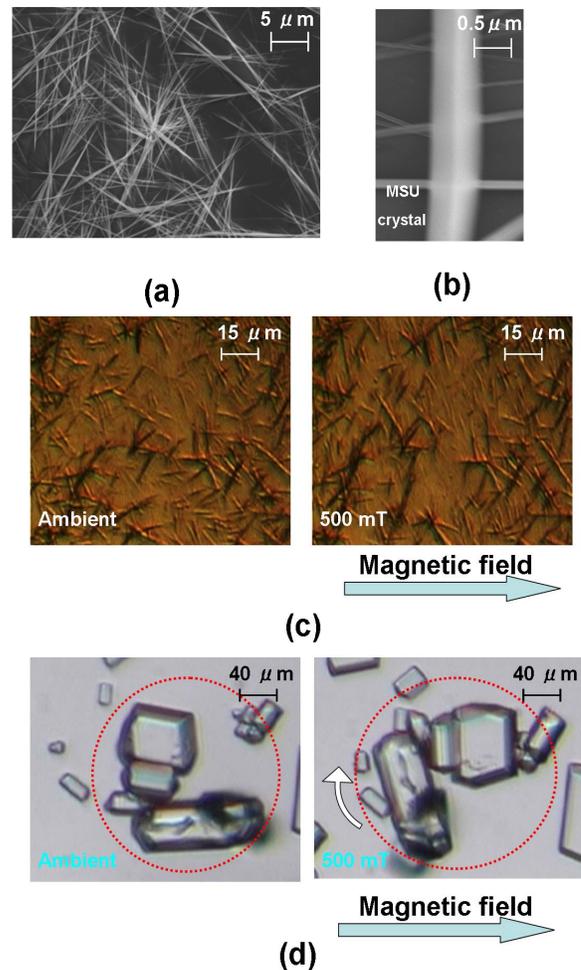

Fig. 2. (a) Scanning electron microscope (SEM) image of MSU crystals. (b) SEM image of the left image scaled up ten times. (c) Microscopic images showing the diamagnetic orientation in MSU crystals under the ambient fields and magnetic under a magnetic field of 500 mT. (d) Microscopic images of the magnetic rotation of oxalic acid crystals under the ambient fields and under a magnetic field of 500 mT.

a time course change from the suspension of floating of MSU crystals. The reflected light intensity was continuously measured both with and without applied magnetic fields of several hundred millitesla, as shown in Fig. 3(a)–(d). The changes in light intensity were detected using a spectrometer, and the results clearly show that the reflected light intensity increased under magnetic fields between 130 and 500 mT when the magnetic field was switched on, and that it gradually decreased as the magnetic field was switched off. At 500 mT, the light intensity increased 0.88% from free exposure, and it decreased 0.74% with postexposure. Additionally, the light intensity decreased as the magnetic field decreased. Fig. 3(e) shows the change in the scale of the vertical axis shown in Fig. 3(d). When the magnetic field was 100 mT, the light intensity increased 0.14% from free exposure, and it decreased 0.07% at post exposure.

It was different only slightly. Hence, the MSU crystal showed orientation under magnetic fields of 100 mT. It is believed magnetic field threshold level for a MSU crystal of about 15 μm in length is 100 mT or less.
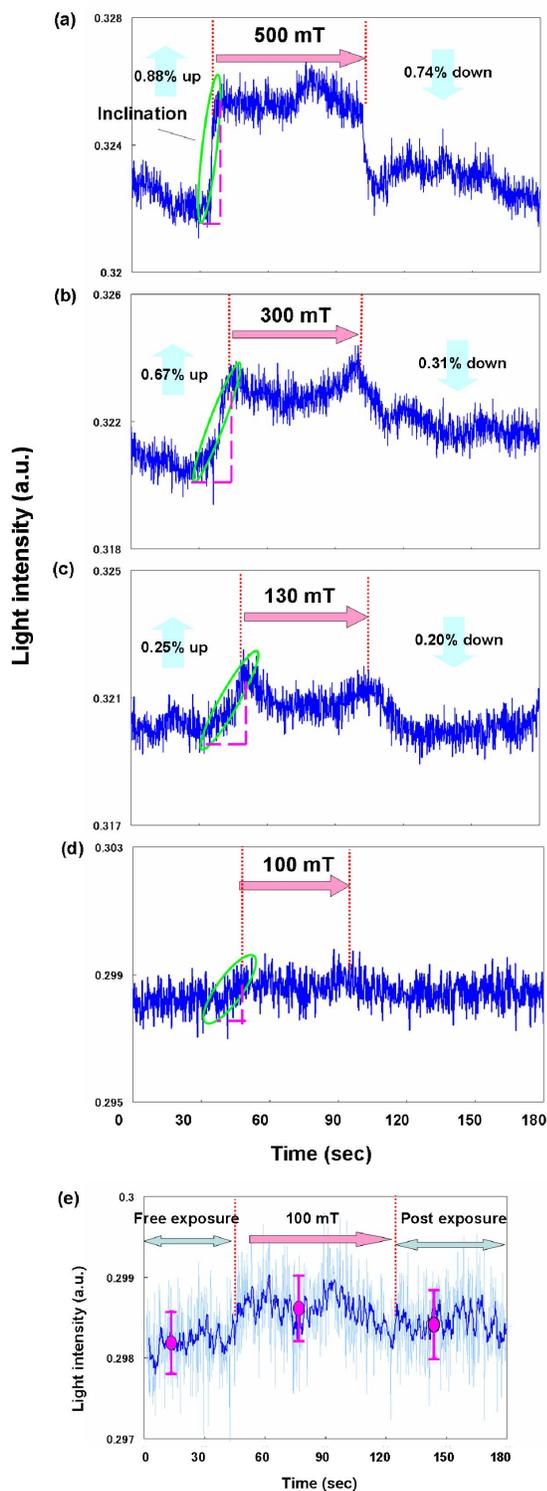
Fig. 3. (a)–(d) Time course evolution of the reflected light intensity from MSU crystals with and without magnetic field of 100, 130, 300 and 500 mT. (d′) Changed the scale of the vertical axis in (d). The mean value of reflected light intensity and ± standard deviation are shown.

Additionally, we obtained the inclination from the point at which the magnetic field was turned on to the point at which the maximum light intensity was attained by approximation. Fig. 4 shows dependency graph of the inclination relative to the magnetic field. The inclination shows the rate of change
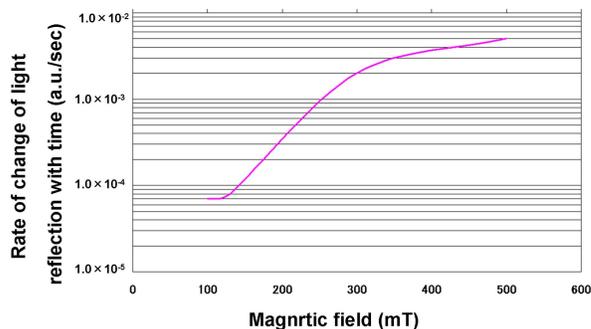

Fig. 4. Dependence of rate of change of light reflection with respect to time in MSU crystals under magnetic fields of 500 mT to 100 mT.
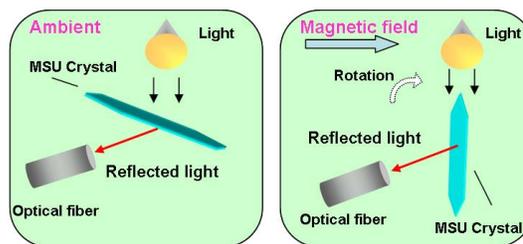

Fig. 5. Illustration diagram of rotation of MSU crystal.

of light reflection with time. It increases as the magnetic field increases, and has a tendency to saturate by degrees. This result indicates that the orientational speed of the crystals was negatively correlated with the magnitude of the field. We were able to detect the magnetic orientations of these needle-like MSU crystals quantitatively.

This phenomenon means that the crystals oriented their long axes and surfaces to be perpendicular to the magnetic field because the MSU crystals have a slight surface, as shown in Fig. 2(b); the light was then reflected by the crystal's surface, and was detected by the spectrometer, which was set up perpendicular to the magnetic field (Fig. 5). Therefore, the light intensity increased with the magnetic field orientation.

This indicates that the uric acid molecule that the forms part of the MSU crystal and the oxalic acid molecule was diamagnetism and that the MSU crystal and the oxalic acid crystal contain neither paramagnetic nor ferromagnetic. It can be concluded that the crystal orientation is induced by the diamagnetic anisotropy of these crystals.

IV. MODEL FOR THERAPEUTIC

The results indicated that the magnetic orientations of the MSU crystal and the oxalic acid crystal effectively enable a less physical stimulation under medical treatment. For example, in the gout treatment, we consider a situation where the MSU crystals are growing in an arthrosis of the finger, as shown in Fig. 6. The growing MSU crystals can be aligned by external magnetic fields of several hundreds of mT order. The alignment of diamagnetic fiber-like material using diamagnetic torque rotation can cause the polymerization of the fiber-like crystals. Consequently, this can provide pain relief by orienting the crystals in the magnetic field direction. The suggested
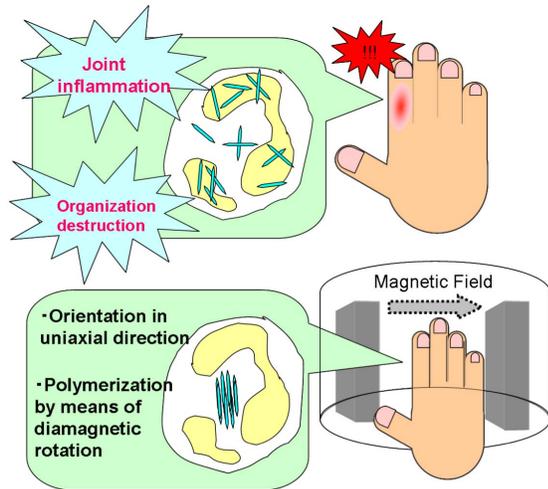
Fig. 6. Model for the diamagnetic alignment of MSU crystals. Top: no-magnetic field treatment condition, spiny assembly of needle-like MSU crystals can easily penetrate the cell tissues. Bottom: magnetic field exposure at 500 mT can form a less spiny assembly, which can reduce the damage to the surrounding cellular tissue.

treatment based on this paper is to provide pain relief by controlling the crystals.

V. CONCLUSION

In conclusion, the magnetic orientations of MSU crystals and oxalic acid crystals under 500 mT magnetic fields were clarified. These crystals were precipitated artificially. Using an electromagnet, MSU crystals and oxalic acid crystals were oriented perpendicular to the magnetic fields. The spectra of the MSU crystals were measured to determine the reflected light both with and without the static magnetic field in time course change. It was found that the light intensity definitely responded to a magnetic field of 100 mT. An analysis of the rate of change of light reflection of the MSU crystals with respect to time under applied magnetic fields of 100–500 mT revealed a dependence on the applied magnetic field.

REFERENCES

[1] C. Y. Pak, "Kidney stones," *Lancet*, vol. 351, no. 9118, pp. 1797–1802, 1998.

[2] H. Okabe, T. Hosoya, M. Hikita, M. Saji, K. Ichida, and I. Ohno, "Analysis of urolithiasis in patients with gout and hyperuricemid using ultrasonography," *Jpn. J. Rheumatol.*, vol. 9, no. 3, pp. 239–244, Sep. 1999.

[3] T. F. Yü and A. B. Gutman, "Uric acid nephrolithiasis in gout: Predisposing factors," *Ann. Int. Med.*, vol. 67, no. 6, pp. 1138–1148, 1967.

[4] B. Shekarriz and M. L. Stoller, "Uric acid nephrolithiasis: Current concepts and controversies," *J. Urology*, vol. 168, no. 4, pp. 1307–1314, Oct. 2002.

[5] A. P. Hall, P. E. Barry, T. R. Dawber, and P. M. McNamara, "Epidmiology of gout and hyperuricemia: A long-term population study," *Amer. J. Med.*, vol. 42, no. 1, pp. 27–37, Jan. 1967.

[6] H. Okabe and T. Hosoya, "Clinical feature of urolitiasis in patients with gout," *Hyperuricemia Gout*, vol. 8, no. 1, pp. 47–50, 2000.

[7] E. L. Prien and E. L. Prien, Jr., "Composition and structure of urinary stone," *Amer. J. Med.*, vol. 45, no. 5, pp. 654–672, Nov. 1968.

[8] F. L. Coo, A. Evan, and E. Worceter, "Kidney stone disease," *J. Clin. Invest.*, vol. 115, no. 10, pp. 2598–2605, Oct. 2005.

[9] S. Yamaguchi, "Hyperuricemia as a risk factor for urolithiasis," *Hyperuricemia Gout*, vol. 18, no. 1, pp. 53–58, 2010.

[10] S. I. Hung *et al.*, "HLA-B*5801 allele as a genetic marker for severe cutaneous adverse reactions caused by allopurinol," *Proc. Nat. Acad. Sci. USA*, vol. 102, no. 11, pp. 4134–4139. Mar. 2005.

[11] N. Kaniwa *et al.*, "HLA-B locus in Japanese patients with anti-epileptics and allopurinol-related Stevens-Johnson syndrome and toxic epidermal necrolysis," *Pharmacogenomics*, vol. 9, no. 11, pp. 1617–1622, Nov. 2008.

[12] C. Lonjou *et al.*, "A European study of HLA-B in Stevens-Johnson syndrome and toxic epidermal necrolysis related to five high-risk drugs," *Pharmacogenetics Genomics*, vol. 18, no. 2, pp. 99–107, Feb. 2008.

[13] Y. Takeuchi, Y. Mizukawa, Y. Miyashita, and M. Iwasaka, "Two-stage magnetic orientation of uric acid crystals as gout initiators," *Appl. Phys. Lett.*, vol. 104, no. 2, p. 024109, Jan. 2014.

[14] D. H. Kim *et al.*, "Biofunctionalized magnetic-vortex microdiscs for targeted cancer-cell destruction," *Nature Mater.*, vol. 9, no. 2, pp. 165–171, Feb. 2010.

Two-stage magnetic orientation of uric acid crystals as gout initiators

Y. Takeuchi, Y. Miyashita, Y. Mizukawa, and M. Iwasaka

Articles you may be interested in
Kerosene wick lamp flame deformation in gradient magnetic fields
Appl. Phys. Lett. **104**, 114104 (2014); 10.1063/1.4868877

Magnetic field-controlled two-way shape memory in CoNiGa single crystals
Appl. Phys. Lett. **84**, 3594 (2004); 10.1063/1.1737481

Relativistic effects on the nuclear magnetic shielding tensor
J. Chem. Phys. **118**, 471 (2003); 10.1063/1.1525808

Early stages of mechanical crystallization of amorphous FeZrBCu soft magnetic material
J. Appl. Phys. **87**, 2464 (2000); 10.1063/1.372203

Control of the orientation of human erythrocytes by magnetic and electric fields
J. Appl. Phys. **85**, 5711 (1999); 10.1063/1.370260

Two-stage magnetic orientation of uric acid crystals as gout initiators

Y. Takeuchi,[1] Y. Miyashita,[1] Y. Mizukawa,[1] and M. Iwasaka[1,2,a]

[1]*Graduate School of Engineering, Chiba University, 1-33 Yayoi-cho, Inage-ku, Chiba-city, Chiba 263-8522, Japan*
[2]*PRESTO, Japan Science and Technology Agency, Kawaguchi, Saitama 332-0012, Japan*

The present study focuses on the magnetic behavior of uric acid crystals, which are responsible for gout. Under a sub-Tesla (T)-level magnetic field, rotational motion of the crystals, which were caused by diamagnetic torque, was observed. We used horizontal magnetic fields with a maximum magnitude of 500 mT generated by an electromagnet to observe the magnetic orientation of the uric acid microcrystals by a microscope. The uric acid crystals showed a perpendicular magnetic field orientation with a minimum threshold of 130 mT. We speculate that the distinct diamagnetic anisotropy in the uric acid crystals resulted in their rotational responses. © 2014 AIP Publishing LLC. [http://dx.doi.org/10.1063/1.4862271]

Recently, gout, a serious disease, has become one of the most prevalent diseases caused by eating disorders and excessive alcohol intake. Generally, gout is caused by a high concentration of uric acid in the bloodstream. This leads to inflammation in the joints, such as the ankle. Like many other diseases, chemical medicines can be an efficient therapeutic method for gout. However, excess intake of such medicines frequently causes serious side effects.[1–3]

The effects of magnetic fields on biological molecules and macromolecules, such as proteins in solution, have been thoroughly studied in magnetic fields of up to 10 T. It has been reported that a magnetic field induces magnetic orientation of modulates the rate of crystal growth.[4–12] As well as condensed crystals, lipid crystals can adopt magnetic orientation under magnetic fields of sub-T order.[13] However, there are few reports concerning the possible applications of magnetically controlled crystallization as a therapeutic method. Of several kinds of physical stimulation, a direct-current magnetic field is a candidate that can provide noncontact noninvasive treatments of living tissue. Our previous studies on biogenic crystals of guanine, which are chemical analogues of uric acid, revealed that it shows distinct magnetic orientation and light-scattering anisotropy under magnetic fields in the range of 100–500 mT.[14–18] In our studies on guanine crystals and its analogues, we found that magnetic fields induced similar light-scattering change in uric acid crystals, which were obtained by precipitation under lowering temperatures.

In the present study, we examine the magnetorotational properties of uric acid crystals. We confirm the existence of two stages of rotation during the formation of magnetically oriented uric acid crystals. Both stages of magnetic rotation appear under magnetic fields of 100 and 500 mT.

Uric acid powder (Wako, 216-00222, 98% purity, 10 mg) was completely dissolved in an aqueous solution of sodium hydroxide (0.075 mol/l, 5.0 ml), after which hydrochloric acid (2.88 mol/l, 1.3 ml) was added to precipitate uric acid crystals in the bottom of the incubation tube upon neutralization. The obtained crystals were transferred to a microchamber, with a cover glass window (18×18 mm, 0.12–0.17 mm thick). The microchamber was positioned in a charge-couple device (CCD) microscope, which was then placed in an electromagnet (resistive type, 50 mm between the magnetic poles, Hayama Co. Ltd., Fukushima, Japan), as shown in Figure 1(a), to observe the dynamic motion of the uric acid crystals.

Images of the crystals were recorded on an MPEG-2 recorder, and the obtained static images were analyzed with capture and analysis software (Image-J). Parameters such as the angular velocity and volume of the crystals were
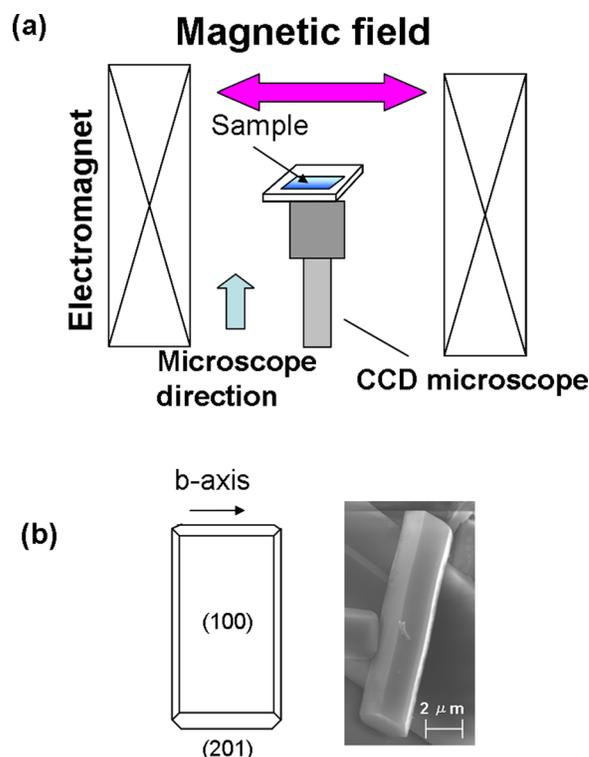

FIG. 1. (a) Experimental system used to observe the effects of magnetic fields on the behavior of uric acid crystals. (b) On the left is a model of a uric acid crystal. On the right is a scanning electron microscope image of a uric acid crystal.

a)iwasaka-m@umin.ac.jp

calculated. We also observed the sample using the CCD microscope placed in the bore of the electromagnet. A magnetic field of up to 500 mT was generated by the electromagnet. The magnetic field was generated to 500 mT within 1 s.

The uric acid crystals that were recrystallized from the saturated solution of uric acid powder are as shown in Figure 1(b). Crystals were rectangular in shape. According to the literature,[19,20] the broadest surface of a uric acid crystal corresponds to the (100) plane and the length of the broadest plane is perpendicular to the *b*-axis.

Figure 2 shows photographs of uric acid crystals and time courses of angular velocity both with and without a static magnetic field of several hundred mT. The X-axis and Y-axis are defined as the directions parallel and perpendicular to the magnetic fields, respectively. The Z-axis is the direction of observation and perpendicular to the magnetic field. The observed crystals showed two stages of orientation. In the first stage, the length (morphological long axis) of the crystal rotated around the Z-axis with an angular velocity of ω_z, and consequently the length was perpendicularly directed to the magnetic field. After the first magnetic rotation, the second stage of magnetic rotation occurred around the Y-axis with an angular velocity of ω_y, which caused the morphologically broadest surface of the crystal to be oriented perpendicularly to the magnetic field. As the magnetic field increased, the duration of the rotations shortened and rapid rotations of the crystals were observed. These phenomena occurred between 200 and 500 mT. When the magnetic field was 130 mT, the length of the crystal rotated around the Z-axis with an angular velocity ω_z and was oriented perpendicularly to the magnetic field, but a second magnetic rotation did not occur. This suggests amount of energy needed for the second orientation was insufficient for the observed size of crystal. The crystal showed no movement in the absence of magnetic fields.

The uric acid molecule is diamagnetic and the crystal contains neither paramagnetic nor strong magnetic species. It is possible to conclude that the orientation of the crystal was induced by the diamagnetic anisotropies in the recrystallized uric acid. The speed of diamagnetic rotation was reduced when the maximum intensity of the magnetic field was decreased.

Figure 3(a) shows the dependence of the angular velocity of crystals diamagnetically rotating around the applied magnetic fields $\vec{B}$ of up to 300 mT. The angular velocity clearly increased as the broadest area of the uric acid crystal decreased. These results indicate that the orientational speed of the crystal was negatively correlated with the crystal's broadest area. In other words, the orientational speed increases as the average moment of inertia is decreased.

Figure 3(b) shows the dependence of the angular velocity on the aspect ratio of the crystals diamagnetically rotating around the applied magnetic fields $\vec{B}$ of up to 300 mT. The aspect ratio was defined by measuring the length and the width of the broadest surface of a crystal whose area was between 800 and 1100 μm^2. The angular velocity of diamagnetic rotation was clearly increased by decreasing the aspect ratio. The result denotes that the slender crystal shape is faster on the angular velocity, and the crystal shape definitely had an effect on angular velocity.
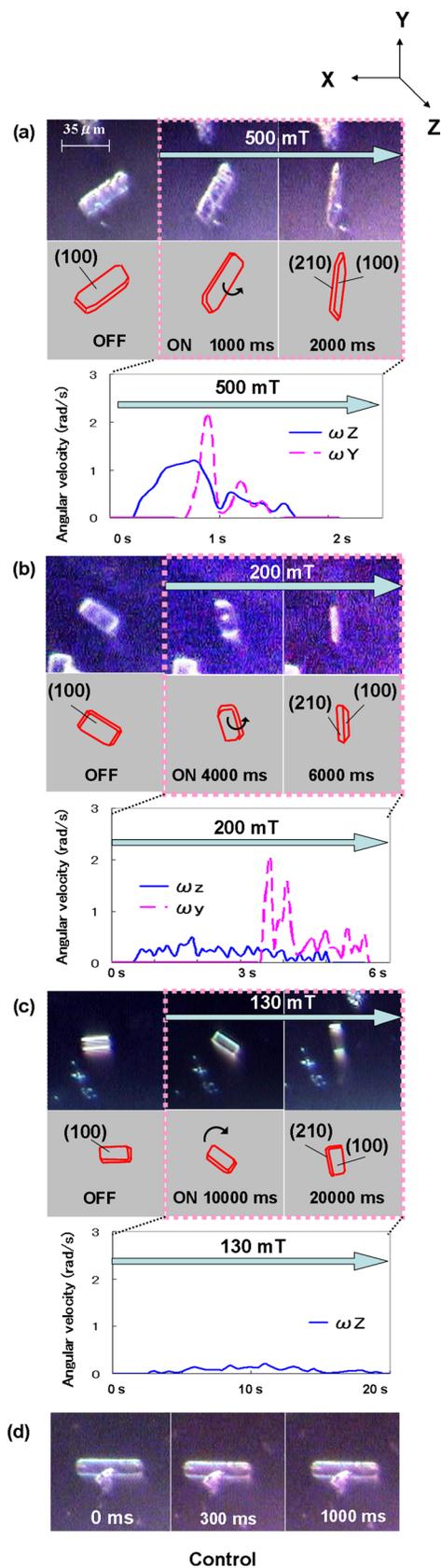

FIG. 2. (a)–(c) Microscopic images showing the two stages of magnetic orientation of uric acid crystals under magnetic fields of several hundreds of mT. The graphs show the change in angular velocity over time after the magnetic field is applied. The solid line is the angular velocity of a uric acid crystal around its Z-axis. The dotted line is the angular velocity around the Y-axis. (d) Microscopic images of uric acid crystals not exposed to a magnetic field.

FIG. 3. (a) Dependence of angular velocity of the area of each uric acid crystal diamagnetically rotating around an applied magnetic field of 300 mT. (b) Dependence of angular velocity on the aspect ratio of uric acid crystals diamagnetically rotating around an applied magnetic fields at 300 mT.

under magnetic fields of more than 200 mT. The thickness was measured using images of completely aligned crystals. ΔE of the crystals at 130 and 200 mT using the averaged volume is 6.3×10^{-11} and 1.4×10^{-10} erg, respectively. ΔE at 200 mT is therefore about 10^4 times larger than the thermal energy kT at 300 K, which is 4.14×10^{-14} erg. It is speculated that the constraint factors such as the viscosity of the surrounding water and friction with the glass surface limit the velocity of diamagnetic rotation of the crystals, and consequently only the one-stage rotation occurred at 130 mT.

In conclusion, the orientation of uric acid crystals under magnetic fields of several hundred mT was examined. Uric acid crystals were recrystallized from a saturated aqueous solution of uric acid powder. Using an electromagnet with a maximum field of 500 mT, we were able to induce two stages of orientation in the crystals. First, the length of the uric acid crystal showed the orientation perpendicular to the magnetic field. Then, a second magnetic rotation occurred to make the morphologically broadest surface of the crystal, so that it was oriented perpendicularly to the magnetic field. Analysis of the angular velocity of the uric acid crystals diamagnetically rotating around applied magnetic fields $\vec{B}$ of 130–500 mT revealed that the angular velocity depended on the applied magnetic field $\vec{B}$, and the area and shape (aspect ratio) of the crystal.

L. Pauling analyzed the anisotropy of the diamagnetic susceptibility of aromatic molecules[21,22] and obtained the diamagnetic anisotropy of molar benzene as -49.4×10^{-6} cm^3 mol^{-1} based on the following equation:

$$\Delta\kappa = \frac{3e^2a^2}{2m}, \quad (1\text{-}1)$$

where e is the elementary charge, a is the distance between two carbon atoms, and m is the mass of an electron. In the case of a five-membered ring compound, $\Delta\kappa$ is calculated to be -14.2×10^{-6} cm^3 mol^{-1}. The molar diamagnetic anisotropy of a uric acid molecule is estimated to be -63.6×10^{-6} cm^3 mol^{-1}, because it contains both six- and five-membered rings.

The anisotropy of volumetric susceptibility $\Delta\chi$ is given by $\Delta\chi = \Delta\kappa\rho/M$, where ρ is density and M is molar mass. $\Delta\chi$ is calculated to be -3.7×10^{-7}. The diamagnetic anisotropic energy ΔE can be estimated using the following equation:

$$\Delta E = -\frac{\Delta\chi V B^2}{2\mu_0}, \quad (1\text{-}2)$$

where V is the volume of the crystal, and μ_0 is magnetic permeability in a vacuum. We calculated the average volume of uric acid crystals as 1.9×10^{-10} cm^3 based on the length and width of each crystal on its broadest surface and thickness, which were determined from the images of rotating crystals

[1]S. I. Hung, W. H. Chung, L. B. Liou, C. C. Chu, M. Lin, H. P. Huang, Y. L. Lin, J. L. Lan, L. C. Yang, H. S. Hong, M. J. Chen, P. C. Lai, M. S. Wu, C. Y. Chu, K. H. Wang, C. H. Chen, C. S. Fann, J. Y. Wu, and Y. T. Chen, Proc. Natl. Acad. Sci. U.S.A. **102**, 4134 (2005).

[2]N. Kaniwa, Y. Saito, M. Aihara, K. Matsunaga, M. Tohkin, M. Kurose, J. Sawada, H. Furuya, Y. Takahashi, M. Muramatsu, S. Kinoshita, M. Abe, H. Ikeda, M. Kashiwagi, Y. Song, M. Ueta, C. Sotozono, Z. Ikezawa, and R. Hasegawa, Pharmacogenomics **9**, 1617 (2008).

[3]C. Lonjou, N. Borot, P. Sekula, N. Ledger, L. Thomas, S. Halevy, L. Naldi, J. N. Bouwes-Bavinck, A. Sidoroff, C. de Toma, M. Schumacher, J. C. Roujeau, A. Hovnanian, and M, Mockenhaupt, Pharmacogenet. Genomics **18**, 99 (2008).

[4]M. Fujiwara, M. Tamaru, M. Hara, K. Suzuki, and K. Mukai, J. Phys. Chem. B **111**, 9492 (2007).

[5]M. Fujiwara, M. Fukui, and Y. Tanimoto, J. Phys. Chem. B **103**, 2627 (1999).

[6]T. Kohama, H. Takeuchi, M. Usui, J. Akiyama, M. G. Sung, K. Iwai, and S. Asai, Mater. Trans. **48**, 2867 (2007).

[7]C. Uyeda, R. Takashima, and K. Tanaka, Appl. Phys. Lett. **86**, 094103 (2005).

[8]C. Wu, S. Li, K. Sassa, Y. Chino, K. Hattori, and S. Asai, Mater. Trans. **46**, 1311 (2005).

[9]T. Kawai, R. Iijima, Y. Yamamoto, and T. Kimura, J. Phys. Chem. B **105**, 8077 (2001).

[10]S. Li, K. Sassa, K. Iwai, and S. Asai, Mater. Trans. **45**, 3124 (2004).

[11]Y. Kawamura, I. Sakurai, A. Ikegami, and S. Iwayanagi, Mol. Cryst. Liq. Cryst. **67**, 77 (1981).

[12]G. Sazaki, E. Yoshida, H. Komatsu, T. Nakada, S. Miyashita, and K. Watanabe, J. Cryst. Growth **173**, 231 (1997).

[13]I. Sakurai, Y. Kawamura, A. Ikegami, and S. Iwayanagi, Proc. Natl. Acad. Sci. U.S.A. **77**, 7232 (1980).

[14]M. Iwasaka, J. Appl. Phys. **107**, 09B314 (2010).

[15]M. Iwasaka, Y. Miyashita, M. Kudo, S. Kurita, and N. Owada, J. Appl. Phys. **111**, 07B316 (2012).

[16]M. Iwasaka and Y. Mizukawa, Langmuir **29**, 4328 (2013).

[17]M. Iwasaka, Y. Miyashita, Y. Mizukawa, K. Suzuki, T. Toyota, and T. Sugawara, Appl. Phys. Express **6**, 037002 (2013).
[18]Y. Mizukawa and M. Iwasaka, IEEJ Trans. Fundam. Mater. **133**, 383 (2013).
[19]A. Z. Zellelow, K. A. Cox, D. A. Fink, C. E. Ford, K. H. Kim, R. E. Sours, and J. A. Swift, Cryst. Growth Des. **10**, 3348 (2010).

[20]R. E. Sours, D. A. Fink, and J. A. Swift, J. Am. Chem. Soc. **124**, 8630 (2002).
[21]L. Pauling, J. Chem. Phys. **4**, 673 (1936).
[22]A. Weiss and H. Witte, *Magnetochemie Grundlagen und Anwendungen*, translated by M. Sorai (Misuzu Shobo, Tokyo, 1980).

参考論文

(1)　Effects of magnetic fields on dissolution of arthritis causing crystals

　　Y. Takeuchi and M. Iwasaka

　　Journal of Applied Physics **117** 17D152 (2015).

(2)　Magnetic rotations of uric acid crystals and uranic crystals by static magnetic fields of up to 500 mT

　　Y. Takeuchi, Y. Mizukawa and M. Iwasaka

　　35th Annual International Conference of the IEEE Engineering in Medicine and Biology Society (EMBC2013), Conf Proc IEEE Eng Med Biol Soc. 2013:3261-4, Osaka, Japan, July 3-7 (2013).

Effects of magnetic fields on dissolution of arthritis causing crystals

Y. Takeuchi and M. Iwasaka

Articles you may be interested in

Finite element analysis of magnetohydrodynamic effects on blood flow in an aneurysmal geometry
Phys. Fluids **26**, 101901 (2014); 10.1063/1.4895893

Down-regulation of adipogenesis of mesenchymal stem cells by oscillating high-gradient magnetic fields and mechanical vibration
Appl. Phys. Lett. **105**, 103702 (2014); 10.1063/1.4895459

Effect of erythrocytes oscillations on dielectric properties of human diabetic-blood
AIP Advances **1**, 012104 (2011); 10.1063/1.3556986

Despite widespread use there is no convincing evidence that static magnets are effective for the relief of pain
Med. Phys. **35**, 3017 (2008); 10.1118/1.2901092

Polymerization and dissolution of fibrin under homogeneous magnetic fields
J. Appl. Phys. **83**, 6453 (1998); 10.1063/1.367735

Effects of magnetic fields on dissolution of arthritis causing crystals

Y. Takeuchi[1,a)] and M. Iwasaka[1,2,3]

[1]*Graduate School of Advanced Science of Matter, Hiroshima University, 1-3-1 Kagamiyama, Higashi-Hiroshima, Hiroshima 739-8530, Japan*
[2]*RNBS, Hiroshima University, 1-4-2 Kagamiyama, Higashi-Hiroshima, Hiroshima 739-8527, Japan*
[3]*PRESTO, Japan Science and Technology Agency, Kawaguchi, Saitama 332-0012, Japan*

The number of gout patients has rapidly increased because of excess alcohol and salt intake. The agent responsible for gout is the monosodium urate (MSU) crystal. MSU crystals are found in blood and consist of uric acid and sodium. As a substitute for drug dosing or excessive water intake, physical stimulation by magnetic fields represents a new medical treatment for gout. In this study, we investigated the effects of a magnetic field on the dissolution of a MSU crystal suspension. The white MSU crystal suspension was dissolved in an alkaline solution. We measured the light transmission of the MSU crystal suspension by a transmitted light measuring system. The magnetic field was generated by a horizontal electromagnet (maximum field strength was 500 mT). The MSU crystal suspension that dissolved during the application of a magnetic field of 500 mT clearly had a higher dissolution rate when compared with the control sample. We postulate that the alkali solution promoted penetration upon diamagnetic rotation and this magnetic field orienting is because of the pronounced diamagnetic susceptibility anisotropy of the MSU crystal. The results indicate that magnetic fields represent an effective gout treatment approach. © 2015 AIP Publishing LLC. [http://dx.doi.org/10.1063/1.4919037]

INTRODUCTION

Gout is one of these diseases and the main symptom is the presence of monosodium urate (MSU) crystals, which is a compound created by excess uric acid and sodium in the blood. The inability to excrete sufficient amounts of uric acid, and thus the formation of MSU crystals, is often caused by excess intake of food substances that contain high volumes of purine bodies. MSU crystals are usually located around the thumb joint at low temperatures, leading to joint inflammation and acute pain. The treatment of gout involves chemical medicines such as uricosuric and a urinary alkalizer. The urinary alkalizer is dispensed to return the acidic pH of urine of gout patients to a normal level. However, excess intake of such medicines is reported to lead to side effects.[1,2] Moreover, an overdose of these medicines increases the risk of urinary stones.[3–5]

Various research efforts examining the influence of magnetic fields on diamagnetic materials have reported that such materials align under high magnetic field strengths.[6–14] For example, in biomolecules, such as proteins, the application of a magnetic field changes the dissolution rate and increases the viscosity of the suspension. Moreover, crystal growth rates varied because of the drift effect of the charged particles based on the Lorentz force.[15,16] Nonetheless, there are only a few reports describing the use of crystal control *in vivo* using magnetic fields as a potential treatment method of diseases that have metabolite crystals as the main symptom.

We previously reported that uric acid crystals respond in a magnetic field of 130 mT. This observation shows that uric acid crystals have a large anisotropy of the diamagnetic susceptibility tensor.[17] In this report, the dissolution rate of MSU crystals, which are responsible for gout, was investigated under the influence of magnetic fields and gradient magnetic fields (GMFs) of several hundred mT.

METHODS

Sample preparation

We prepared MSU crystals by adding 40 ml sodium hydroxide (0.025 mol/l) to 120 mg of uric acid powder (Wako, 99% and used without further purification) and dissolved the mixture at room temperature. The MSU crystals were obtained by standing for 2 days at 4 °C after naturally cooling this solution. The MSU crystals were placed into plain plastic tubes and centrifuged gently (2000 rpm, 5 min).

Measurements

The obtained MSU crystals were transferred to a quartz cell ($1.0 \times 1.0 \times 4.5$ mm) and dissolved in 0.35 ml of an alkaline solution. The MSU crystal suspension, which was added to the alkaline solution, was dissolved under an applied magnetic field using an electromagnet. The MSU crystal suspension under the applied magnetic field was removed from the electromagnet after 2.5 min and before equilibrium was reached, and the dissolution of the crystals was measured by a transmitted light measuring system. The transmitted light decreases in proportion to the concentration of the dissolution of the crystals and the light path length. The temperature

a)Electronic mail: yuka880122@hiroshima-u.ac.jp.
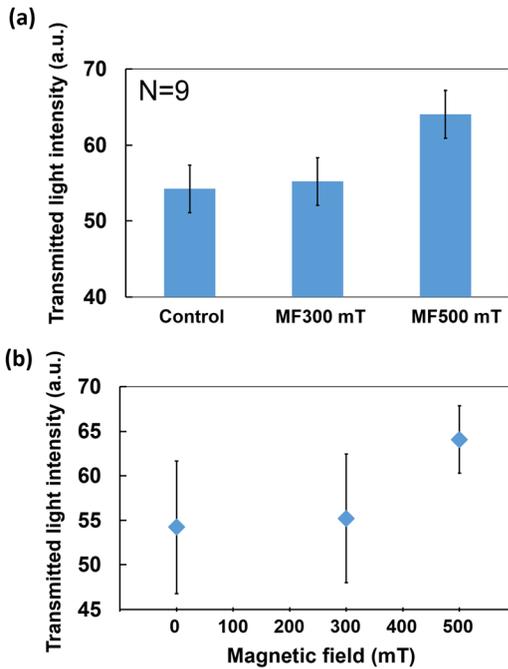
FIG. 1. (a) The mean transmitted light intensity of MSU crystal suspensions in the presence and absence of a magnetic field. Control: ambient field; MF 300 mT: a magnetic field of 300 mT; MF 500 mT: a magnetic field of 500 mT. (b) The dependence of the magnetic field on the transmitted light intensity of the MSU crystal suspension $\pm$ the standard deviation is shown.

was maintained at 28 °C. The transmitted light intensity was measured and analyzed over the wavelength range of 450–800 nm.

RESULTS

Figure 1(a) shows the mean transmitted light intensity of the dissolution process measured for the MSU crystal suspension and the effect of a magnetic field on this process. Error bars show the standard error. The magnetic field intensities examined were 0, 300, and 500 mT. The transmitted light intensity of a MSU crystal solution under a magnetic field of 500 mT was found to be noticeably higher when compared with the result of a MSU crystal solution placed in an ambient field. A magnetic field of 500 mT dissolved the MSU crystal suspension at a faster rate than a solution placed in an ambient field or in a magnetic field of 300 mT. The transmitted light intensity is high if the turbidity is small. A

t-test was used to estimate whether the results were statistically significant. A significant difference was shown between the transmitted light intensity of the solution when place at 500 mT and the transmitted light intensity of the solution at ambient field ($p < 0.05$). However, a significant difference was not found for the transmitted light intensity of the solution placed at 300 mT as compared with the transmitted light intensity of the solution at the ambient field ($p > 0.1$). The applied magnetic field of 500 mT promoted the dissolution rate of the MSU crystal suspension by ∼1.2-times when compared with the ambient field result. Figure 1(b) shows the magnetic field dependence of the mean of transmitted light intensity of the MSU crystals solution. The analysis of the ambient field and magnetic field of 300 mT showed a large dispersion of the transmitted light intensity. The dispersion of the transmitted light intensity under the magnetic field of 500 mT was the smallest.

Figure 2 shows the time course of the transmitted light intensity of the dissolution process of MSU crystals in the presence and absence of the 500 mT magnetic field. The concentration of MSU crystals was tracked to the sampling predetermined time interval and the measured transmitted light to the sample that was placed in the electromagnet. Figure 2(a) shows the measurement system of the transmitted light intensity. The suspension of MSU crystals in the quartz cell was illuminated from a light source placed below the cell; changes in light intensity were detected using a spectrometer placed above the MSU crystal suspension. The MSU crystals were illuminated by a halogen lamp. Figure 2(b) shows the time course of the transmitted light intensity prior to the addition of an alkali solution (equilibrium state) to the MSU crystal suspension. In the case of measuring under an ambient field, the transmitted light intensity at ∼400 s had just reached the equilibrium state. In contrast, in the case of measuring under a magnetic field of 500 mT, the transmitted light intensity showed that at ∼350 s an equilibrium state had been reached. In the course of reaching the equilibrium, the dissolution rate in the MSU crystal suspension was clearly accelerated under an applied magnetic field of 500 mT.

Next, the behavior of the MSU crystals was examined in a state where nothing was added. Figure 3(a) shows a photograph of the MSU crystals, which were transferred to a micro-chamber consisting of a cover glass window
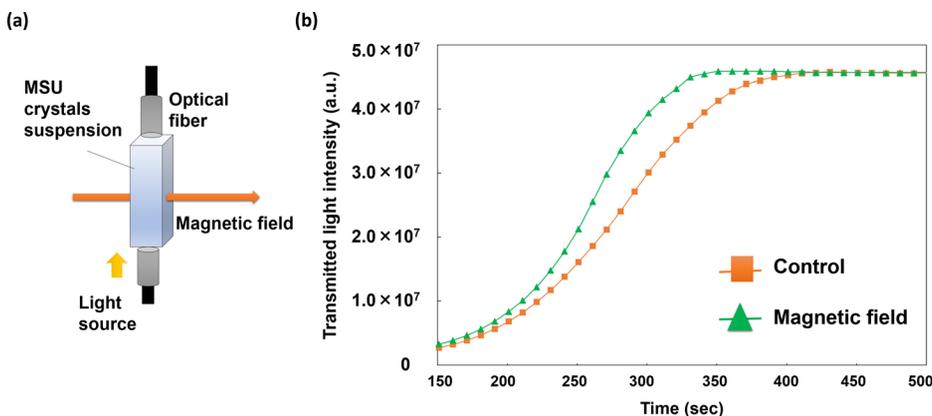

FIG. 2. (a) Schematic showing the measurement of the transmitted light. (b) Time course of the transmitted light intensity in the presence (500 mT) and absence of a magnetic field in the dissolution process following the addition of an alkali solution.
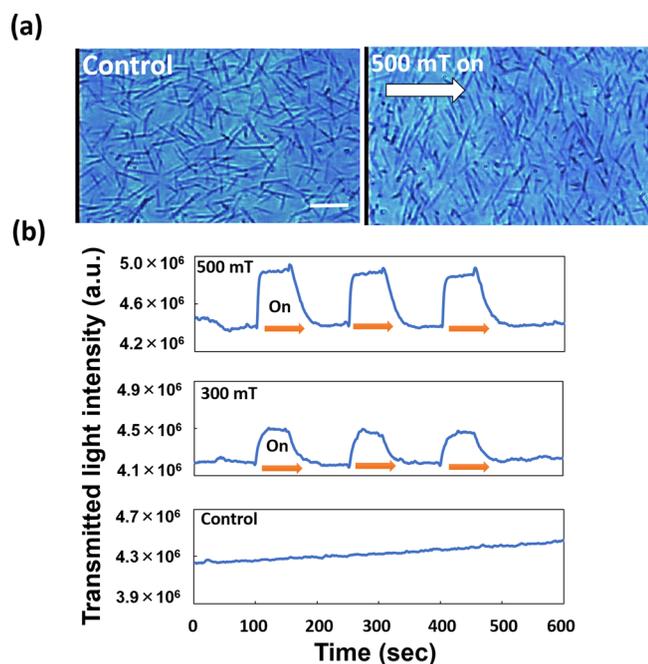
FIG. 3. (a) Microscopic images showing the magnetic orientation of MSU crystals in the presence and absence of a 500 mT magnetic field. Bar, 10 μm. (b) Time course of the transmitted light intensity with 500 mT, 300 mT, and ambient field in a state where nothing was added to the samples.


FIG. 4. The mean transmitted light intensities of MSU crystal suspensions in the presence and absence of a gradient magnetic field. Control: ambient field; GMF 5 T^2/m: gradient magnetic field of 300 mT ($B \cdot dB/dx - 5$ T^2/m); GMF 14 T^2/m: gradient magnetic field of 500 mT ($B \cdot dB/dx - 14$ T^2/m).

(18×18 mm and 0.12–0.17 mm thick) and a rubber sheet under a magnetic field of 500 mT, using an optical microscope whose stage was placed in the space between the poles of an electromagnet. The MSU crystals that were observed to be randomly oriented in the absence of a magnetic field and rapidly oriented (within seconds) when a magnetic field was present. The MSU crystals needle (long) axis rotated in the direction of the diagonal to the magnetic field. Figure 3(b) shows the transmitted light intensity of MSU crystals in a state where nothing was added and continuous measurements were made in the presence and absence of applied magnetic fields of several hundred mT. The intensity of the transmitted light changed and this change was dependent on the magnetic field. Thus, the MSU crystals are sensitive to the applied magnetic field and align rapidly. This phenomenon occurs because of the diamagnetic susceptibility anisotropy of the MSU crystals. Therefore, the dissolution rate of the MSU crystal suspension promoted by the magnetic field is due to the magnetic orientation of the MSU crystals. The addition of an alkali solution penetrates the aligned crystals, whereas such penetration is absent when the crystal is exposed to the ambient field. The results show that the use of magnetic fields is an effective approach for the dissolution of MSU crystals.

Next, we measured the dissolution rate using a gradient magnetic field and a method described previously. The MSU crystal suspension in the quartz cell was exposed to a gradient magnetic field by placing the sample at the edge of a magnet where a magnetic field gradient was obtained. Figure 4 shows the mean transmitted light intensity of the MSU crystal suspension in the presence of the gradient magnetic field. The applied magnetic field was changed to 0, 300, and 500 mT. The gradient magnetic force is $B \cdot dB/dx - 5$ T^2/m at
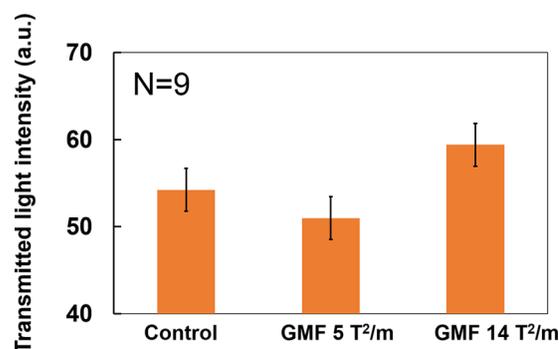
300 mT and 14 T^2/m at 500 mT, respectively. The results of the t-test showed that the transmitted light intensity at a gradient magnetic field of 5 T^2/m at 300 mT was not significantly different to the results (i.e., transmitted light intensity) obtained at the ambient field ($p > 0.1$). The transmitted light intensity at the gradient magnetic field of 14 T^2/m at 500 mT increased the dissolution rate of the MSU crystal suspension, and the t-test result showed that there is marginal significance between 500 mT and the ambient field ($0.05 < p < 0.1$). The increase in the dissolution rate of the solution when exposed to the gradient magnetic field of 14 T^2/m at 500 mT is possibly because of a stirring effect due to magnetic convection. The force of the magnetic field is proportional to $\chi \cdot B \cdot dB/dx$, where χ is the magnetic susceptibility, B is the magnetic field, and a dB/dx is the gradient magnetic field. Thus, stronger gradient magnetic fields may increase the dissolution rate of MSU crystal suspensions.

CONCLUSION

In conclusion, we have presented the effects of a magnetic field and a gradient magnetic field on the dissolution of a MSU crystal suspension when this suspension was added with an alkaline solution to dissolve the crystals. The magnetic field was generated by an electromagnet with a maximum magnetic field of 500 mT. The MSU crystals were precipitated artificially. Application of a magnetic field of 500 mT to a MSU crystal suspension promoted the dissolution rate by $\sim$1.2 times when compared with the MSU crystal suspension placed in an ambient field.

ACKNOWLEDGMENTS

[1]S. I. Hung, W. H. Chung, L. B. Liou, C. C. Chu, M. Lin, H. P. Huang, Y. L. Lin, J. L. Lan, L. C. Yang, H. S. Hong, M. J. Chen, P. C. Lai, M. S. Wu, C. Y. Chu, K. H. Wang, C. H. Chen, C. S. Fann, J. Y. Wu, and Y. T. Chen, Proc. Natl. Acad. Sci. U.S.A. **102**, 4134 (2005).
[2]N. Kaniwa, Y. Saito, M. Aihara, K. Matsunaga, M. Tohkin, K. Kurose, J. Sawada, H. Furuya, Y. Takahashi, M. Muramatsu, S. Kinoshita, M. Abe,

H. Ikeda, M. Kashiwagi, Y. Song, M. Ueta, C. Sotozono, Z. Ikezawa, and R. Hasegawa, Pharmacogenomics **9**, 1617 (2008).

[3]T. F. Yu and A. B. Gutman, Ann. Intern. Med. **67**, 1138–1148 (1967).

[4]A. P. Hall, P. E. Barry, T. R. Dawber, and P. M. McNamara, Am. J. Med. **42**, 27–37 (1967).

[5]E. L. Prien and E. L. Prien, Jr., Am. J. Med. **45**, 654–672 (1968).

[6]M. Fujiwara, M. Tamaru, M. Hara, K. Suzuki, and K. Mukai, J. Phys. Chem. B **111**, 9492 (2007).

[7]J. Torbet, J.-M. Freyssient, and G. Hurdy-Clergen, Nature **289**, 91 (1981).

[8]M. Fujiwara, M. Fukui, and Y. Tanimoto, J. Phys. Chem. B **103**, 2627 (1999).

[9]A. Yamagishi, T. Takeuchi, T. Higashi, and M. Date, Physica B **164**, 222 (1990).

[10]T. Kohama, H. Takeuchi, M. Usui, J. Akiyama, M. G. Sung, K. Iwai, and S. Asai, Mater. Trans. **48**, 2867 (2007).

[11]A. Yamagishi, T. Takeuchi, M. Date, and T. Higashi, Physica B **155**, 433 (1989).

[12]C. Uyeda, R. Takashima, and K. Tanaka, Appl. Phys. Lett. **86**, 094103 (2005).

[13]A. Yamagishi, T. Takeuchi, T. Higashi, and M. Date, Physica B **177**, 523 (1992).

[14]C. Wu, S. Li, K. Sassa, Y. Chino, K. Hattori, and S. Asai, Mater. Trans. **46**, 1311 (2005).

[15]S. Yanagiya, G. Sazaki, S. D. Durbin, S. Miyazaki, K. Nakajima, H. Komatsu, K. Watanabe, and M. Motokawa, J. Cryst. Growth **208**, 645 (2000).

[16]I. Mogi, S. Okubo, and Y. Nakagawa, J. Phys. Soc. Jpn. **60**, 3200 (1991).

[17]Y. Takeuchi, Y. Mizukawa, Y. Miyashita, and M. Iwasaka, Appl. Phys. Lett. **104**, 024109 (2014).

Magnetic rotations of uric acid crystals and uratic crystals by static magnetic fields of up to 500 mT

Yuka Takeuchi, *Non-member,* Yuri Mizukawa, *Member, IEEE* and Masakazu Iwasaka, *Member, IEEE*

Abstract— **In recent years, the disease concerning ureteral calculus is increasing possibly due to the changing lifestyles. For example, it is well known that the urinary calculi have a large impact to gout. As eating habitual diseases, gout and the hyper-uricemia are related to the formation of urinary calculus. In the previous studies, therapeutic agents were developed to enhance the uric acid excretion. From the viewpoint of side effects induction by the chemical agents, we are motivated to explore an alternative method to control the formation of ureteral crystals stimulator by physical stimulations. Therefore in the present study, we focused on the behaviors of uric acid crystals under magnetic fields of several hundreds of mT (Tesla). The uric acid crystals were re-crystallized from a suspension of uric acid powder, and the micro-crystals were prepared to be floating in the solution. We generated horizontal magnetic fields of maximum 500 mT by an electromagnet which contained a CCD microscope. A permanent magnet with magnetic fields of 200~400 mT was also utilized. During the magnetic fields were applied to the uric acid crystals, we observed that the uric acid crystals were oriented by the magnetic fields down to 200 mT at the room temperature. It was speculated that the dimagnetic anisotropy in the uric acid crystals exhibited the rotational responses. The results indicate the possible remote control of the uric acid crystals in living body by the magnetic fields of 200 mT to 500 mT**.

I. INTRODUCTION

In recent years it is well known that there is possibility that one of seven men is ailing urinary tract stone disease [1]. Usually the urine is produced by the kidneys through the ureters. And it is discharged to extracorporeal through the urethra into the bladder accumulate (Fig.1). This course is called a urinary tract. The urinary calculus is a disease to have calculi on this urinary tract. The urinary tract calculi are classified into upper urethra lithiasis and the lower urethra lithiasis which is a calculus in a bladder and the urethra. 95% of people having a urinary tract calculus are ailing upper urethra lithiasis.

The urinary tract calculi are classified in ingredients such as calcium oxalate, calcium phosphate, uric acid and cystine. We focused on the uric acid crystals. It is known as a material that is causing the gout. And it is well known that the urinary

calculi have a large impact to gout [2-5]. As eating habitual diseases, gout and the hyper-uricemia are related to the formation of urinary calculus [6-9]. It has been developed a therapeutic agent which can be used for uric acid excretion stimulator. For the purpose of improving the quality of life, another approach to control the uric acid crystal formation shold ve developed. In the present study, we focused on the magnetic field effects on the characteristics of the uric acid which was a causative agent of the gout. We started a basic study of the magnetic treatment in gout and the urinary tract calculus.

II. METHODS

A. sample preparation

The uric acid powder (98 % of purity, 7.5 mg) was dissolved completely in 2 ml aqueous solution of sodium hydroxide; 2 ml hydrochloric acid was added to generate a precipitate of uric acid crystals in the bottom of incubation tube.

The obtained crystals were transferred to a micro chamber which was consisted of a cover glass window. The thin chamber was set in a CCD microscope which was set in an electromagnet, as shown in Fig. 2. We observed the dynamic motion of uric acid crystals and uratic acid crystals by adding a solvent fluctuation by means of pipetting with 3 ml of pipet (Falcon 3557).

The image of crystals was recorded on a MPEG-2 recorder, and the obtained static images were analyzed on a capture analyzing software, Image-J. Parameters such as the angular velocity of crystals, and so on were calculated.
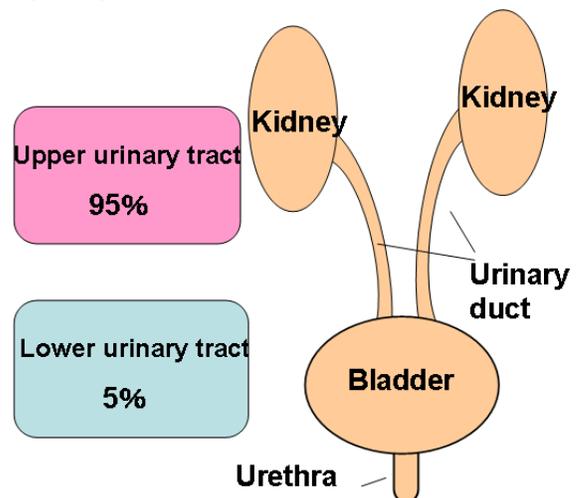

Figure 1. A model of urinay tract.
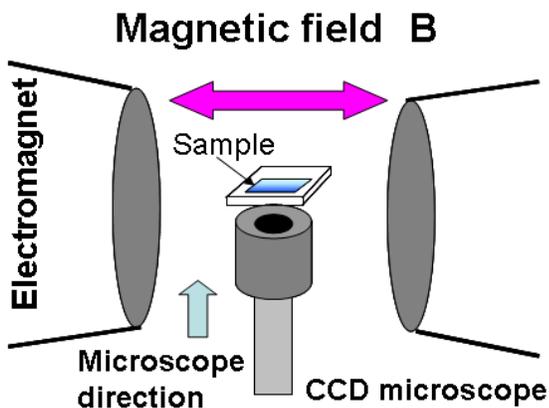
Figure 2. Experiment system for observing the effects of magnetic fields on the behaviors of uric acid crystals.

B. magnetic field generators

We observed the sample on a CCD microscope placed in the bore of the electromagnet to it. The magnet field strength of the electromagnet was set at 0 to 0.5 Tesla (500 mT). The electromagnet (resistive type, 50mm in diameter of magnetic poles, produced by Hayama Corp. Ltd., Fukushima, Japan) generated the maximum magnetic fields of up to 500 mT within 1 second.

III. RESULTS AND DISCUSSION

Figure 3 shows examples of re-crystallized uric acid crystals in a saturated suspension of uric acid powder. By adding hydrochloric acid, the shape and size of uric acid crystals changed. It was speculated that the rod-like shaped crystals had the structure of crystals (uratic crystal) usually observed in ureteral calculus while the "needle assembly" in right upper photo was of uric acid crystals usually generated in the diseased part (gout).

The crystal has been precipitated from the uric acid solution. And rod-shaped and needle-shaped crystals have been arranged at random. Figure 4 shows photos of uric acid crystals under magnetic fields of several hundreds of mT (Tesla). The crystal showed a tendency to orient perpendicular to the magnetic after the magnetic field on. It was oriented at 0.5 Tesla - 0.2 Tesla and was not oriented at 0.1 Tesla. As the magnetic field becomes small, the orientation speed was reduced. The crystal orientation was difficult to. Then stop the magnetic field is applied, it was returned to the environment magnetic field. But oriented crystal did not return to the original.angle

Figure 5 shows angular velocity when changing the magnetic field. The angular velocity is calculated from the rotation angle and the time needed to orient The crystal which were applied to the magnetic field were limited to an size of $2.8nm^2$-$3.4nm^2$. As a result, the angular velocity became large when we increased the magnetic field. The angular velocity

gradually saturated. The result indicates that magnetic fields at 200~500mT was large enough for the orientation of uric acid crystals.
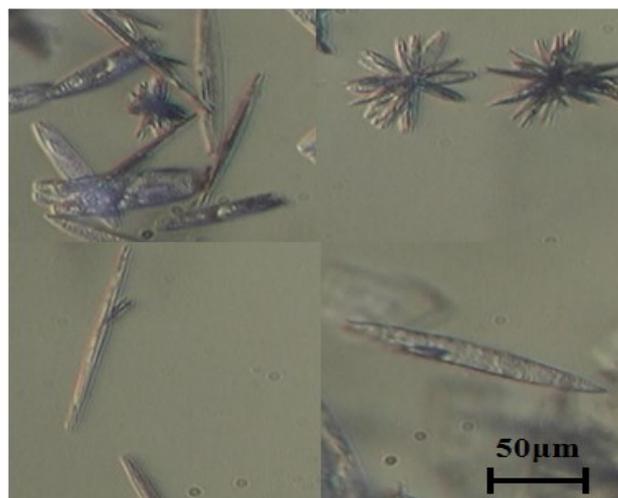

Figure 3. Examples of re-crystallized uric acid crystals in a saturated suspension of uric acid powder.


Figure 4. Magnetic rotation of uric acid crystals under magnetic fields of several hundreds of mT (Tesla).

Figure 5. Angular velocity of the uric acid crystals dia-magnetically rotating around the applied magnetic fields of 200mT – 500mT.

Figure 6 shows the dependence of angular velocity on the aspect ratio of the uric acid crystals dia-magnetically rotating around the applied magnetic fields of up to 500 mT. No apparent dependence of the orientation speed on the aspect ratio was obtained. Probably mixing crystal plates with different size and area randomized the possible dependency.

In order to exclude the effects of the fluctuations of area size, we calculated the new parameter, aspect ratio per area, as shown in Figure 7. The angular velocity of diamagnetic rotation clearly increased when the aspect ratio being divided by area of crystal increased. The results of analyses indicated that the orientation speed of crystal was large when the crystal area is small, i.e. the averaged moment of inertia decreased. It was also speculated that the aspect ratio definitely had an effect on the angular velocity, however, the dispersion of crystal size unrevealed its dependency.

The crystal of uric acid showed orientation under magnetic fields. In the future study, it is needed to clarify the structure of the obtained crystals by X-ray crystal structure analysis for the purpose of revealing the more detailed mechanism.

Figure 6. Dependence of angular velocity on the aspect ratio of the uric acid crystals dia-magnetically rotating around the applied magnetic fields.

IV. A MODEL FOR THERAPEUTIC APPLICATION

Here we propose a model to produce a new therapeutic method for the treatment of gout. We consider a situation where needle types of uric acid crystals are growing in an arthrosis of thumb, as shown in Figure 8. The growing uric acid crystals can be aligned by the external magnetic fields of several hundred of Tesla. The alignments of diamagnetic fiber-like materials by means of diamagnetic torque rotation can cause the polymerization of fiber-like crystals of uric acid, consequently, the grown-up large crystal assembly should appear as less spiny and more rounded micro- to millimeter size of crystals, which will bring less pain to the arthrosis of thumb. The rough model for the diamagnetic alignment of micro-crystals of uric acid is shown in Figure 9.


Figure 7. Dependence of angular velocity on the aspect ratio, which was divided by the area of each of uric acid crystals dia-magnetically rotating around the applied magnetic fields.
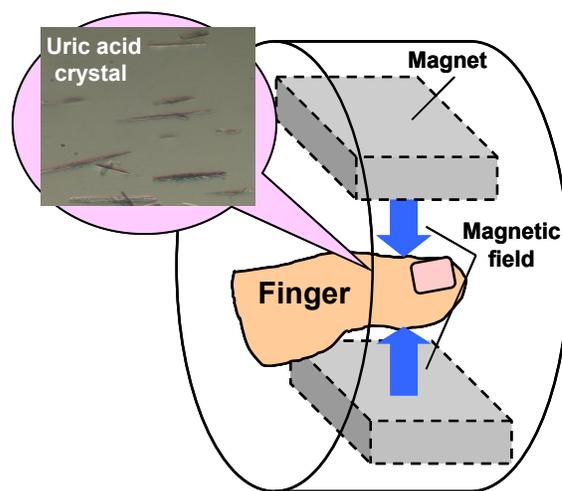

Figure 8. A new therapeutic method for the treatment of gout.
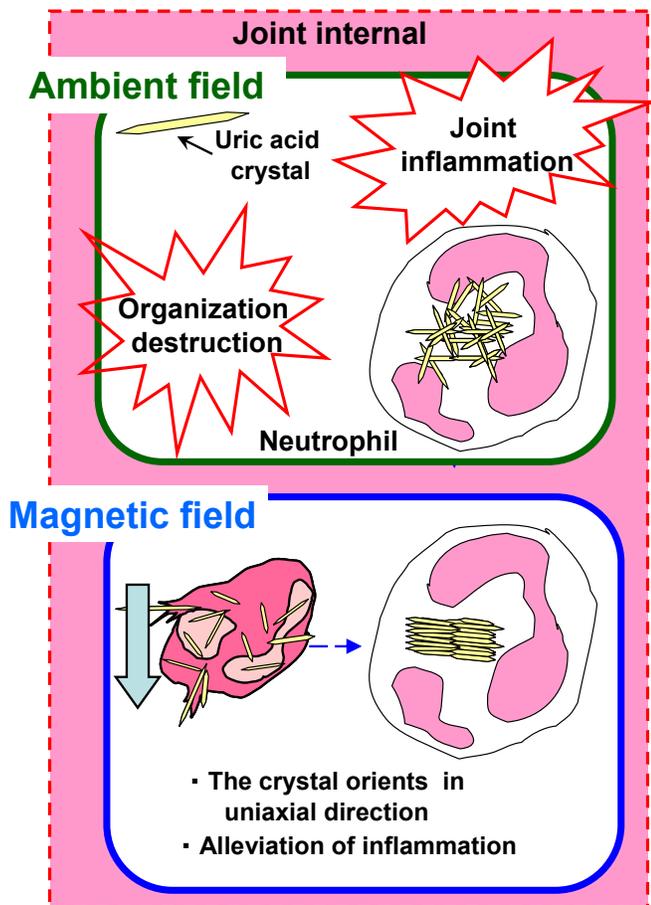
Figure 9. Rough model for the diamagnetic alignment of micro-crystals of uric acid. Upper; under the non-magnetic treatment condition, spiny assembly of needle like uric acid crystals can easily penetrate the cell tissues, Lower; magnetic field exposure at ~500mT can form a less spiny assembly, which can reduce the damage to the surrounding cellular tissue.

V. CONCLUSIONS

Crystals of uric acid were re-crystallized from uric acid powder under a saturated aqueous solution. By utilizing an electromagnet with a maximum field of 500mT, the crystals were oriented perpendicular to the magnetic fields.

An analysis of angular velocity of the uric acid crystals dia-magnetically rotating around the applied magnetic fields of 200mT − 500mT was carried out. It was revealed that the angular velocity depended on magnetic fields and crystal's aspect ratio per area.

REFERENCES

[1] CY. Pak, "Kidney stones," *Lancet*, vol. 351, pp. 1797-1802, 1998.
[2] TF. Yu and AB. Gutman, "Uric acid nephrolithiasis in gout: predisposing factors," *Ann Intern Med*, vol. 67, pp. 1138-1148, 1967.
[3] B. Shekarriz and ML. Stoller, "Uric acid nephrolithiasis, current concepts and controversies," *J Urol*, vol. 168, pp. 1307-1314, 2002.
[4] AP. Hall, PE. Barry, TR. Dawber, and PM. McNamara, "Epidmiology of gout and hyperuricemia .A long-term population study," *Am J Med*, vol. 42, pp. 27-37, 1967.
[5] H. Okabe and T. Hosoya," Clinical feature of urolitiasis in patients with gout," *Hyperuricemia and gout*, vol. 8, pp. 47-50, 2000.
[6] H. Okabe, T. Hosoya, M. Hikita, et al, "Analysis of urolithiasis in patients with gout and hyperuricemid using ultrasonography," *Jpm J Rheum*, vol.9, pp. 239-244, 1999.
[7] EL. Prien and EL. Prien Jr, "Composition and structure of urinary stone," *Am J Med* vol. 45, pp. 654-672, 1968.
[8] FL. Coo , A. Evan and E. Worceter, "Kidney stone disease," *J Clin Invest*, vol. 115 , pp. 2598-2605, 2005.
[9] S. Yamaguchi, "Hyperuricemia as a risk factor for urolithiasis," *Hyperuricemia and gout*, vol. 18, pp. 53-58, 2010.